

DISTRIBUTION STATEMENT A
Approved for public release
Distribution Unlimited

DEPARTMENT OF THE AIR FORCE
AIR UNIVERSITY
AIR FORCE INSTITUTE OF TECHNOLOGY

Wright-Patterson Air Force Base, Ohio

AFIT/GE/ENY/97S-1

IMPROVED LOAD ALLEVIATION
CAPABILITY FOR THE KC-135

THESIS

Adam L. Mortensen, Capt, USAF
AFIT/GE/ENY/97S-1

APPROVED FOR PUBLIC RELEASE

Approved for public release; distribution unlimited

19970923 111

The views expressed in this thesis are those of the author and do not reflect the official policy or position of the Department of Defense or the U.S. Government.

AFIT/GE/ENY/97S-1

IMPROVED LOAD ALLEVIATION
CAPABILITY FOR THE KC-135

THESIS

Presented to the Faculty of the School of Engineering
of the Air Force Institute of Technology

Air University

In Partial Fulfillment of the

Requirements for the Degree of

Master of Science in Electrical Engineering

Adam L. Mortensen, BSAE

Capt, USAF

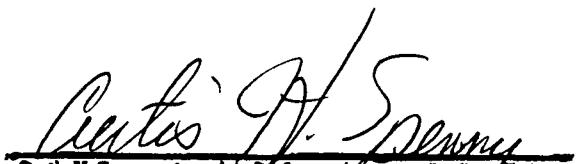
September 1997

Approved for public release; distribution unlimited


IMPROVED LOAD ALLEVIATION
CAPABILITY FOR THE KC-135

Adam L. Mortensen, B.S.
Captain, USAF

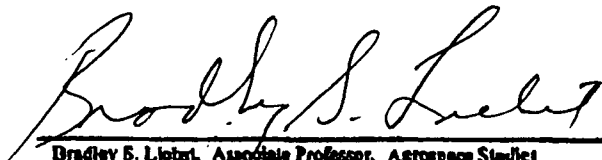
Approved:


Curtis H. Sperry, Associate Professor, Aerospace Studies (Chairman)

5 Sept 97
Date


Dana L. Schneider, Major, USAF, PhD, Electrical Engineering

5 Sept 97
Date


Bradley S. Lieber, Associate Professor, Aerospace Studies

5 Sept 97
Date

ACKNOWLEDGEMENTS

First, I would like to thank my wife, Sabrina, supporting me during my sentence...er...time here at AFIT. While I worked on this thesis project, she took care of just about everything else with only a little help from me. I couldn't have finished this effort without her help. I would also like to thank my thesis advisor, Dr Curtis Spenny, for his help, support, and encouragement. This research would not have been possible without his insight and knowledge. He helped make this work challenging for me and valuable for the Air Force.

I would be remiss if I didn't thank the members of my thesis committee, Drs. Liebst and Schneider. Thanks for being there in my "time of need." Oh, I owe it to those Systems Engineering guys for letting me use the best equipped PC lab at AFIT...Thanks Guys!

It's been a long haul for an Aeronautical Engineer turned Electrical Engineer. It's over... and what an experience! Or is it just the beginning?

Table of Contents

	Page
ACKNOWLEDGEMENTS	V
LIST OF FIGURES.....	VIII
LIST OF TABLES.....	XI
ABSTRACT	XII
I. INTRODUCTION.....	13
Problem	13
Scope	15
Approach/Methodology	15
Materials and Equipment	16
Overview	16
II. LITERATURE REVIEW	17
Air Force Futures	17
KC-135 Dynamic Model.....	18
Robust Controller for Refueling Formation Hold	18
KC-135 Boom Operating Envelope Studies.....	19
KC-10 Refueling Boom Load Alleviation System.....	20
Summary	22
III. METHODOLOGY.....	23
Robotic System Representation.....	24
Boom Loading.....	31
Controller Overview.....	33
KC-135R Aircraft Dynamic Model.....	34
Determining Boom Orientation and Boom Drag	36
Boom Dynamic Model.....	39
Bending Torque Estimation	40
Joint Angle to Base Frame Position Conversion	41
Position Error Conversion to Equivalent Force.....	43
Ruddevator Control Input Equations.....	45
Ruddevator Plant.....	50
Modeling Limitations.....	53
Summary	54
IV. ANALYSIS	55
Simulation Approach.....	55
Controller Performance With Ideal Ruddevator Plant	56
Open Loop Response.....	57
Closed Loop Controller Response	60
Closed Loop Response With Increased Gain on Tip Force Feedback.....	62
Closed Loop Response With Feed Forward	63
Closed Loop Response With Rate Feedback.....	65
Closed Loop Response with Rate Feedback. Gain = 1,000,000.....	66
Closed Loop Response with Feed Forward and Rate Feedback	68
Closed Loop Controller With Non-Ideal Ruddevator Plant.	70

Closed Loop Performance With Non-Ideal Ruddevator Plant.....	75
Non-Ideal Ruddevator Controller With Feed Forward.....	77
Non-Ideal Ruddevator Controller With Rate Feedback.....	78
Non-Ideal Controller With Rate Feedback and τ_{ff}	80
Operating Condition Variations	81
The Coup de Grace	85
Feed Forward Imperfection.....	88
Impact of Controller Performance on UAV Refueling	89
Summary	91
V. CONCLUSIONS AND RECOMMENDATIONS.....	93
Conclusions	93
Recommendations	95
APPENDIX A.....	97
APPENDIX B.....	103
APPENDIX C.....	115
APPENDIX D.....	127
APPENDIX E.....	134
BIBLIOGRAPHY.....	142

List of Figures

	Page
Figure 1: Robotic Representation of KC-135 Refueling System.....	24
Figure 2: Ruddevator Transformation Matrices	28
Figure 3: Boom loads during refueling.....	32
Figure 4: Controller Diagram	33
Figure 5: Aircraft Plant Input To Model.....	34
Figure 6: Calculation of Desired Position and Boom Aero Load.....	37
Figure 7: Controller Boom Plant	39
Figure 8: ΔX_b Due to Boom Bending.....	41
Figure 9 Bending force calculation segment	42
Figure 10: Telescoping Boom Cross-Section [1]	44
Figure 11: Ruddevator Plant Controller Segment.....	46
Figure 12: AOA and Ruddevator Angle Relationship.....	48
Figure 13: Ruddevator Aerodynamic Load Segment	51
Figure 14: Feed-Forward of Boom dynamics.....	52
Figure 15: Direct Feedback of Commanded Torque to Boom Plant	55
Figure 16: 3° Elevator Command and q_l Result	56
Figure 17: Open Loop Torque Error, τ_{root}	58
Figure 18: Open Loop Nozzle Force F_{tip}	58
Figure 19: Open Loop Tip Deviation, Δx_b	59
Figure 20: Open Loop Wind Load	59
Figure 21: Open Loop Gravity Load	60
Figure 22: Closed Loop Tip Force – F_{tip}	61
Figure 23: Closed Loop Torque Command, τ_{root}	61
Figure 24: C.L. Nozzle Force, F_{tip}	62
Figure 25: C.L. Commanded Torque, τ_{root}	63

Figure 26: Nozzle Force, τ_{ff} add.....	64
Figure 27: Commanded Torque, τ_{ff} added	64
Figure 28: Tip Force, F_{tip} and Rate Feedbk.....	65
Figure 29: τ_{root} and rate feedback	66
Figure 30: Rate Feedback Nozzle Force Gain=1M	67
Figure 31: Torque Command, Rate Feedback.....	67
Figure 32: Nozzle Force, τ_{ff} , and Rate Fdbk	68
Figure 33: Torque Command, τ_{ff} , and Rate Fbk	69
Figure 34: N.F., τ_{ff} and Rate Feedback G = 1M	69
Figure 35 Torque Command for G = 1M	70
Figure 36: δ_r , δ_r^c Error, P controller gain = 10,000.....	72
Figure 37: τ_{root} , $\tau_{root-actual}$ Error, P controller gain = 10,000	72
Figure 38: δ_r , δ_r^c Error, P controller gain = 30,000.....	73
Figure 39: τ_{root} , $\tau_{root-actual}$ Error, P controller gain = 30,000	73
Figure 40: δ_r , δ_r^c Error, P gain = 30K, Elev. input = 15°.....	74
Figure 41: τ_{root} , $\tau_{root-actual}$ Error, P gain = 30,000, Elevator input = 15°.....	74
Figure 42: Nozzle Force of Non-Ideal Controller	76
Figure 43: τ_{root} With Non-Ideal Ruddevator.....	76
Figure 44: Nozzle Force With Feed Forward	77
Figure 45: τ_{root} With Feed Forward	78
Figure 46: Nozzle Force With Rate Feedback, G=400,000.....	79
Figure 47: τ_{root} With Rate Feedback, G=400,000.....	79
Figure 48: Nozzle Force with τ_{ff} and Rate Feedback, G=400,000	80
Figure 49: τ_{root} With τ_{ff} and Rate Feedback, G=400,000	80
Figure 50: 15° Elevator Command and q_1 Result	81

Figure 51: Nozzle Force Resulting From Large Magnitude Aircraft Motion.....	82
Figure 52: Torque Produced to Neutralize Aircraft Transient.....	82
Figure 53: Ruddevator Error, P gain = 30K, Elev. comm = 15°, w/ hyd. T.F.	83
Figure 54: Torque Error, P gain = 30K, Elev comm = 15°, w/ Hyd. T.F.	83
Figure 55: Nozzle Force With Large Elevator Input and Servo T.F.	84
Figure 56: $\tau_{root-actual}$ to Minimize Nozzle Forces.....	84
Figure 57: Nozzle Force, Controller w/ Moving F.P.....	86
Figure 58: $\tau_{root-actual}$, Controller /w Moving F.P.....	86
Figure 59: Nozzle Force, Controller w/ Feed Forward and Moving F.P.	87
Figure 60: $\tau_{root-actual}$, Controller /w Feed Forward, Moving F.P.	88
Figure 61: Structural and Mass Properties of Boom [1].....	112
Figure 62: Ruddevator Moment of Inertia Estimate[16]	113
Figure 63: Aircraft Plant Block	128
Figure 64: Controller Model.....	128
Figure 65: Kinematic, Boom Mass and Aerodynamics Calculation Block	129
Figure 66: Freestream Wind Conversion to Boom Axes Block	129
Figure 67: Boom Dynamic Plant Block.....	130
Figure 68: Inertia Block and Division Block.....	130
Figure 69: Boom Dynamics Coriolis and Gravity Calculation Blocks.....	130
Figure 70: Conversion of Position Error, ΔX , ΔY , ΔZ Vector from Inertial Frame, "R03"	131
Figure 71: Ruddevator Plant and Feed Forward Inputs.....	131
Figure 72: Ruddevator Aerodynamics Calculation Block	131
Figure 73: Transformation of Ruddevator Forces to Boom Frame	132
Figure 74: Subblock of Figure 73, Actual Transformation Block.....	132
Figure 75: Feed Forward Signal Calculation Block	132
Figure 76: Inverse Boom Plant Subsystem from Figure 75.....	133

List of Tables

	Page
Table 1: Envelope Limits for KC-135 Refueling Operations (Philips)	20
Table 2: DH Parameters	25
Table 3: Refueling Boom Weights, Distributed Weights	30
Table 4: Refueling Boom Weight Distribution, Fixed Weights	30
Table 5: Aircraft Flight Condition data	36
Table 6: Ruddevator Aerodynamic Properties	47
Table 7: Summary of Additional Simulation Runs	139

ABSTRACT

The Air Force will greatly increase its use of Unmanned Aerial Vehicles (UAVs) in the next century and the latter part of this decade. These UAVs will require refueling like their manned counterparts. The KC-135 and the KC-10 are candidates to provide this refueling task. The KC-10 is equipped with an automatic load alleviation system on its refueling boom which minimizes radial loads at the receiver of the aircraft being refueled. The KC-135 does not have such a system on its boom. Because the boom operator relies on visual cues to tell him when the boom is bending to adjust the boom's ruddervators, large loads may be imparted to receiver aircraft at the fuel receiver port. While load alleviation is required for all aircraft in order to ensure that binding of the nozzle does not prevent disconnect, load alleviation may also be important for the lightweight UAV in order to prevent unwanted disturbance to its flight control system.

A controller was designed to control the longitudinal motion of the boom. This controller can control the angle of the boom so no forces are imparted to the nozzle as the tanker moves from its nominal orientation. The optimal controller design uses both feed forward and rate feedback to modulate the commanded torque signal sent to the ruddervators. The results show that using an automatic controller promises to provide accurate control of the KC-135 refueling boom during refueling operations with minimal nozzle forces being imparted to the receiver aircraft.

IMPROVED LOAD ALLEVIATION CAPABILITY FOR THE KC-135

I. Introduction

In 1996 the Air Force performed a study titled Air Force 2025 [2, 7, 18] in which the authors projected how the Air Force of 2025 would operate. It is clear from this study that Unmanned Aerial Vehicles, UAVs, will be a key force enhancement system for all aspects of air operations by 2025. The authors envision UAVs in offensive, defensive and long duration reconnaissance missions either as part of a total package including piloted vehicles or alone to accomplish tedious or high risk missions. Using UAVs in such a variety of roles adds new and sometimes more stringent requirements to those levied on the personnel and systems currently supporting the Air Force's manned platforms. One system sure to be affected by this transition to UAVs is the Air Force's aerial refueling aircraft. Specifically, the KC-135 Stratotanker which lacks the improvements made in the KC-10 Extender to allow automatic load alleviation while the refueling boom is connected to the receiver aircraft. This lack of load alleviation could prove a mission limiter for the KC-135. If future UAVs are relatively lightweight in comparison to their manned counterparts, they may be more susceptible to departure from controlled flight as a result of excessive force applied by KC-135 boom operators.

Problem

The Air Force has had a requirement for aerial refueling since its inception in 1948. Since that time the technology to perform this task has progressed to the point where the boom operator can steer the boom remotely. Currently, in the KC-135 the boom operator controls the boom using a set of ruddervators located at the end of the upper section of the boom. Ruddervator control is achieved by translating control inputs of the boom operator (boomer) through a hydro-mechanically linked joystick into changes in the angle of attack (AOA) for each of the ruddervators. The extension of the boom's lower segment is also controlled by another

hydro-mechanically linked joystick. Using these two joysticks, the boomer is capable of controlling the spatial position of the refueling boom's tip with relatively coarse resolution.

As the Air Force moves toward UAVs, the coarseness of the boomer's inputs may be a critical limitation to the safe operation of the UAVs. The physical characteristics of future UAVs are unknown. Currently, the boomer attempts to alleviate the loads at the receiver by visual observation of the bend in the refueling boom and then attempts to straighten the boom by increasing the control inputs in the direction away from the bend. When the bending is present but of small magnitude, the boomer cannot observe the loading and thus may subject the receiver aircraft to adverse loads at the receiver port. Also, because of the position of the boomer in relation to the boom he has limited capability to discern bending when the bend is in the vertical axis. If UAVs turn out to be relatively lightweight creations, as current UAVs are¹, the coarse nature of the boomer's control while connected to a UAV being refueled could result in accidental introduction of the UAV to unsafe flight conditions that may overpower the UAV autopilot. This is more of a problem if the relative mass and control authority of the UAV are not of sufficient magnitude to offset the forces introduced to the receiver port while the UAV is connected. One solution to this problem would be to take the boomer out of the loop or augment his control of the refueling boom with a computer controller. The KC-10 uses load alleviation on its boom. In modified form, this system is one candidate for use on the KC-135.[1]

¹ It's likely that UAVs won't be as heavy as their present day manned counterparts primarily because without a pilot on board up to fifteen percent of the aircraft weight comprising the pilot support systems can be eliminated.

By implementing a computer-controlled architecture, the boom operator could act as a monitor during that part of the refueling operation where the tanker and the UAV were actually connected. Then, if the refueling operation stayed within controllable bounds, the boomer would not have to intervene at all. If, on the other hand, something occurred that posed a safety risk to the tanker or the refueled aircraft, the boomer could intervene as necessary to correct the situation or abort the refueling attempt. The boomer would only be responsible for oversight of the refueling operation during the actual connected portion of the refueling.

Scope

This research will develop a longitudinal boom control architecture. After I design the controller, I will benchmark a load alleviation system for UAV applications or for any other aircraft with the capability to maintain a fixed position relative to the center of gravity of the tanker aircraft.

Approach/Methodology

To perform this research, the following tasks were accomplished:

- a. A study of work already done to characterize the operational dynamics of the KC-135 boom was accomplished.
- b. Work done to date that would be useable as a part either of the model or as basis for the assumptions made in the research was incorporated into the study.
- c. The major components of the controller architecture were developed. These major components included the boom dynamics, the KC-135 aircraft dynamic equations, the aero-loading model for the boom, the dynamic equations for the boom, and the aircraft control input profile for driving the simulation

- d. Once the simulation model of the boom controller was completed, it was tested with the longitudinal aircraft disturbance. The boom's response was determined and the effectiveness of the boom's ruddervators at compensating for the disturbances was evaluated.

Materials and Equipment

All materials and equipment are already available for this thesis. The simulation work will be done using the Sun computer systems and appropriate software, such as Matlab, Mathematica, Simulink, and Robotica Front End for Mathematica available in the simulation laboratory

Overview

This thesis report is divided into five chapters. Chapter I contains background information and is an introduction to the topic. Chapter II is a literature review of current KC-135 Refueling System work. Chapter III describes the procedure used to develop the new architecture, followed by an analysis of the results in Chapter IV. Finally, Chapter V contains my conclusions drawn from this research and recommendations for future research.

II. LITERATURE REVIEW

In this literature review, I introduce studies that indicate UAVs will be a prevalent part of the Air Force of the next century. Additionally, I will present recent work which focused on methods of extending the useful service envelope of the KC-135 refueling boom, and work aimed at developing formation autopilots for refueling tasks.

Air Force Futures

In the last six years with the advent of the end of the cold war and the fall of a visible permanent foe, the Air Force has experienced a downsizing trend unmatched since World War II. This shrinking of all branches of the military promoted the Chief of Staff, General Ronald Fogelman to commission a study on the future of the Air Force. He directed the Air Force's Air University at Maxwell Air Force Base to evaluate all aspects of the way the Air Force does business and postulate its shape and mission in the year 2025. A large segment of this report dealt with aerial operations. Three of the white papers on air operations forecast the growth of and importance of UAVs and the reduction of the use of manned intra-atmospheric aircraft. While none of the papers directly states that manned atmospheric, combat related flight will be eliminated, they do argue that many of the more dangerous or arduous missions currently performed by pilots could be accomplished by UAVs. This trend is due to several overarching issues. First, the Air Force will concentrate a larger share of its resources on exo-atmospheric operations thus opening a whole new arena in which pilots may still play an important role. Second, the technology to operate unmanned aircraft will have matured to the point that it is no longer necessary to have a pilot in situ to adequately control the aircraft.

As the demand for increased loiter times for the reconnaissance UAV's grows, one possible solution for enabling long loiter times is on station refueling. On station refueling of these vehicles presents a special challenge to the refueling boom operator. The fact that current

UAV reconnaissance platforms are very lightweight [1, 7, 18] means the boom operator must have a very steady hand or risk damaging or even disabling the UAV. The reconnaissance scenario painted by the authors lends itself well to the development of an automated refueling system. The possible range of UAV weights ranges from as little a 6,000 lbs to 30,000 lbs. [6]

KC-135 Dynamic Model

Several theses completed at the Air Force institute of Technology used the KC-135 platform as a basis for different research topics. Two of these theses addressed the design of multiple input, multiple output flight control architectures for the KC-135. [13, 8] A third thesis, completed in 1993 by Dennis Trosen, used the work of the previous two theses as a baseline for the Development of an Air-To-Air Refueling Automatic Flight Control System Using Quantitative Feedback Theory. [17]

Robust Controller for Refueling Formation Hold

In his thesis, Trosen created an architecture based on the dynamic model of the KC-135R that was capable of holding that aircraft in a specified position with relatively tight tolerances. This work is used to make one of the initial assumptions for my research. He shows that a receiver can track the tanker to within 0.425 feet longitudinally, 0.0025 feet vertically, and 1.9 feet laterally. The position tracking requires that the receiver aircraft “knows” quite accurately where it should be relative to the tanker. How this information is passed is not discussed. His controller is capable of controlling a KC-135 aircraft whether it is empty and light or heavy and full of fuel. The position keeping in both cases is very precise.

In order to hold formation behind another aircraft while refueling, the tolerances must be tight. Trosen’s design demonstrated that capability. The controlled aircraft stays well within the operational refueling envelope of the KC-135. These tight tolerances allow the assumption that if the receiver aircraft knows where it should be, it can maintain that position without deviation.

With an autopilot that holds tolerances as tightly as Trosen's does the basis exists for development of a boom controller which has a primary task of holding the boom's tip position constant as the tanker is buffeted or as the pilot steers the aircraft. Trosen's autopilot is capable of controlling the receiver aircraft to tight tolerances but it isn't very good at adjusting for changes in position of the ideal point in the short period. Several studies have addressed the issue of the operational envelope and methods that could be used to increase that envelope.

KC-135 Boom Operating Envelope Studies

Although the KC-135 is an effective refueling platform, many in the refueling community would like to see the spatial working envelope of the boom increased. Two studies have addressed this issue to date. The first study was completed in 1989 in a team thesis done by several AFIT students [1]. This study primarily evaluated the overall effectiveness of the KC-135 refueling boom with regard to boom loads and operational envelope. It also began to address methods to increase the spatial envelope such as increasing the ruddvator size and incorporating a rolling ruddvator system. The study indicated incorporation of a rolling ruddvator would enable the boom to operate through a larger spatial volume. Another study expanded on this work. In addition to identifying the size of the spatial envelope achieved by incorporating a rolling ruddvator, Debra Nawrocki's thesis [10], also evaluated the benefit of altering the shape of the boom from its current ovoid cross-section to one more teardrop shaped. Her work showed that the envelope could be increased in the lower extreme quadrants of the envelope if the shape of the boom cross section were changed. Nawrocki found the tear drop cross-section actually augmented the down force of the boom when it was at high azimuth angles. The operational envelope of the KC-135 is shown in Table 1. Note that the connection limits of the boom in all cases exceed the position where fuel cutoff occurs.

Table 1: Envelope Limits for KC-135 Refueling Operations (Philips)

Nominal position of boom	
Elevation (deg)	-30
Azimuth (deg)	0
Length (ft)	39.8
Envelope to Maintain Connection	
Elevation (deg)	-34 to -26
Azimuth (deg)	-10 to 10
Length (ft)	38.7 to 40.9
Envelope For Continuous Refueling	
Elevation (deg)	-20 to 40
Azimuth (deg)	-15 to 15
Length (ft)	33.7 to 45.9

Again the aim of both studies was to expand the envelope for continuous refueling.

Nawrocki's research accomplished this by using a rolling rudder and a new teardrop shaped boom cross-section. The 1989 systems effectiveness study only addressed how changes to the rudder system could increase the envelope of the boom. Their biggest benefit to my research comes from the comprehensive aerodynamic, structural and static control models they developed.

KC-10 Refueling Boom Load Alleviation System

There are two methods used to minimize the loading at the tip of the KC-10 refueling boom during coupled operation[4]. The first method attempts to command the control surfaces on the boom to settings that will hold the boom constant at the angle sensed. This method samples the boom position and, using an open loop controller, gains the signal to values equivalent to the correct elevator and rudder settings for the existing boom position. This method of control is very coarse and is not normally used. Normally, a closed loop algorithm called the Automatic Load Alleviation System or ALAS is used. This system uses a series of strain gauges located at the inboard end of the telescoping boom segment to sense the loads on the telescoping section resulting from boom bending. This force information is used in a closed

loop controller that attempts to modify the control surface deflections in order to zero out the forces seen at the strain gauges. Though ALAS does ensure that loads stay below 100 lbs, its ability to determine loading at the *tip* of the boom is limited. Situations can exist in which there is no bending imparted to the boom but significant loads still remain at the boom tip. While load alleviation is required for all aircraft in order to ensure that binding of the nozzle does not prevent disconnect, it is even more important to ensure no side loads are imparted to a receiver aircraft through the receiver port. The ALAS could allow large forces to go undetected which could have significant effect on the receiver aircraft if that aircraft had limited control authority. Lightweight UAVs could be adversely affected by loads of this nature; they could lack the control authority to overcome the effects of forces imparted by a boom under ALAS control. Current UAVs and those being developed, range in weight from 6000 lbs up to 30,000 lbs for the larger systems.[6] In adverse conditions it is not inconceivable that loads of up to one twentieth of the weight of a small UAV can be seen at the boom tip even with the ALAS controller performing optimally.[4]

One characteristic of the KC-10 ALAS bears further discussion. The signals used to drive the controllers for both the open and closed loop algorithms only rely on information about bending in the boom and the elevation and azimuth angles of the boom. This implies that the KC-10 system is only designed to provide optimal load alleviation when the tanker aircraft is not pitching and rolling about its CG. The performance of the KC-10 load alleviation system likely degrades when the aircraft is pitching, yawing, or rolling. The architecture designed in this study will incorporate information about the orientation of the KC-135 and will be able to respond to transients in this orientation. Additionally, the new controller will be able to better respond to changes in the receiver's position that can be sensed.

Summary

UAVs will be ubiquitous in the Air Force of 2025. Because of this, new methods of refueling these aircraft should be designed. Study of the KC-135 has addressed autopilot design for flight of the KC-135, automatic formation flight of another aircraft with the KC-135, and possible modifications to the boom which would increase its useful operational envelope. The load alleviation system used on the KC-10 was studied to determine its benefits and weaknesses. This is the starting point for my research. I will design a longitudinal boom controller based on the robot design methods outlined in Spong's text in order to utilize the Robotica system development software which automates the process of calculating the kinematic and dynamic equations of any system represented using his method. This boom design will compensate for the short period changes in position of the receiver aircraft and minimize the nozzle forces imparted to a receiver aircraft.

III. Methodology

This chapter describes the methodology used to develop the longitudinal controller for the KC-135 refueling boom. The first section will give an overview of the boom system representation used for this research and a description of the coordinate frames for each joint of the boom system. After this overview, the aircraft plant that provides the input for the control system will be briefly described. Next will be a discussion of the overall control architecture followed by descriptions of the blocks that make up the control architecture. Comparison of design options for the controller architecture is the primary emphasis of this study.

As outlined in chapter two, the formation hold autopilot designed by Trosen [17] had the fidelity to maintain position behind a tanker well enough that it could track to a position which was fixed relative to the center of gravity (CG) of the tanker aircraft. This point is called the *formation point* for this research. Trosen's model could track any tanker motion with a period of more than six seconds. With such a formation hold autopilot, as the tanker aircraft pitches about its CG, the formation point does not move with these rotations. The task of remaining connected is divided between the receiver aircraft and the tanker aircraft. The formation hold autopilot for the trailing aircraft is responsible only for maintaining *position* with respect to the tanker CG as it translates in the inertial frame. The boom controller is responsible for adjusting the rudder angle of attack (AOA) to produce a torque that minimizes boom bending. This action is referred to as *load alleviation* and ensures minimum contact force with the receiver port of the trailing aircraft which is important from a safety viewpoint of reducing the possibility of nozzle binding that could prevent disconnection of the boom. There are several assumptions made to facilitate this research. These assumptions are:

1. This research will study only the longitudinal motion of the boom while connected to a receiver aircraft.

2. The tanker and the receiver maintain constant position relative to one another. This is based on the predicted capability of Trosen's formation hold controller research.
3. The angular motion of the tanker is unaffected by boom dynamics. Its motion is only a function of the commanded control surface input.
4. Only first mode bending of the boom is modeled.

Associated with the first major assumption, it is also convenient to assume the ruddervators have no dihedral angle relative to the boom. (Nonzero dihedral gives lateral force producing capability). Finally, this study does not examine control of a free flying boom.

Robotic System Representation

Before the dynamic system is developed, the coordinate system for each part of the robot representation must be identified so the coordinate transform matrices can be assembled. Additionally, the dynamics of the boom must be documented and calculated. The dynamic equations depend upon the choice of coordinate frames for the system. One could simply use the standard coordinate frames associated with aeronautics. If instead, a method outlined in Spang [14] is used, the job of creating the kinematic and dynamic equations can be accomplished using a computer tool called Robotica Front End (RFE) [15], developed by Doctor Spang.

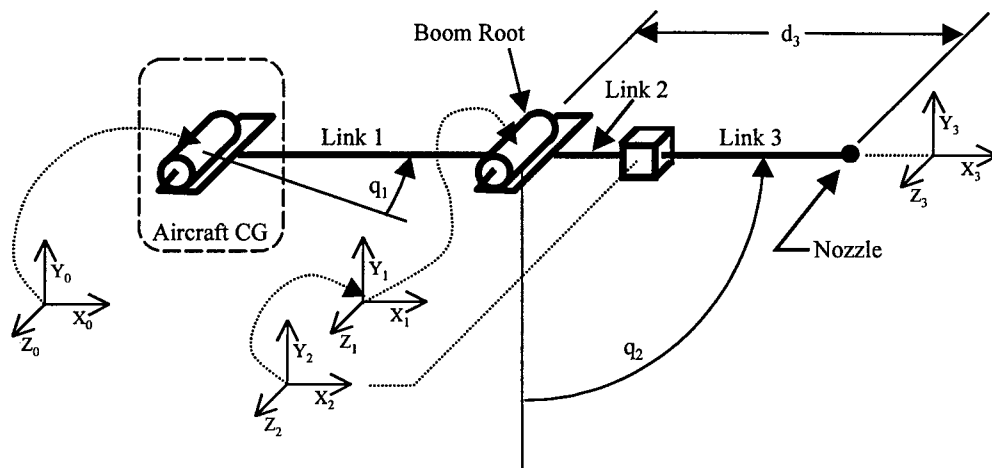


Figure 1: Robotic Representation of KC-135 Refueling System

This software which runs on top of Matlab, aids in development of the symbolic kinematic and dynamic equations for any simple kinematic chain. Figure 1 is the robot representation of the refueling boom system for this study. Note the system's base frame is located at the aircraft CG and its axes' directions remain fixed relative to the earth inertial frame. The frame with origin O_1 is fixed to the end of link one and frame O_2 is attached to the end of link two. Link two for this robotic representation has no length, therefore frame O_2 is co-located with frame O_1 . The last frame O_3 is fixed to the end of link three. Each frame O_i is attached to the end of its respective link i and moves with that link. As link i rotates, the angle between O_i and O_{i-1} is the angle q_i . The variable controlled for each joint is the angle between the frame fixed to the joint and the previous frame, denoted using a q_i , except for the distance between frames two and three which is denoted using a d . Links one and two have control variables q_1 and q_2 respectively, Link three has control variable d_3 . For this study, q_1 is prescribed by aircraft plant motion, q_2 is controlled, and d_3 , normally controlled during free flight, is allowed to free float during refueling and therefore, is not controlled. Using the Denavit-Hartenberg (DH) method outlined in Spong [14] for developing the kinematic equations simplifies the task of assembling the parameters that describe the orientation and position of each joint with respect to its predecessor joint. The items that describe each frame's orientation and position within DH are compiled in Table 2 below.

Table 2: DH Parameters

Link	a_i	α_i	d_i	θ_i
1	49	0	0	q_1
2	0	$\pi/2$	0	q_2
3	0	0	d_3	0

The link parameters in Table 2 are explained in Spong [14] as follows.

a_i = distance along x_i from O_i to the intersection of the X_i and Z_{i-1} axes in feet.

d_i = distance along Z_{i-1} from O_{i-1} to the intersection of the X_i and Z_{i-1} axes in feet.

d_i is variable if joint i is prismatic (sliding).

α_i = the angle between Z_{i-1} and Z_i measured about X_i in radians.

θ_i = the angle between X_{i-1} and X_i measured about Z_i in radians. θ_i is variable if joint i is revolute.

To clarify, the frame with origin O_1 rotates about the Z_0 axis. Frame O_2 rotates about the Z_1 axis. Finally, frame O_3 translates in the common Z_2 direction. For all frames, positive rotation or translation is according to the right-hand-rule. Since the boom length is represented by d_3 , which originates at the boom root coincident with joint two, care must be given to ensure the limits of the actual telescopic segment match the extension and contraction limits of the boom. For the remainder of this paper, the frame attached to the boom, frame three, will be referred to as the boom frame. Vector components in this frame will be referenced with a subscript b. For example, the X component of frame three is denoted as X_b .

After collecting the descriptive information, a series of transformation matrices are created to represent the transformation from one joint to the next. When each of these matrices is multiplied together, the resulting matrix is a representation of kinematic equations for both rotation and translation.

$$T_0^3 = \begin{vmatrix} R_0^3 & d_0^3 \\ 0 & 1 \end{vmatrix} \quad (3.1)$$

The most commonly used kinematic relation in this research describes the transformation from the distal joint's coordinate frame to the base frame. This kinematic equation is termed the T_0^3 transformation matrix. This single matrix contains the kinematic equations for both translation and rotation of the boom tip with respect to the system base frame. The rotational

transformation, matrix which converts frame three vector components into frame 0 components is the upper left 3x3 matrix of equation (3.1) denoted by R_0^3 . The top three rows of column four, d_0^3 are components of a vector that define the position of the nozzle with respect to frame 0. For the kinematic chain of Figure 1, the T_0^3 matrix is

$$T_0^3 = \begin{vmatrix} c12 & 0 & s12 & 49c1 + d3s12 \\ s12 & 0 & -c12 & -d3c12 + 49s1 \\ 0 & 1 & 0 & 0 \\ 0 & 0 & 0 & 1 \end{vmatrix} \quad (3.2)$$

where the c or s preceding each number represents the Sin or Cosine of the angle indicated by the number and the angle q_1 is denoted by the number 1, and similarly the angle q_2 is denoted by the number 2. A combination like $c12$ means $\text{Cos}(q_1+q_2)$. The variable d_3 represents the time dependent length of joint three. The matrices T_0^1, T_1^2, T_2^3 are formed similarly.

Figure 3-2 shows the orientation of the coordinate frames for both the left and right ruddevators, and their orientation with respect to the boom. There are two coordinate transformations necessary to move from the boom frame to the ruddevator frame. The first is the boom to dihedral transformation frame, R_b^d . The dihedral coordinate frame is rotated about the Y_d axis to an angle, d . For simplicity in this study of longitudinal motion, d is set to zero degrees. This results in an small increase in the force the ruddevators can provide versus the real system, but the results are still valid because the performance of the controller for each simulation scenario is based on the same ruddevator conditions.

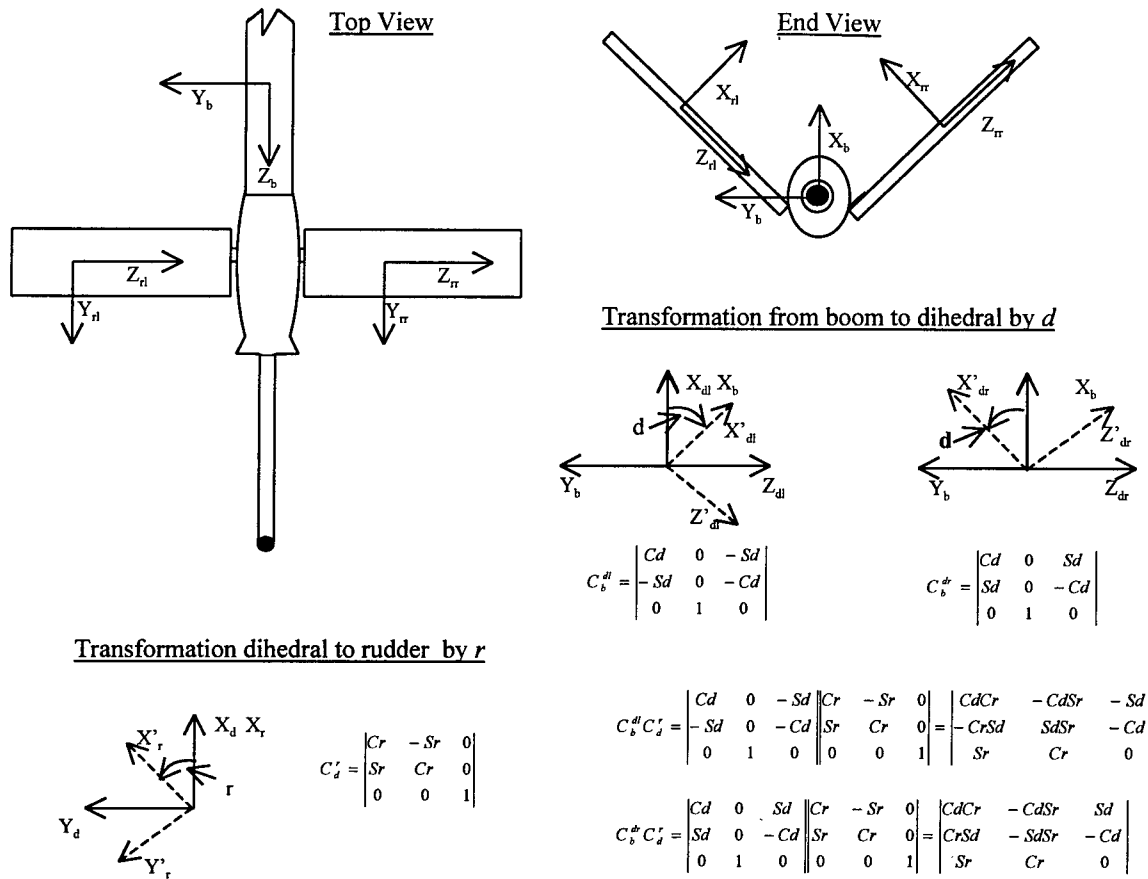


Figure 2: Ruddevator Transformation Matrices

The dihedral coordinate frame for the left ruddevator is rotated clockwise (looking from the boom tip), the right ruddevator frame is rotated counter-clockwise. Both ruddevators use a common transformation to the ruddevator angle δ_{br} . Note the transformation matrices created throughout this research always represent the distal coordinate frame in terms of the coordinate frame nearest the base frame. For example, R_b^{dr} represents the transformation matrix where the right ruddevator *dihedral* frame is represented in the boom frame. Similarly, the product of the transformation matrices $R_b^{dr} R_{dr}^r$ represents the right *ruddevator* frame in the boom frame coordinates.

The dynamic equation created from Robotica is implemented in the boom plant system block. The general form of the dynamic equation which describes the torques on each joint as a function of inertia, coriolis and gravity is

$$\begin{bmatrix} \tau_1 \\ \tau_2 \\ \tau_3 \end{bmatrix} = \begin{bmatrix} M_{11} & M_{12} & M_{13} \\ M_{21} & M_{22} & M_{23} \\ M_{31} & M_{32} & M_{33} \end{bmatrix} \begin{bmatrix} \ddot{q}_1 \\ \ddot{q}_2 \\ \ddot{q}_3 \end{bmatrix} + \begin{bmatrix} C_{11} & C_{12} & C_{13} \\ C_{21} & C_{22} & C_{23} \\ C_{31} & C_{32} & C_{33} \end{bmatrix} \begin{bmatrix} \dot{q}_1 \\ \dot{q}_2 \\ \dot{q}_3 \end{bmatrix} + \begin{bmatrix} g_1 \\ g_2 \\ g_3 \end{bmatrix} \quad (3.3)$$

where τ_i is the net torque on joint i due to all external sources (including Gravity), M_{ij} is the moment of inertia acting on joint i due to acceleration of joint j , C_{ij} is the coriolis force resulting from interaction between joints i and j . The last term, g_i is the torque on joint i due to gravity acting on link i . For the boom system, we are only interested in the torque acting on joint two. This is because the torque on joint 1 and the resultant angle are driven by the AOA of the tanker model when an elevator deflection is commanded. Also, because this controller is designed to operate when the boom is connected to a receiver aircraft, joint three must be allowed to “float”. Any frictional forces occurring at joint three do not contribute to the torque on joint two. With these assumptions, only the second row of equation (3.3) is relevant.

$$\left(\sum \tau\right)_2 = M_{21}(d_3, q_2)\ddot{q}_1 + M_{22}(d_3)\ddot{q}_2 + C_{21}(d_3)\dot{q}_1\dot{d}_3 + C_{22}(d_3)\dot{d}_3 + C_{23}(d_3)\dot{q}_1\dot{q}_2 + g_2 \quad (3.4)$$

The left side of equation (3.4) is the summation of all of the torques on the system. These torques include rudder torque, τ_r , wind drag on the boom, τ_w , and the reaction torque due to boom deflection, τ_b . The right side consists of the torque due to inertia, non-linear coupling, and gravity. The KC-135 aircraft model that drives the simulation actually describes the first link’s motion. This is possible because the AOA of the KC-135 is actually the negative of the joint angle, q_1 . This assumption means that for the purposes of the Robotica calculations, joint

one can be assumed to have no mass or moment of inertia. The mass properties of the KC-135 refueling boom are shown in Table 3 and Table 4. Figure 61 of Appendix B shows the pieces of

Table 3: Refueling Boom Weights, Distributed Weights

Section	Item	Weight (lbs)
1,2,3	Structure Tube	166.9
	Fairing	142.7
	Fuel	129.4
	Hydraulics	58.1
	Fixed Inner Tube	31.0
	Electrical	15.4
	Fuel System	13.2
2,3,4	Telescoping Inner Tube	(total) 245.7
	Telescoping Tube Lining	

Table 4: Refueling Boom Weight Distribution, Fixed Weights

Section	Item	Weight (lbs)
1	Snubber	28.9
	Hydraulic Drive	64.3
	Stowage Provisions	13.3
	Instrumentation	10.0
	Attachment Provisions	6.0
2	Rollers and Supports	23.4
3	Ruddevators and Supports	208.2
	Recoil Assembly	54.3
	Ruddevator Controls	48.8
	Ruddevator Locking	9.9
	Dumping Provisions	8.0
5	Nozzle	31.0
	Shock Absorber	31.0

the boom system and shows the method for calculating the mass dynamically during simulation runs. The equations represented by each of the coefficients, M , C , or g defined in equation (3.3) are documented in Appendix A along with the T matrix coefficients. All kinematic and dynamic data for the boom structure were derived using RFE from the parameters outlined at the beginning of Appendix A.

Boom Loading

The boom loads shown in Figure 3 are the rudder force perpendicular to the boom, F_{bxr} , nozzle load in the X_b direction due to bending in the boom or inaccurate position keeping, F_{bxb} , distributed wind load, P_w , and the distributed gravity load, P_g . The rudder force, F_{bxr} , consists of both lift and drag. The goal of this controller is to control the rudder forces to ensure the lateral force, F_{bxb} , on the boom nozzle is minimized.

Due to restrictions of the DH method of representing kinematic structures, q_2 will actually be measured as shown in Figure 1 from the Y_0 axis upward versus from the X_0 axis down. Therefore, an angle of 30 degrees down elevation for the boom is equivalent to 60° for angle q_2 . On the KC-135 the boom rests at an angle of 29.6 degrees, measured from the horizontal plane downward, for the flight conditions used in this project [9]. Using the coordinate system of this study, the initial angle for the real KC-135 at the prescribed flight conditions, would be 60.4 degrees. The model used in this study is in equilibrium at $q_2 = 56.2^\circ$. The angular difference between our model's set point and the actual set point for the boom at these flight conditions would put us out of the nominal refueling envelope for the KC-135, but it is acceptable for purposes of this study. A formation point was chosen such that the force of wind on the boom was exactly cancelled by the force of gravity acting counter to it. The position of the formation point in the base frame is approximately 82.1 feet back from the aircraft CG and 22.2 feet down. At this position, the boom is depressed 33.8 degrees down from horizontal. A

corresponding initial rudder angle setting was determined for which lift and drag create no net moment about the boom root (joint 2). If the rudder had been initialized with zero AOA, the position of the boom would have been closer to the set point of the actual KC-135. However, this would make simulations for the ideal rudder cases of chapter four more difficult. There was no noticeable deviation from the nominal position upon initiation of the simulation with q_1

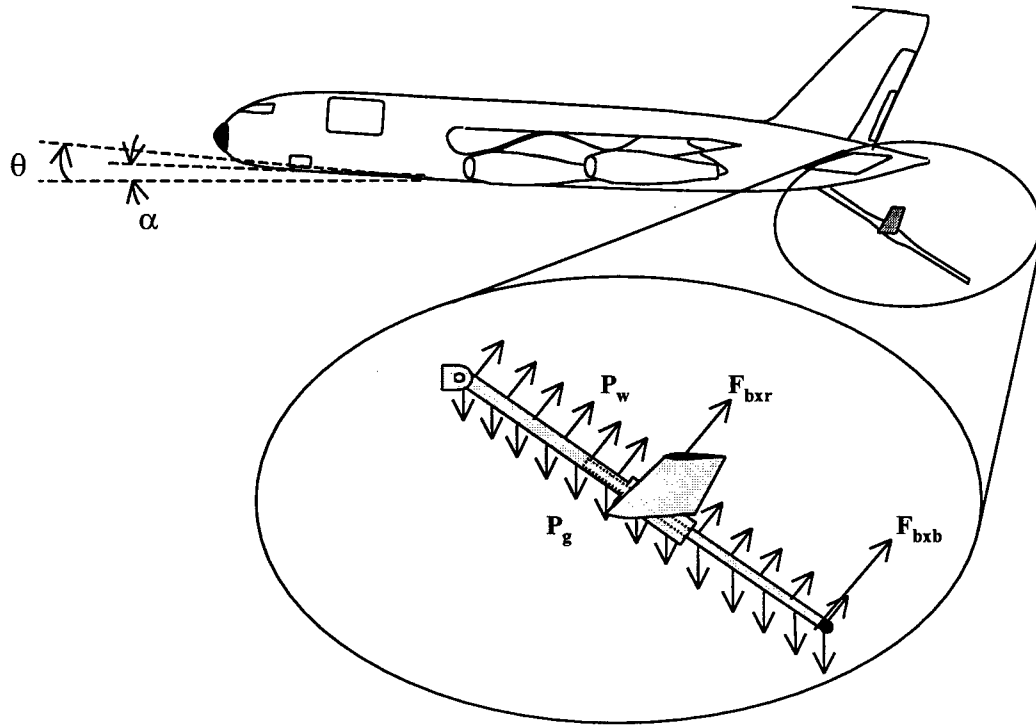


Figure 3: Boom loads during refueling

constant at 0 degrees. This approach to selecting the formation point ensured the model started from a nearly quiescent condition so any motion seen in the boom during simulation would be the results of dynamic interaction of the joints as the aircraft changed angle of attack. Then the initial rudder angle was selected to provide zero force in the X_b direction. One could bias the starting position of the boom by adjusting the rudder angle to provide enough lift to offset the additional gravity load associated with moving the boom up 3.8 degrees. However, this is not necessary for modeling purposes.

Controller Overview

To hold the boom nozzle position constant at the formation point, the force required by the rudddevator is adjusted to offset the difference in torque resulting from the boom dynamics as the tanker aircraft changes pitch. This is the closed loop design. Driving the rudddevator in order to provide the necessary force requires additional levels of feedback control for the rudddevator. The controller design includes a proportional feedback loop which controls the output torque of the rudddevator, a feed forward term which attempts to anticipate net torque required for the prescribed tanker input, a joint rotation rate error feedback signal, and a feedback loop around the rudddevator plant integrator. The overall architecture is shown in Figure 4. The major parts of this controller such as the boom aerodynamics, the boom plant the feedback equations and the rudddevator plant are detailed in the remaining sections of this chapter. Detailed drawings of the controller architecture as represented in Simulink are in Appendix D.

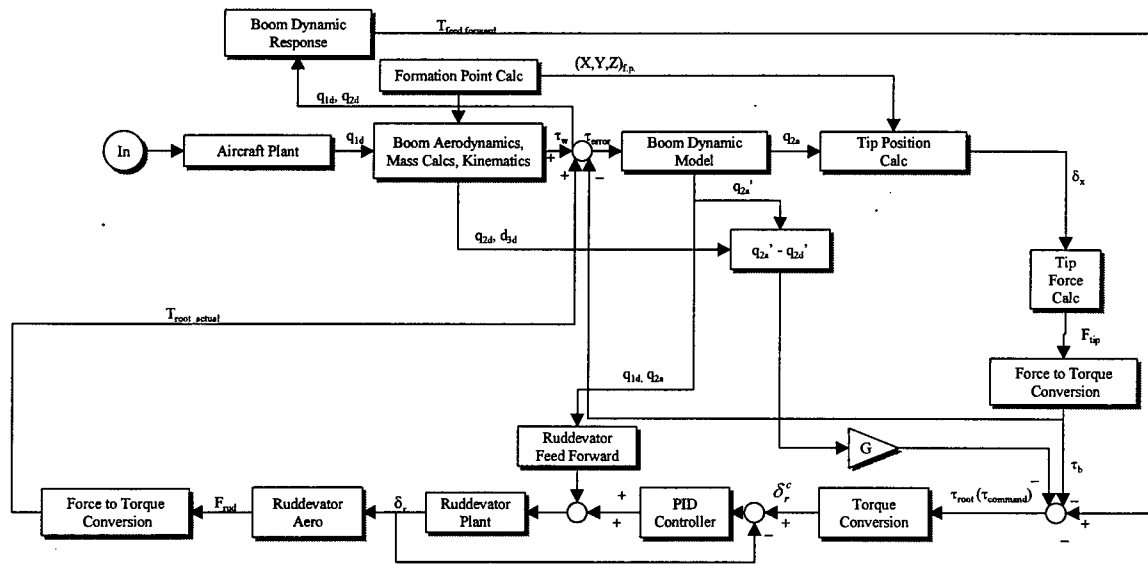


Figure 4: Controller Diagram

KC-135R Aircraft Dynamic Model.

As discussed in the literature review, the dynamic model for the KC-135R is well documented. The development of the basic equations represented in the state equation form of

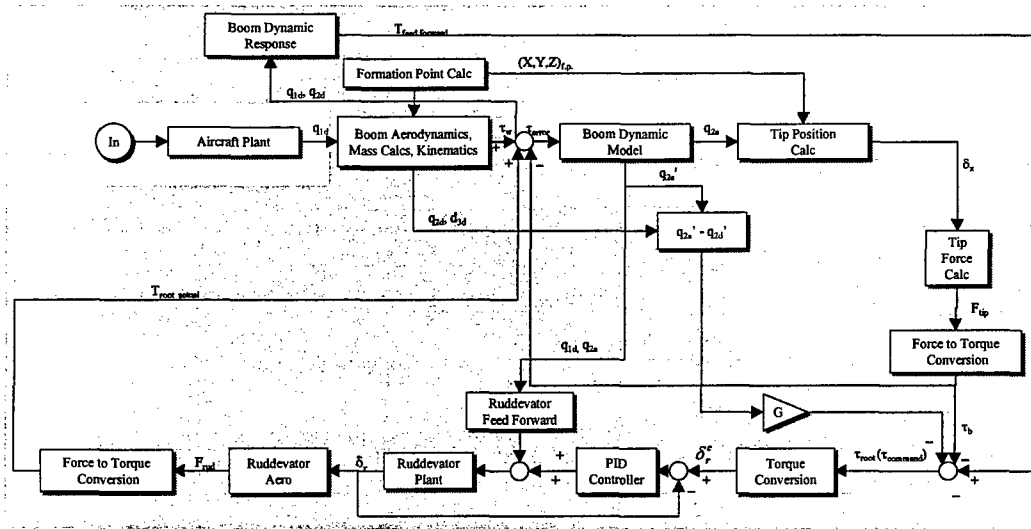


Figure 5: Aircraft Plant Input To Model

the model follows Roskam's text [12]. Equation (3.3) is the general form of the state space model.

$$\begin{aligned}\dot{\bar{x}} &= A\bar{x} + Bu \\ \bar{y} &= C\bar{x}\end{aligned}\quad (3.5)$$

where

$$\dot{\bar{x}} = [\dot{\phi} \dot{\beta} \dot{p} \dot{r} \dot{h} \dot{\theta} \dot{u} \dot{\alpha} \dot{q}]^T$$

$$\bar{x} = [\phi \beta p r h \theta u \alpha q]^T$$

$$\bar{u} = [\delta_r \delta_w \delta_e \delta_{sb} \delta_T]^T$$

$$\bar{y} = [\phi \beta h \theta u]^T$$

The model represents a system of linearized equations. To use it, we assumed only small disturbances to the steady state motion of the aircraft are modeled. With the equations for lateral and longitudinal responses decoupled and since the design theory requires an equal number of model inputs and outputs, the lateral equations are driven using two inputs, rudder (δ_r), and combined aileron and spoiler inputs (δ_w). The expanded form of the coefficient matrix, A, the non-dimensional stability axis derivative matrix, B, and the output matrix, C, are shown in Appendix B. The derivatives were calculated using a Matlab script file programmed with the coefficient and derivative equations. That script file is also in Appendix B.

With the matrix coefficients and stability derivatives calculated, the aircraft motion model is incorporated into the controller simulation model. For this study, the longitudinal response is driven using three inputs, elevator (δ_e), speedbrake (δ_{sb}), and thrust (δ_T). The longitudinal dynamics will be excited using a δ_e of sufficient magnitude to ensure the boom will stay within its continuous refueling envelope if the boom tracks the formation point. When the aircraft model receives a commanded δ_e , a response is output on the five selected variables from the plant state space equations. For this model the last five outputs from the vector x in equation (3.5) were selected. They include: altitude, h , flight path angle, θ , climb rate, u , angle of attack α , and pitch rate, q . The only output used for this study is the angle of attack. A change in the flight path angle results in translation of the aircraft CG. Responsibility for tracking the tanker's CG is left to the receiver aircraft's formation hold autopilot. Where the flight path angle indicates translation, changes in AOA indicate rotation about the aircraft CG. The AOA will appropriately drive the boom controller. The other three inputs describe translation of the aircraft, and therefore, are not used. Using the programs Matlab and Simulink, the equations for the nondimensional stability derivatives, and dimensionalized input and output coefficients were calculated according to Harvey Russell's equations [13]. Coefficients for the flight conditions

used for this project are shown in Table 5: Aircraft Flight Condition data. The Matlab files performing the derivative calculations are in Appendix B. These flight conditions and aircraft characteristics are the nominal flight condition for refueling operations in the KC-135 as verified by personnel at Boeing Company [9, 11].

Table 5: Aircraft Flight Condition data

Variable	Value	Units
Altitude	28,500	ft
Mach	0.77	--
Weight	284,000	Lbs
Center of Gravity	24.2	%MAC
q dynamic. pressure	279.7	lbs/ft²
s wing area	2433	ft²
b wing span	130.83	ft
c wing MAC	20.16	ft
U₀ (true)	770	ft/sec
θ₀ (body)	2.4	deg
α₀ (wing)	4.4	deg
α₀ (body)	2.4	deg
I_{xx}	2,930,000	slug ft²
I_{yy}	4,660,000	slug ft²
I_{zz}	7,480,000	slug ft²
I_{xz}	--	--
Inertias in body axis system		

Determining Boom Orientation and Boom Drag

The highlighted section of Figure 6 performs all the calculations necessary to determine the aerodynamic loading of the boom. The block immediately following the aircraft plant block performs several functions preparatory to computing the aerodynamic loading. The contents of this block are shown in Figure 65 of Appendix B. To calculate q_2 and d_3 the following equations are used. First, the end of link one is located in base frame coordinates using

$$\begin{Bmatrix} x \\ y \\ z \end{Bmatrix}_{o_0} = \begin{Bmatrix} 49 \cos(q_1) \\ 49 \sin(q_1) \\ 0 \end{Bmatrix} \quad (3.6)$$

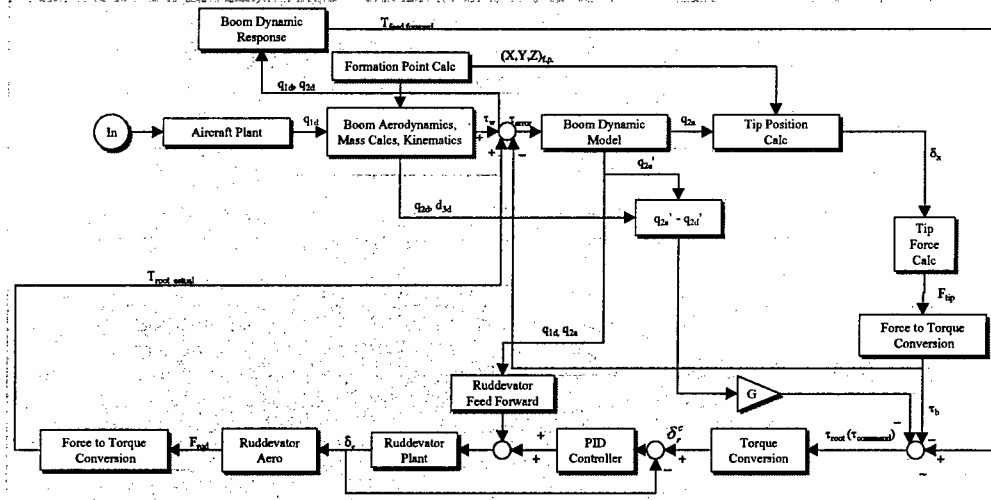


Figure 6: Calculation of Desired Position and Boom Aero Load

Then, finding the magnitude of the component distances Δ_x and Δ_y from this position to the formation point and using these values in the equation

$$q_2 = \tan^{-1}\left(\frac{\Delta_y}{\Delta_x}\right) + \frac{\pi}{2} - q_1 \quad (3.7)$$

q_2 is found. Finally using the pythagorean theorem and the distances Δ_x and Δ_y , d_3 is calculated. This computation is performed in the file, "Inv_kinematics_23.m" included with all other controller function xxx.m files in Appendix C. Next, the center of mass, mass, and aerodynamic centers of pressure are determined according to the method used in the Matlab function file, "boomwgt.m". This file, found in Appendix C, performs the mass, center of mass, centers of pressure, and inertia calculations. The method used follows the method of the GSE study [1]. The boom is divided up into five segments as shown in Figure 61 of Appendix B. The mass of each segment is determined based upon what major assemblies are within that segment.

For example, the segment identified as “Mass 4” consists of part of the fixed boom tube and its subassemblies, part of the telescoping tube, and part of the fairing surrounding the rudder control equipment. As the telescoping segment of the boom extends and contracts, the mass of this segment of the boom will change. Similarly, the mass of the other boom segments is continuously changing too. As the boom moves then, the mass of each section is calculated, the center of mass is determined, then the masses are added up. The moment of inertia is calculated for motion about the boom root in the GSE study. Robotica however, requires a moment of inertia based on rotation about the center of mass of the boom. To accomplish this the moment of inertia equation of the GSE study is modified by adding terms to translate the moment of inertia from the boom root to the boom’s center of mass. Finally the center of pressure for each segment is calculated from the lengths of the different boom sections. It is assumed that the center of pressure of each segment is located at the middle of each segment. Concurrent with the mass calculations, q_1 , q_2 , and d_3 are used in the function, “convaxes.m” to transform the freestream velocity into the boom frame using the kinematic relation R_0^3 . This is done because the drag acting on the boom is only a function of the wind velocity normal to the boom in the X_b direction. The resulting velocity vector, V_b is used in the boom aerodynamic loading function, “boom_aero_moment.m”, and in the rudder lift and drag calculation function, “rud_aero_force.m”. If the rudder was normally at a zero dihedral angle and never moved laterally, transforming the wind vector into the rudder frame would be unnecessary because the entire wind force would be acting to provide lift. But since the real rudder has a dihedral and since it can be moved laterally, only that fraction of the wind velocity that acts parallel to the rudder wing chord provides lift or drag in a useful direction. For this study, transforming to the rudder frame is an unnecessary step but was done as a check to verify the aerodynamic equations were working correctly. Finally, using the joint angles and the centers of pressure, the

moment about joint two due to boom drag is calculated. The calculation of the aerodynamic drag is done in the function “aero_boom_moment.m”. The output of this controller segment is the load on the boom root due to aerodynamic loading, τ_w . The torque, τ_w , is fed forward and summed with the feedback root torque $\tau_{root-actual}$, created by the rudder plant, and reactionary bending moment due to bending of the boom. The block just above the highlighted area, “Formation Point Calcs” calculates the formation point position using the kinematic equation d_0^3 from the T matrix. This block wasn’t included in the Boom Aerodynamics block because the formation point is also used by the nozzle position error calculation block downstream. To include it in the Boom Aero block makes passing the data forward more difficult in the simulation program Simulink.

Boom Dynamic Model

Input to the boom plant is the sum of the aerodynamic moment, boom bending moment and rudder torque. The boom plant, highlighted in Figure 7, uses the summed torques as input to drive the dynamic response of the boom. The output of the boom plant is the angle q_2 .

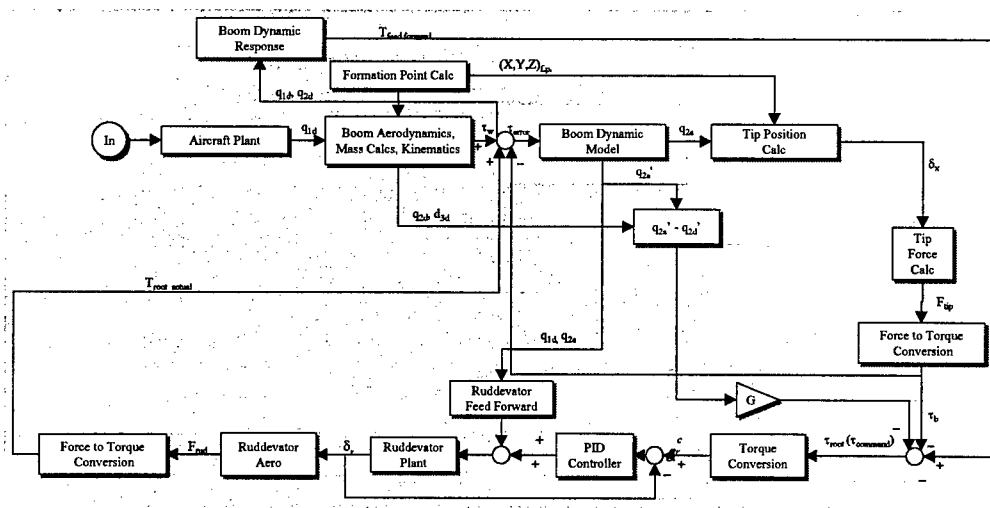


Figure 7: Controller Boom Plant

The ultimate goal of this controller is to maintain the position of joint two so no net force is produced at the nozzle tip. To do this, the position of the tip must be known. The dynamic equations provide knowledge of the actual angle of joint two as the boom bends. To determine the angle q_2 , equation (3.4) is solved for \ddot{q}_2

$$\ddot{q}_2 = \frac{\tau_2 - (M_{21}(d_3)\ddot{q}_1 + C_{21}(d_3)\dot{q}_1\dot{d}_3 + C_{22}(d_3)\dot{d}_3 + C_{23}(d_3)\dot{q}_1\dot{q}_2 + g_2)}{M_{22}(d_3, q_2)} - K_d\dot{q}_2 \quad (3.8)$$

then integrated twice to arrive at q_2 . The equation represented by each of the uppercase letters is listed in Appendix A. To represent the physical system better, a damping term $K_d\dot{q}_2$ was included.

Bending Torque Estimation

The output of the boom plant is the actual angle of the boom. If the boom were allowed to move freely instead of being bound to the receiver port, it would move as described by the output of the plant. Since it is held in place by the receiver aircraft, the angle computed in the boom plant block represents bending in the boom as the tip is held in place by the receiver aircraft. While more than one bending mode can occur in the boom for this model, we assume the boom motion is represented reasonably accurately with only the first bending mode. As the boom bends, it creates a reaction force, F_{tip} , at the boom nozzle which causes a torque at the boom root. This torque, τ_b , is calculated in order to determine its contribution to the boom dynamics. With the actual angle for joint 2, q_{2a} , calculated, it must be converted to a force.

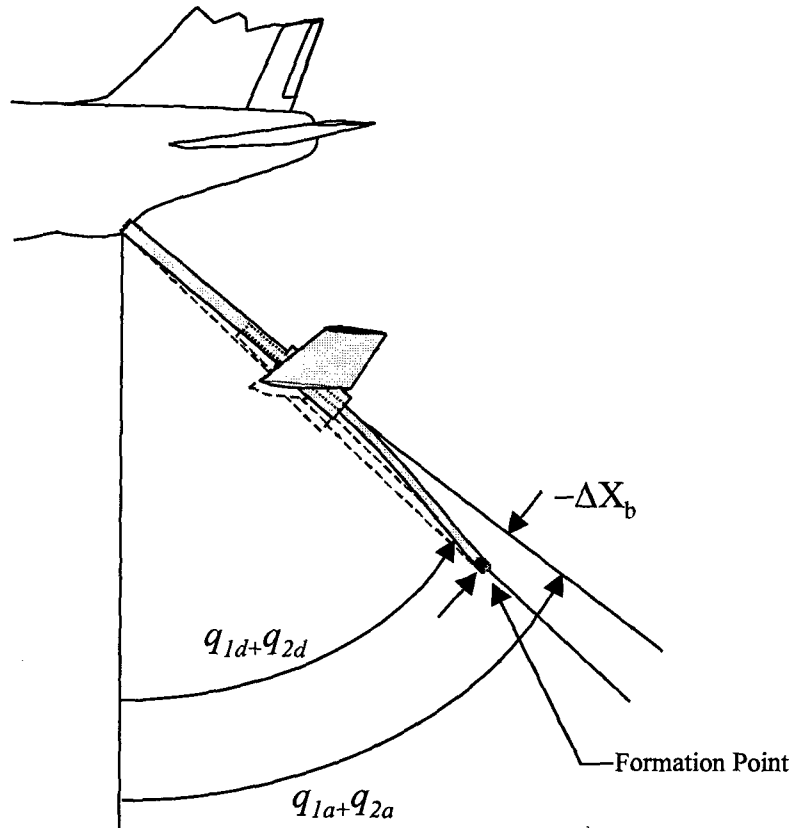


Figure 8: ΔX_b Due to Boom Bending

Joint Angle to Base Frame Position Conversion

To calculate F_{tip} , start by assuming Δx_b represents the position of the boom nozzle if it were not bound to the receiver aircraft as shown in Figure 8. Then, one of two methods is used to calculate the tip displacement. Some assumptions are made to simplify the F_{tip} calculation. First, for the longitudinal controller, only the motion in the X_b, Z_b plane is of interest. In Figure 1, frame 3 with origin O_3 , is equivalent to the boom frame with origin O_b . This convention is used throughout this document for clarity. Second, by assuming the distance between the actual angle, q_{2a} and the desired angle, q_{2d} , is small, one can use the small angle approximation to calculate the distance from the boom tip to the formation point. The equation

$$x = r d\theta \quad (3.9)$$

gives the distance in the X_b direction. Similarly, calculating the forward kinematics gives the position of the boom tip represented by q_{2a} . This cartesian position of the boom tip is transformed into to base frame coordinates using the inverse kinematic equations for rotation, R_0^3

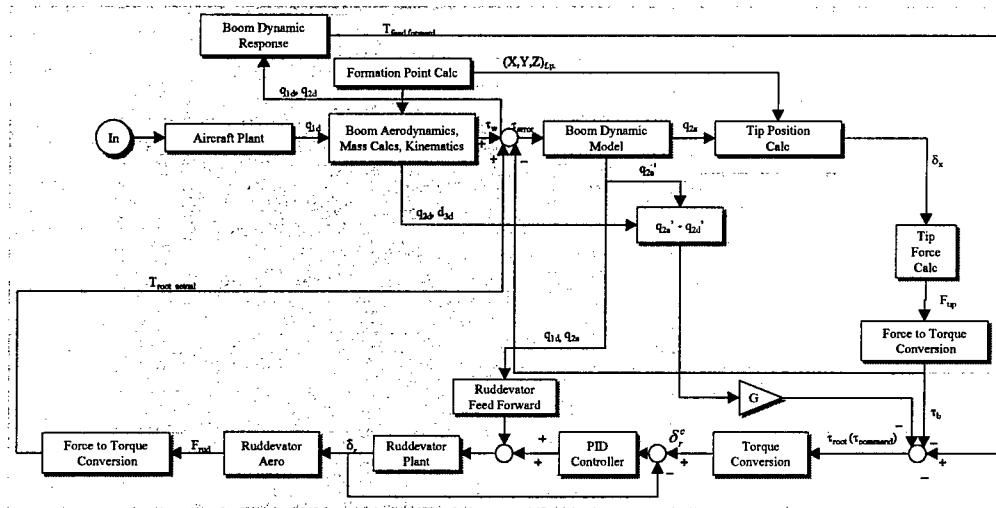


Figure 9 Bending force calculation segment

The with the tip position represented in the base frame the distance between its position and the formation point can be calculated as follows:

$$\begin{Bmatrix} \Delta X_0 \\ \Delta Y_0 \\ \Delta Z_0 \end{Bmatrix} = \begin{Bmatrix} X_{tip} - X_{FP} \\ Y_{tip} - Y_{FP} \\ 0 \end{Bmatrix} \quad (3.10)$$

These distances are assumed equivalent to the displacement as the boom bends. This vector is then transformed into the boom frame to find the component perpendicular to the boom by multiplying it with the transformation matrix R_3^0 . The perpendicular component, ΔX_b , is the fraction of the boom bending that contributes to the torque on the boom. For purposes of this controller, the displacement distance, ΔX_b , is positive when the boom is displaced downward

from the formation point. Figure 8 shows a negative ΔX_b which results from the boom being displaced *above* the formation point.

Position Error Conversion to Equivalent Force

Equation (3.12) represents the distance a cantilevered beam will bend when a load P is applied at a position ℓ from the cantilevered end.

$$\delta = \frac{P\ell^3}{3EI} \quad (3.12)$$

This equation will be used to determine the equivalent stiffness of the distal boom section due to axial nozzle loads. Rearranging equation (3.12) gives

$$\frac{P}{\delta} = \frac{3EI}{\ell^3} \quad (3.13)$$

Equation (3.13) has units of force/length. This is the same as the constant k in the spring equation

$$F = -Kdx \quad (3.14)$$

or

$$K_{spr} = \frac{P}{\delta} = \frac{3EI}{\ell^3} \quad (3.15)$$

Then, given the displacement of a beam, the force applied can be determined.

For a hollow beam the area moment of inertia is calculated using the equation

$$I_y = \pi(.25)(R_o^4 - R_i^4) \quad (3.16)$$

where R_o and R_i are the inner and outer radii of the beam. In the 1989 GSE study [1], another factor is included in (3.16) to account for the non-circular cross-section of the telescoping tube.

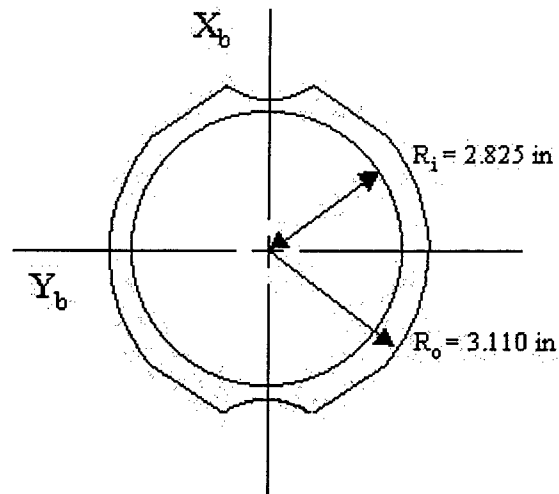


Figure 10: Telescoping Boom Cross-Section [1]

A coefficient of $-4.55in^4$, is added to equation (3.12) to correct for the radial difference in shape of the telescoping boom segment's cross section. Figure 10 shows the actual cross-section of the telescoping boom segment. To use equation (3.11) for this controller we assumed the non-telescoping upper section of the boom was much stiffer than the telescoping section. Therefore, the bending is confined to the telescoping boom segment. The length of the cantilever beam is denoted as ℓ . For this problem ℓ is equivalent to the nominal length of the telescoping boom section, 12.2 feet. The modulus of elasticity, E is 10.4×10^6 for 7075-T6 aluminum alloy. For the nominal position of the telescoping boom segment, $I = 18.9013in^4$. Therefore, $K = 191.07 lb/in$. F_{tip} can now be calculated using equation (3.14) where dx is ΔX_b , the position error in the X_b direction.

$$F_{tip} = -K(\Delta X_b) \quad (3.17)$$

The torque τ_b is found from

$$\tau_b = F_{ip}(d_3) \quad (3.18)$$

This torque τ_b is used as the initial input to τ_{root} or $\tau_{command}$ which drives the ruddervator plant. It is also used to represent the reaction force on the nozzle as the boom is subjected to bending. This signal is fed back by the wire connecting the signal τ_b to the summer upstream of the boom dynamic model. This is the wire shown departing the lower left corner of the highlighted section of Figure 9

Ruddervator Control Input Equations

As seen in Figure 11 the controller model had a summer prior to the ruddervator plant. This summer is necessary to ensure all signals being fed back are done so in such a manner that they represent the physical system of the refueling boom. To treat the ruddervator as an ideal system, this can be done by tapping the signal τ_{root} and feeding it back to the boom plant directly. This is equivalent to setting τ_{root} equal to $\tau_{root-actual}$. This procedure will be used for the analysis of the simulation model. Otherwise, τ_{root} should be passed to the ruddervator plant in order to create a δ_r to drive the ruddervator response model. The torque due to bending, τ_b is further broken into two different values to clarify ruddervator modeling. First, the torque required to counteract the boom bending will be called τ_b . It is calculated from the torque equation of (3.18). This torque drives the ruddervator operation. The output of the ruddervator plant is $\tau_{root-actual}$. The last torque being fed into the first summer is the feed-forward torque τ_{ff} . This torque derived from the feed-forward block represents the anticipated load the system will experience as motion is imparted to the boom system. It is the sum of the torque due to

boom plant dynamics and boom aerodynamic drag. The sum of the torques being added together is τ_{root} . The equation for τ_{root} is $\tau_{root} = \tau_b - \text{rate damping} + \tau_{ff}$. This force is fed forward to the next summer only after being multiplied with a transfer function that

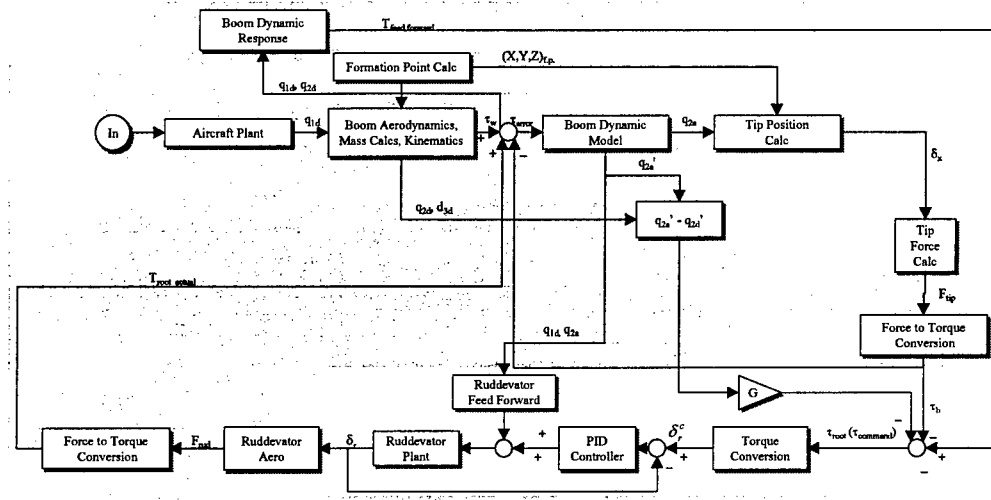


Figure 11: Ruddevator Plant Controller Segment

represents the relationship between torque on the ruddevator, τ_{rud} , and τ_{root} . To develop this transfer function several relationships must be identified. First, due to the aerodynamic load on the ruddevator, there is a net torque acting on it.

$$\tau_{rud} = I\ddot{\alpha} + k\dot{\delta} - C_{m\dot{\alpha}}\dot{\alpha} \quad (3.19)$$

where I is the moment of inertia of the ruddevators, α is the AOA and the dots represent first or second time derivatives, k is a coefficient that describes the torque on the ruddevator caused by friction on the ruddevator shaft due to ruddevator rotation, $\dot{\delta}$, and $C_{m\dot{\alpha}}$ is the coefficient of moment due to rate of change of AOA. Another equation relates the lift force on the ruddevator in the X_b direction to the AOA:

$$F_L = C_{l\alpha}\alpha qS + C_{l\dot{\alpha}}\dot{\alpha} qS \quad (3.20)$$

Where $C_{l\alpha}$ and $C_{l\dot{\alpha}}$ are the coefficient of lift with respect to AOA and the coefficient of lift with respect to rate of change in AOA. The equation for drag is

$$F_D = C_D q S \quad (3.21)$$

where

$$C_D = C_{D0} + \frac{(C_{l\alpha}\alpha)^2}{\pi A Re} \quad (3.22)$$

AR is the aspect ratio of the wing, and e is an efficiency factor. $C_{l\dot{\alpha}}$ was calculated according to the method outlined in Appendix B according to Etkin [5]. For this study, the range of AOAs commanded of the rudder are so small that the right-most quantity of equation (3.22) was eliminated from the aerodynamic calculations. The values for the coefficients in equations (3.21) and (3.22) are included in Table 6.

Table 6: Rudder Aerodynamic Properties

Coeff.	Value	Units
q	275.7	psf
S	6.01	ft ²
C_{D0}	0.006	-
AR	1.9675	-
e	0.73	-
$C_{l\dot{\alpha}}$	-24.5044	1/rad

Equation (3.23), relates the AOA to the angles q_1 , q_2 , and δ_r .

$$\alpha = -q_1 - q_2 + \delta_r + \frac{\pi}{2} \quad (3.23)$$

This relationship between the AOA, the joint angles and the rudddevator angle is shown in Figure 12. Finally, an equation for τ_{root} , the boom torque relates lift and drag to the resultant torque in the X_b direction by incorporating equation (3.23).

$$\tau_{root} = \ell_{rud} F_l \sin(q_1 + q_2) + \ell_{rud} F_d \cos(q_1 + q_2) \quad (3.24)$$

By combining equations (3.19) through (3.22), and (3.24) we can get a relationship between the torque on the boom root, and the angles α , q_1 , and q_2 . The result is

$$\tau_{root} = \ell_{rud} \sin(q_1(s) + q_2(s)) q S [C_{L\alpha} + s C_{L\dot{\alpha}}] \alpha(s) + \ell_{rud} \cos(q_1(s) + q_2(s)) q S [C_{D0} + 7.878 \alpha^2(s)] \quad (3.25)$$

This is not easily solved for $\alpha(s)$. To make an approximation to it we assume drag is not a

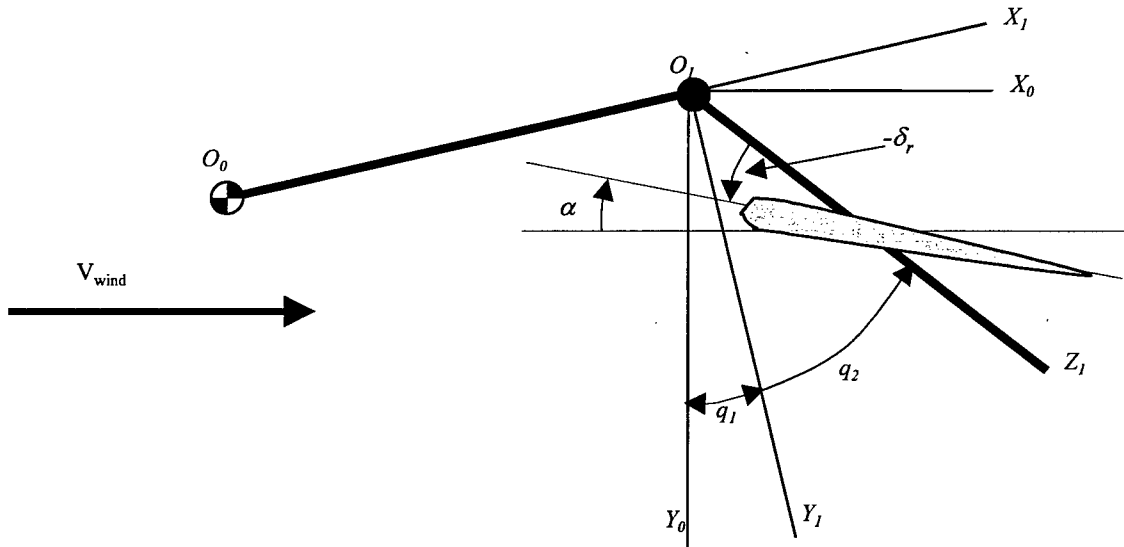


Figure 12: AOA and Ruddevator Angle Relationship

function of angle of attack. This is true for our case as the boom only traverses a small angular distance. With this assumption, equation (3.25) becomes

$$\alpha(s) = \frac{[\tau_{root}(s) - \ell_{rud} \cos(q_1(s) + q_2(s)) q S C_{D0}]}{q \ell_{rud} \sin(q_1(s) + q_2(s)) (s C_{L\dot{\alpha}} + C_{L\alpha})} \quad (3.26)$$

Finally, substituting for $\alpha(s)$ from equation (3.23) we get a relation in terms of the rudder angle commanded

$$\delta_r^c(s) = q_1(s) + q_2(s) - \frac{\pi}{2} + \frac{[\tau_{root}(s) - \ell_{rud} \cos(q_1(s) + q_2(s))qSC_{Do}]}{q\ell_{rud} \sin(q_1(s) + q_2(s))(sC_{L\dot{\alpha}} + C_{L\alpha})} \quad (3.27)$$

This equation can be thought of as a command (everything on the r.h.s. is known in the simulation). Then, position feedback control of the rudder angle can be used to deliver the commanded $\delta_r(s)$. Start by taking the time derivative of equation (3.23)

$$\dot{\alpha} = -\dot{q}_1 - \dot{q}_2 + \dot{\delta}_r \quad (3.28)$$

Then differentiating equation (3.28) again with respect to time we have

$$\ddot{\delta}_r = \ddot{\alpha} + \ddot{q}_1 + \ddot{q}_2 \quad (3.29)$$

Using equations (3.28) and (3.29) to substitute for the derivatives of AOA in equation (3.19) and then rearranging, the result is an equation relating the rudder torques to the rudder angle

$$\tau_{rud} + I(\ddot{q}_1 + \ddot{q}_2) + C(\dot{q}_1 + \dot{q}_2) = I\ddot{\delta}_r + (C_{m\dot{\alpha}} + k)\dot{\delta}_r \quad (3.30)$$

For ease of use, take the Laplace transform of (3.30) to get

$$\tau_{rud} + Is^2(q_1 + q_2) + Cs(q_1 + q_2) = [Is^2 + s(C_{m\dot{\alpha}} + k)]\delta_r(s) \quad (3.31)$$

Then solving (3.31) for $\delta_r(s)$ the equation becomes

$$\delta_r(s) = \frac{\tau_{rud} + I_{rud}s^2(q_1 + q_2) + C_{m\dot{\alpha}}s(q_1 + q_2)}{[I_{rud}s^2 + s(C_{m\dot{\alpha}} + k)]} \quad (3.32)$$

Then by making $\tau_{rud}(s)$ the required motor torque, proportional to error in δ_r , and perhaps its derivative,

$$\delta_r(s) = \frac{[K(\delta_r^c(s) - \delta_r(s)) + Ks(\delta_r^c(s) - \delta_r(s))] + I_{rud}s^2(q_1 + q_2) + C_{m\dot{\alpha}}s(q_1 + q_2)}{[I_{rud}s^2 + s(C_{m\dot{\alpha}} + k)]} \quad (3.33)$$

we have a PD controller around the actual rudder angle which is used to drive the rudder plant. Equation (3.33) describes the inputs to an equation relating δ_r^c to δ_r . With equation (3.27) as the input to equation (3.33), we have a complete relationship between a force commanded and the resulting rudder angle. The non-ideal rudder is created by including I_{rud} and $C_{m\dot{\alpha}}$ in the rudder equations along with a P.D. controller to control the rudder angle. Note that equation (3.33) includes the rudder dynamics in the numerator representing a feed forward model as well as in the denominator where it is thought of as the system plant being controlled. When the feed forward model in the numerator is omitted the rudder response is degraded even further from the ideal case. Since the feed forward term is the same as the actual rudder plant transfer function, the only error seen in this rudder plant is due to the error in the P.D. controller which arises as a result of imperfect gain selection. During the simulation process an additional transfer function representing the response of the rudder servo-actuators will be included. This function will not be added to the feed forward term. This will demonstrate further the effect of having an imperfect feed forward model of the rudder plant.

Rudder Plant

The highlighted segment of the controller in Figure 13 calculates the actual load for a given rudder angle. The first step in this block is to transform the boom velocity V_b into the rudder frame using the R_r^b transformation. Then, the angle of attack is calculated using

trigonometry and the transformed velocity vector. The calculation of the aerodynamic load for each rudder is performed in the “rudder aero” block of Figure 13. The Matlab function

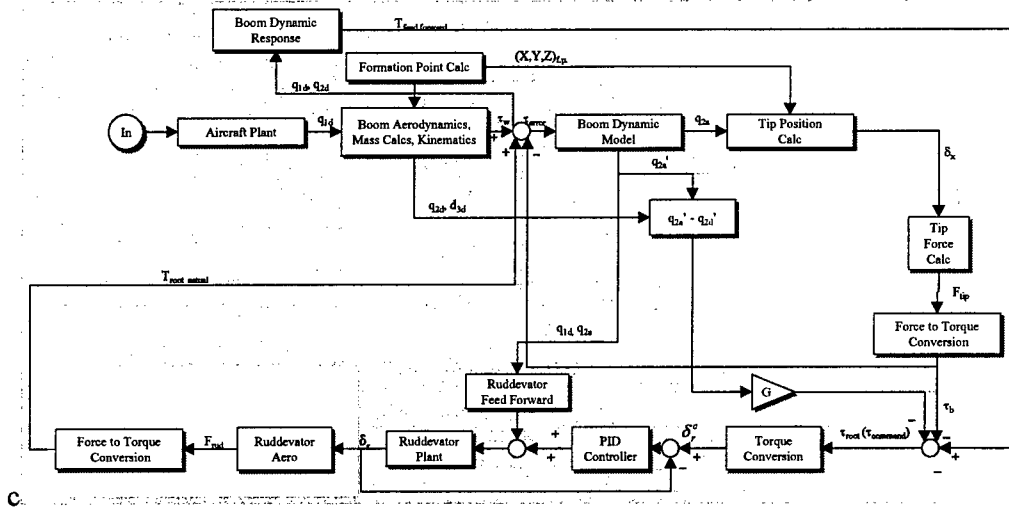


Figure 13: Ruddervator Aerodynamic Load Segment

that performs the actual calculation, “rud_aero_moment.m” is included in Appendix C. The lift and drag are computed using equations (3.14) and (3.15). Once the lift and drag are calculated for each rudder, they are decomposed into forces in the rudder frame. The result of this calculation is a force vector in the rudder frame. This vector is passed to the final block “force to torque conversion” which transforms the rudder forces to the boom coordinate system. The X_b component from each rudder is summed and multiplied by ℓ_{rud} to find $\tau_{root-actual}$. This signal is passed to the summer upstream of the boom plant. The feed-forward block highlighted in Figure 14 is used to give the controller a prediction of the torque error which will occur when the system is excited from steady state. This helps controller keep the boom tip in place by augmenting the required torque signal with an anticipatory additional force. Contained within this block is an exact duplicate of the “boom aerodynamics, mass calculations and Kinematics” block. This block calculates the wind load on the boom using the desired angle for q_2 where the similar block in front of the boom plant calculates the wind load as the boom

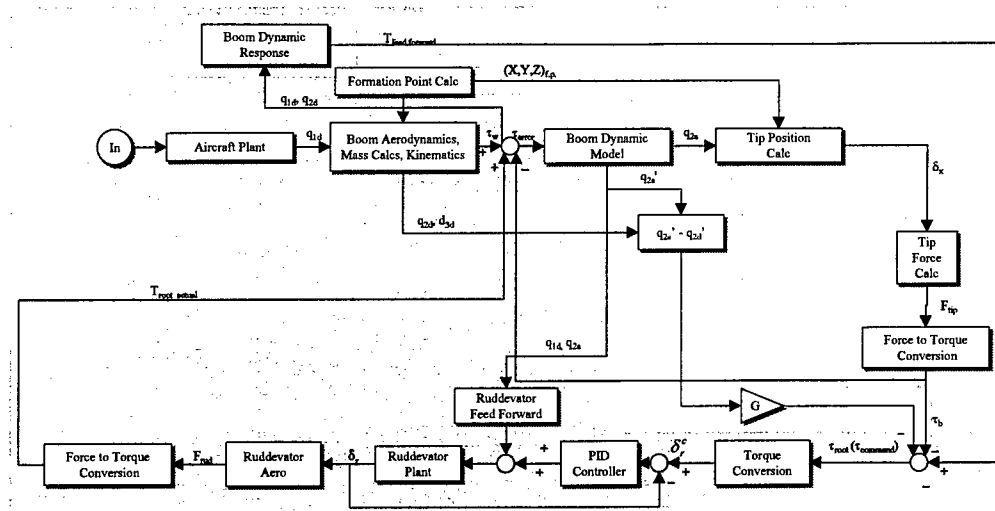


Figure 14: Feed-Forward of Boom dynamics

moves about as a result of the boom dynamics. Additionally, a copy of the boom plant is included in the feed forward block which is solved for the resultant torque due to boom dynamics and gravity effects instead of being solved to find the angular acceleration of q_2 . This torque is subtracted from the torque due to wind, also calculated in the feed forward block, to produce an error signal that is fed to the summer upstream of the boom dynamics block. The result of this feed forward term is that when the feed forward calculation contains an exact match of the boom plant equations, the error coming from the boom plant should be zero.

One additional feedback term is used to augment the rudder torque command signal. Highlighted at the bottom right corner of Figure 29, this rate error feedback is designed to speed damping of the oscillation in the controller. This signal is the difference between the derivatives of the actual and desired angles for joint two, $\Delta q_2' = q_2'_{desired} - q_2'_{actual}$. It is multiplied by a gain to make its output the same magnitude as the torque signals feeding this summer. Since the derivative of the angle q_2 leads the angle, this phase shifted signal helps damp oscillation in the system.

Modeling Limitations

While it is useful to use simulation to determine the performance of a system under development, there are limitations in the simulator's ability to represent the real system. Differences between the real system and the simulation range from a lack of sensor noise in the simulated system to the use of perfect system plants to represent the real system. For example, in this study's simulation, rate feedback is used to damp out the oscillations inherent in the uncontrolled boom. While rate feedback performs this function well, as will be shown in the following chapter, in the real system, rate information must usually be derived by taking the time derivative of position information or the integral of accelerometer information. Using either of these methods may be useful when the original signal is differentiated or integrated once, but if the same signal is then differentiated or integrated again, the signal to noise ratio becomes very small and using the resultant signal to control the real system may lead to unwanted or unplanned system performance. Also, as is the case for the KC-10[4], the sensors used to measure the forces and angles are imperfect. To solve this problem on the KC-10 uses an elaborate filter system in order to have a useful signal for controlling the boom. In a real system, the rate feedback derived from the desired and actual boom angles may produce unanticipated results. For the ideal case, the rate feedback is useful because it always provides a 90 degree phase lead to the commanded torque which always results in perfect damping of the boom's oscillatory nature. If the rate signals were noisy as in the real case, the resultant phase difference could be unreliable, leading to inaccurate or ineffective damping of the oscillatory response. Conversely, using the mathematical equivalent of time differentiation or integration in the controller simulation model may produce results that don't reflect real world operation. A complaint commonly voiced about simulation models is that designers tend to use a perfect copy of the boom plant in the feed forward signal calculations. In actuality, it is nearly impossible to

duplicate the performance of the real system to the degree it can in a designer's model. One common method of addressing this complaint is to degrade the model used in the feed forward signal so it doesn't exactly duplicate the plant response. Alternatively, the simulation model could reflect some of the plant characteristics perfectly and selectively ignore other plant characteristics. In the non-ideal rudder plant tested in chapter four, this method is employed to show that the rudder plant still performs effectively even when the feed forward terms do not include all rudder system characteristics. Specifically, the transfer function for the control surface hydraulic servo-actuators is incorporated into the rudder plant response model but is purposely left out of the feed forward terms. All of these limitations of modeling real systems can be accounted for in a simulation model with the result being an accurate portrayal of the real system.

Summary

This chapter describes the design of the controller and the equations it operates on. The controller is designed to allow systematic testing of the controller as its complexity is increased. As the different feedback signals which create τ_{root} are closed around the rudder controller, the response of the rudder to the required offsetting torques should improve. This improvement will show up as a decrease in the magnitude of the bending force on the boom as the controller's complexity increases. Issues associated with modeling real systems were addressed and some solutions have been incorporated into the model.

IV. Analysis

Simulation Approach

Simulations for this study are separated into two parts. The first group of simulations treats the ruddervator as an ideal system. This means that any commanded torque is immediately provided by the ruddervator. This is done in the simulation by bypassing the ruddervator calculation segment and passing the total commanded torque, τ_{root} , from the first summer after the boom bending gain straight to the summer preceding the boom plant block. This perfect ruddervator signal is shown as the dark arrow in Figure 15. Treating the ruddervator as an ideal

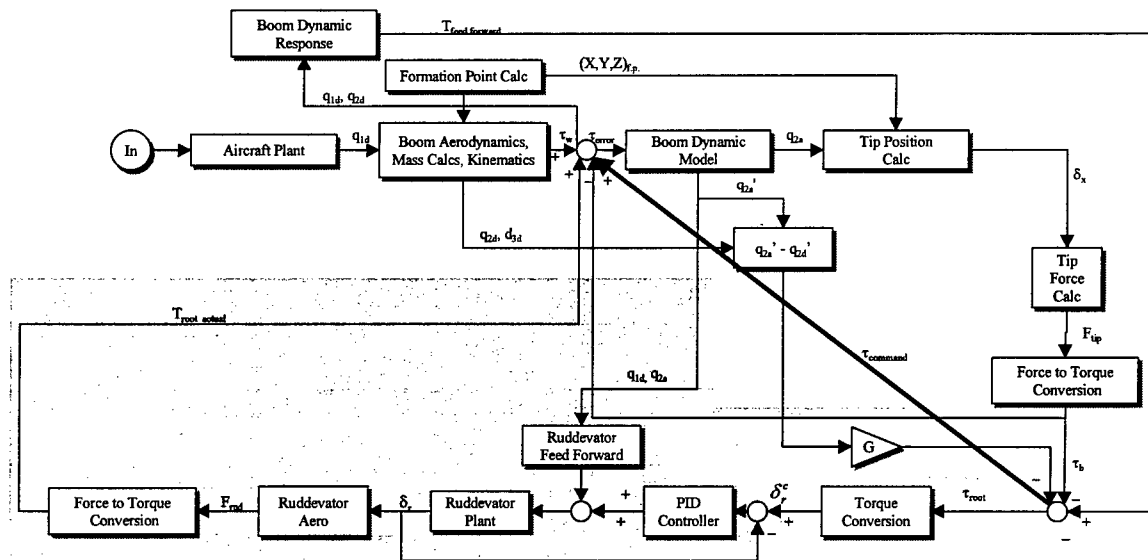


Figure 15: Direct Feedback of Commanded Torque to Boom Plant

component in this manner simplifies validation of the model. More significantly, having an ideal ruddervator aids the visualization of how the different combinations of feedback, feed forward, and their relative magnitudes affected the performance of the controller. With an ideal ruddervator, the different combinations of controller feedback signals can be evaluated without trying to separate out the effects caused by ruddervator plant error. After the alternatives are evaluated, the non-ideal ruddervator is connected and the most promising alternatives for

ruddevator control are evaluated. All simulations in this section, and those in the non-ideal ruddevator section are conducted with an elevator doublet command signal of three degrees upward deflection followed by three degrees of downward deflection unless otherwise noted. This command input results in an initial upward pitching of the aircraft as predicted by the KC-135 aircraft dynamic model. The elevator command and the resulting forced angle for q_1 are plotted together in Figure 16.

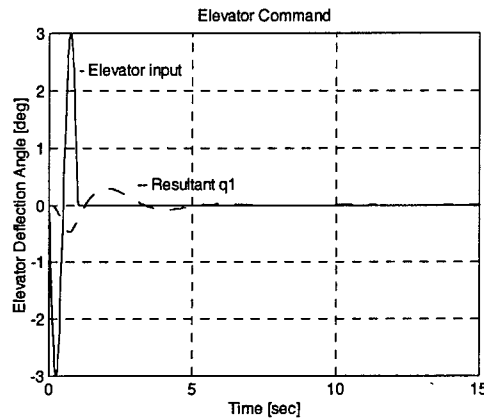


Figure 16: 3° Elevator Command and q_1 Result

Controller Performance With Ideal Ruddevator Plant

Before evaluating any of the closed loop designs the open loop system response must be evaluated for stability and design correctness. Then the controller can be closed by feeding back τ_{root} to simulate a perfect ruddevator. This design's stability will also be verified. Before any of the alternatives were tested, the actual lift capability of the boom was determined by driving the ruddevator from positive stop to negative stop and noting the maximum values obtained. The ruddevator aerodynamics block uses equations (3.20) and (3.21) to calculate the lift and drag on the ruddevator for any angle of attack. The ruddevators are capable of providing approximately 50,000 lbs of lift with the ruddevator configuration currently used, and flight

conditions as identified in Table 5. Recall, the rudddevator's in this system don't have any dihedral, therefore, in the real system the actual lift capability of the rudddevator's is slightly less.

Open Loop Response

To test the open loop response, the signal fed back, either τ_{root} from the command input, or $\tau_{root-actual}$ from the rudddevator plant is disconnected. Doing this is analogous to disabling the rudddevator or letting it weathervane just as it does on the KC-135. (Recall from chapter three that when τ_{root} or $\tau_{root-actual}$ is disconnected the rudddevator drag is omitted and hence the equilibrium is actually associated with a nonzero rudddevator AOA.) With the rudddevator model removed, the only forces acting on the boom are the aerodynamic drag on the boom, gravity, and the spring force associated with bending of the boom. In equilibrium, the torques about the root created by the gravity forces balance the boom aerodynamic force and the bending torque is zero. Any disturbances away from this equilibrium position should produce damped oscillatory motion since all forces acting on the boom act to restore the boom to the equilibrium position. To ensure the steady state is the starting point for the simulation, the angle for q_2 is established such that gravity and drag counteract each other as closely as possible. This controller is quiescent at $q_2 = 56.2^\circ$. With the steady state response verified, joint one was excited with an input from the aircraft plant. The controller is excited by transmitting the AOA from the aircraft plant, which results from the one second pitch doublet initiated by a negative three degree commanded elevator input. An initial negative elevator input results in a pitch up of the aircraft and a negative rotation of q_1 . The system's response was checked to verify the components in the open loop control system acted according to physical principals. Figure 17 and Figure 18 show the system responded as expected.

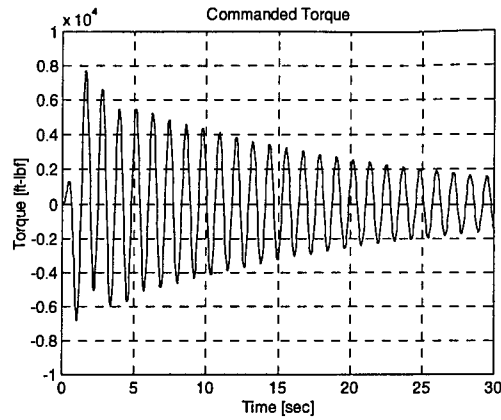


Figure 17: Open Loop Torque Error, τ_{root}

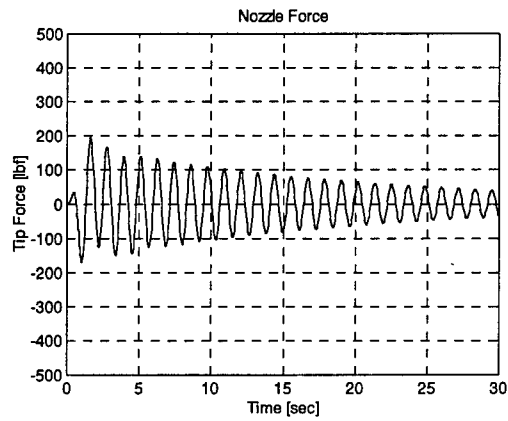


Figure 18: Open Loop Nozzle Force F_{tip}

Figure 17 is the commanded torque at the input to the ruddvator plant. At simulation start, there was no error in the boom position and therefore no torque commanded. The torque builds up as the boom root initially moves down with the aircraft. The position error is at a maximum at the end of two seconds as seen in Figure 18. This coincides with the end of the aircraft pitch doublet. After one second the system response begins to damp out. As the boom angle, q_2 , does not increase fast enough to remain at the formation point, the error results in a displacement of the nozzle downward as the aircraft pitches up. This response is proven in Figure 18. Thus, the torque represented by F_{tip} is a restoring torque as expected. Figure 19 verifies the tip position is in fact acting as expected. If the tip is below the formation point, the deviation in position, as

measured from the boom tip to the formation point, is in the positive X_b direction. This error measurement is demonstrated in Figure 8. Finally, Figure 20 and Figure 21 show the torques due

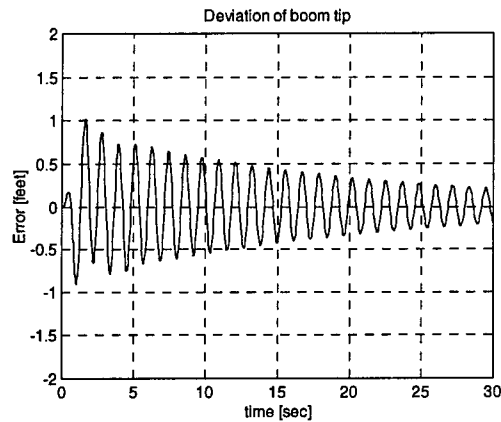


Figure 19: Open Loop Tip Deviation, Δ_{xb}

to wind and gravity respectively. As link 1 rotates clockwise initially, link 2 must rotate counter-clockwise to remain at the formation point. As this happens, the boom's angle of incidence with respect to the wind decreases resulting in decreased boom drag. Similarly, as the motion in link one occurs and the boom rotates

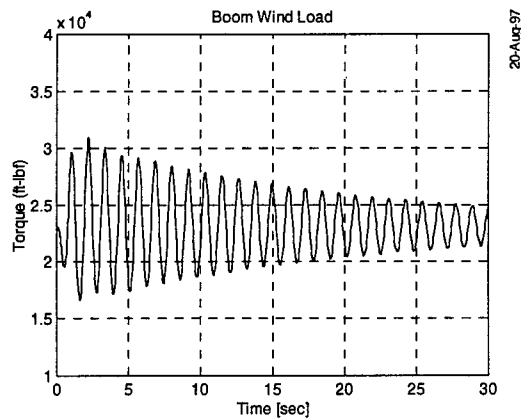


Figure 20: Open Loop Wind Load

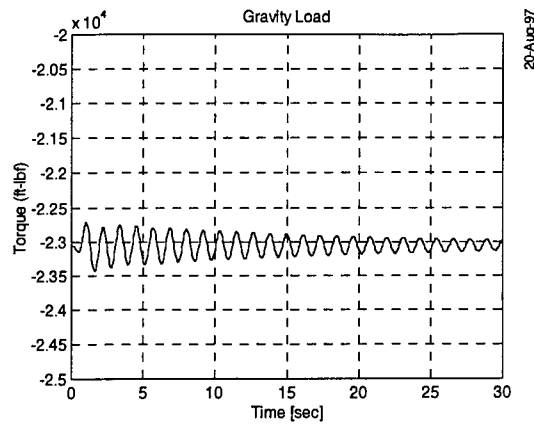


Figure 21: Open Loop Gravity Load

downward, the moment caused by gravity is also expected to decrease. With the system's performance verified and shown to be stable but oscillatory, the controller's feedback loop is then closed. Upon closing the feedback loop, the system's natural frequency should increase and its deviations from the formation point should decrease.

The open loop response is analogous to the first coupled control algorithm used on the KC-10 which was discussed in chapter two.. In our system an initial angle was selected such that the wind and gravity forces were perfectly counteracting each other. The result of this angle selection is that the boom stays motionless if the aircraft plant isn't excited by elevator deflection. For the initial boom angle the rudder has been set so it provides no net force from lift and drag to the boom. Similarly in the KC-10 open loop control algorithm, a rudder angle is selected that allows the boom to remain stationary at its current position.

Closed Loop Controller Response

Recall from chapter three, in order to simulate the ideal rudder, τ_{root} is fed back without being fed to the rudder plant. Figure 22 is the tip force or bending force in the boom

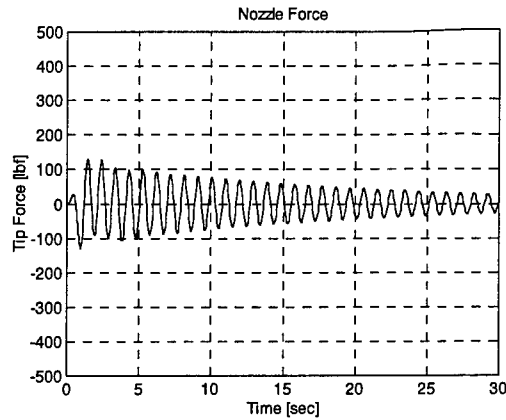


Figure 22: Closed Loop Tip Force – F_{tip}

as a result of tracking errors. The peak tip force is 125 lbs compared to 200 lbs in Figure 18, the open loop case. Additionally, the frequency of the oscillation has increased slightly. In the open loop simulation of Figure 18, the oscillation frequency was approximately 0.9 Hz. The frequency increased to approximately 1.2 Hz for the closed loop simulation. System performance will ultimately be driven by the ruddvator’s ability to respond at the required .

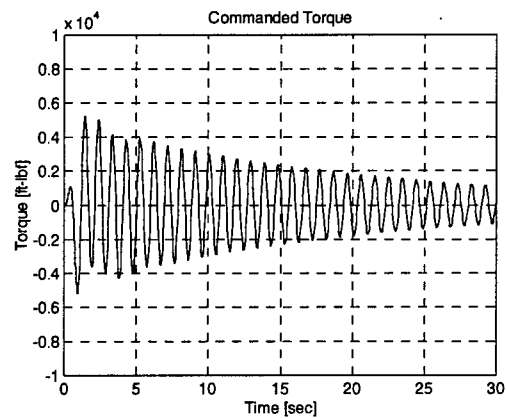


Figure 23: Closed Loop Torque Command, τ_{root}

frequency. Figure 22 shows that the closed loop controller does decrease the bending in the boom. The commanded torque has decreased from 7900 ft-lbs in the open loop case of Figure

17, to about 5200 ft-lbs in the closed loop case of Figure 23. This is the expected result when the control loop is closed.

Closed Loop Response With Increased Gain on Tip Force Feedback

The results of the open loop and closed loop simulations demonstrate that the model is well behaved but still could use improvement. Next, the results from different improvement methods are discussed. The first alternative to improve the system was to increase the gain on the F_{tip} force. This would drive the ruddvator to provide greater forces with a shorter period. The result should be an improvement in the tracking of the formation point. The gain used in this simulation was $G = 10$. There are two limitations experienced if this method is used. These limitations are shown in Figure 24 and Figure 25. In Figure 24 the tip forces have decreased by approximately half of the previous value. The drawback is that the frequency of the system has increased dramatically. Previously, the frequency was about 1.2 Hz. Now the frequency has risen to approximately 2.7 Hz. Also note in Figure 25, the improvement in F_{tip} is obtained at the cost of increased ruddvator operation frequency which will result in higher natural frequency,

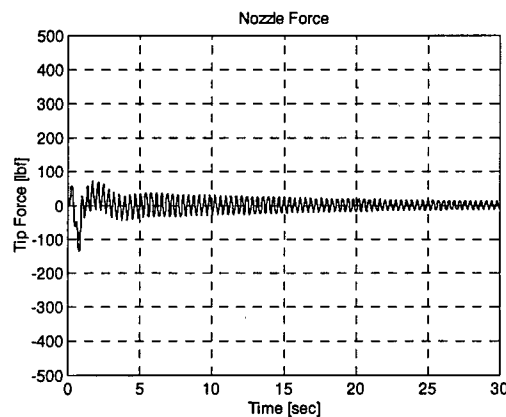


Figure 24: C.L. Nozzle Force, F_{tip}

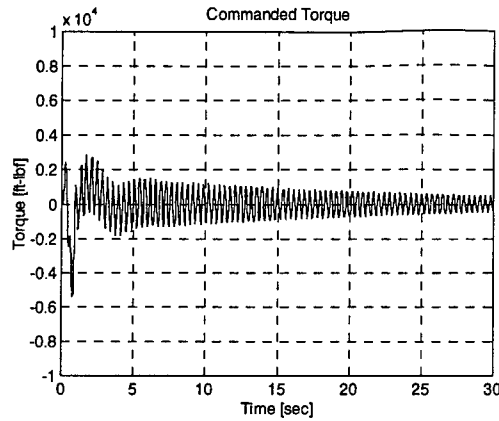


Figure 25: C.L. Commanded Torque, τ_{root}

and possible excitation of additional structural vibration modes. While the torque commanded (Figure 25) in this simulation is achievable, the frequency of the oscillations would likely introduce unwanted vibration and possibly lead to premature failure of the boom or the ruddervators. Figure 25 appears at first to be a desirable result, but the cost to the ruddervator for this decreased τ_{root} is increased operating frequency. Therefore, increasing the gain on F_{tip} is not a viable alternative. The next alternative considered is the use of a feed forward signal.

Closed Loop Response With Feed Forward

As discussed in chapter three, using a feed forward signal should help the control system by providing the ruddervator controller with a prediction of the torque required to drive the system during a known disturbance in order to produce no tip motion. The feed forward signal is the difference between the expected wind load and the load due to system inertia and gravity. For this run the gain on F_{tip} was set to unity. The feed forward torque, τ_{ff} , is always fed back with unity gain. The resulting tip force in Figure 26 for the doublet input indicates the addition of the feed forward signal does improve the system's performance by anticipating the errors in commanded torque which will occur as a result of boom dynamics. Where the nozzle force was originally 125 lbs for the basic controller the addition of feed forward has cut the nozzle force to

approximately 50 lbs. Additionally, using feed forward improves system performance without increasing the system response frequency. This improvement is the result of the controller commanding larger loads from the ruddervators in anticipation of deviations which will occur as

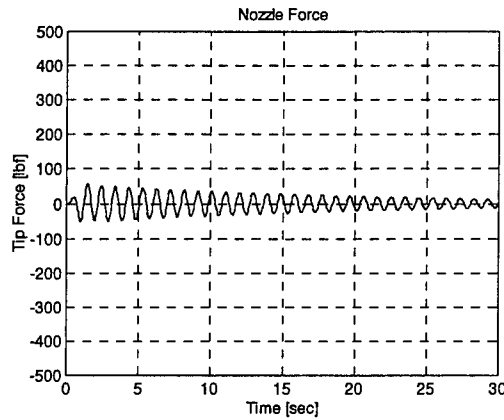


Figure 26: Nozzle Force, τ_{ff} add

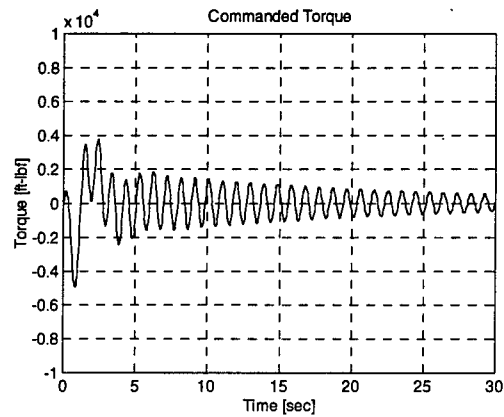


Figure 27: Commanded Torque, τ_{ff} added

the boom's inertia resists motion. The improvement in tip force is moderate but definite. The initial commanded torque hasn't dropped significantly but the magnitude of the overshoot has decreased from 5500 to about 3750 ft-lbs. Feed forward is clearly useful for handling known disturbances such as the pitch doublet from the aircraft plant. However, τ_{ff} can only be used when there is a *measurable* deviation to normal operation. If the disturbance is similar to a wind

gust that affects the receiver position, and the feed forward plant can't be informed of the disturbance, feed forward will fail to cancel out the loads effectively. The effectiveness of feed forward is also reduced when the feed forward model is not precise. An alternative that helps in cases of unknown external forces is the use of a rate feedback signal.

Closed Loop Response With Rate Feedback

Figure 28 and Figure 29 demonstrate how effective the use of rate feedback is. For this project the rate signal used was the difference in the rates of q_2 *actual* and q_2 *desired*. This signal when properly gained provides a lead signal which damps out system overshoot. The only drawback to using rate feedback arises when a high fidelity response is desired to an aggressive input signal. Because it is a damper, it has the detrimental effect of preventing desirable motions

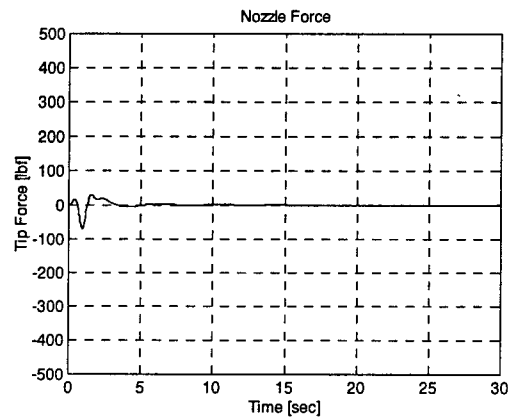


Figure 28: Tip Force, F_{tip} and Rate Feedbk.

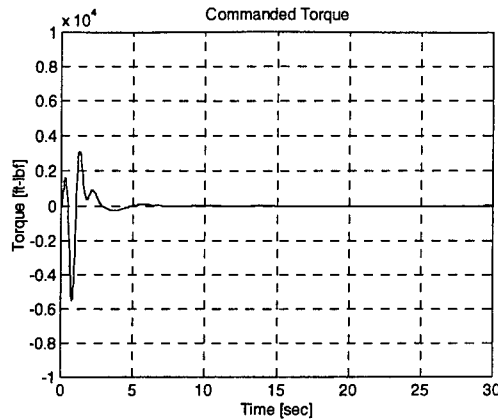


Figure 29: τ_{root} and rate feedback

as well as those that are undesirable. The goal of using rate feedback is to determine a gain value that provides good settling times but doesn't overdamp the system. However, since we are trying to damp out system transients, the gain must be sufficiently high to cause little error in boom tip position. Care must be taken to ensure the resultant τ_{Root} is an achievable magnitude for the rudder system. When using simulations, this isn't readily evident unless one observes the magnitude of τ_{root} . The torque commanded from the rate feedback had no effect on the resultant τ_{Root} until the gain was approximately 50,000. At this magnitude, the torque command from the rate feedback was of the same order of magnitude as the other input forces. The result shown in Figure 28 and Figure 29 was achieved using a gain of 100,000. Though it has done a good job of damping out the oscillation, τ_{root} has increased in comparison to the no damping case. Where it was about 5500 ft-lbs with no damping, τ_{root} has increased in magnitude to roughly 5750 ft-lbs. The trend is for the maximum τ_{root} to increase as the damping gain is increased.

Closed Loop Response with Rate Feedback. Gain = 1,000,000

As expected, the magnitude of τ_{root} increased as the gain was increased. The gain on the damping term for this simulation was 1,000,000. Figure 30 and Figure 31 show the result.

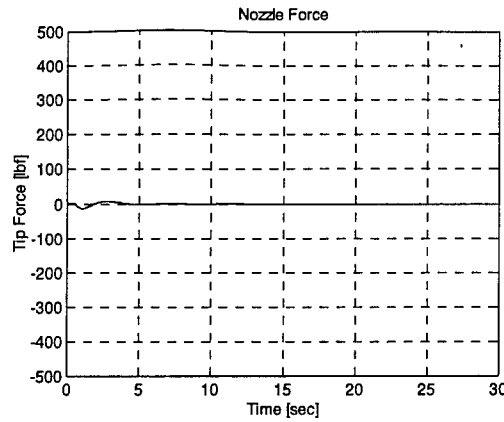


Figure 30: Rate Feedback Nozzle Force Gain=1M

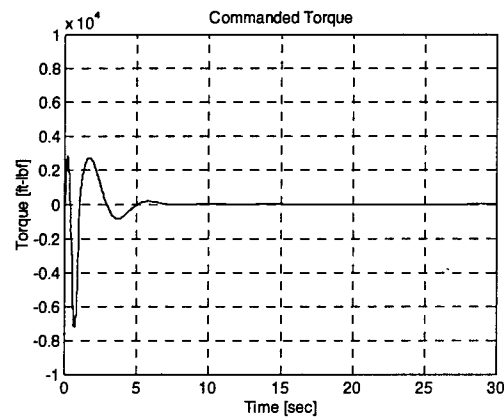


Figure 31: Torque Command, Rate Feedback

The nozzle force seems to be very desirable but the commanded torque has risen even further to roughly 7000 ft-lbs. While it damps oscillations very well, τ_{root} is now increasing the demand on the rudder. Even though τ_{root} is increasing, it is still well within the limits of the rudder's capabilities. This turns out to be a very desirable outcome. It is clear that some combination of τ_{ff} and rate feedback is desirable in order to minimize the initial τ_{root} due to tracking error and to minimize the system oscillation. As expected, as the controller complexity increases, the output response is better.

Closed Loop Response with Feed Forward and Rate Feedback

By combining rate feedback and feed forward, the resulting controller responds to predicted inputs while being relatively well damped in response to unmeasured system disturbances.

Figure 32 and Figure 33 demonstrate the traits of both types of feedback systems. While the result is oscillatory, it is reasonably damped. The damping gain for this case was 100,000. The nozzle force shown in Figure 32 isn't smaller than that of Figure 30, but the settling time is shorter. Since the goal of our controller design was to minimize the nozzle forces in the short period which result from nozzle tracking errors, the decrease in oscillation is desirable. Also, the magnitude of τ_{root} has decreased. This is due to the effectiveness of the feed forward term. As it anticipates the torque needed, the controller reacts sooner to tracking errors. This results in smaller overshoots during the forced motion segment of the simulation.

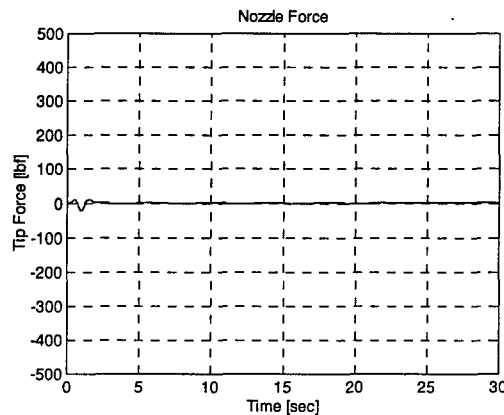


Figure 32: Nozzle Force, τ_{ff} , and Rate Fdbk

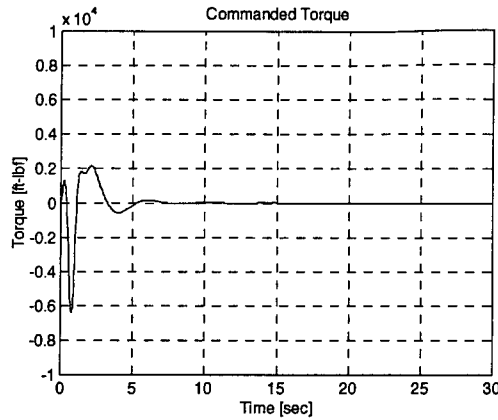


Figure 33: Torque Command, τ_{ff} and Rate Fbk.

To validate the trend in performance, the simulation was run again with a damping feedback of 1,000,000. The results are shown in Figure 34 and Figure 35.

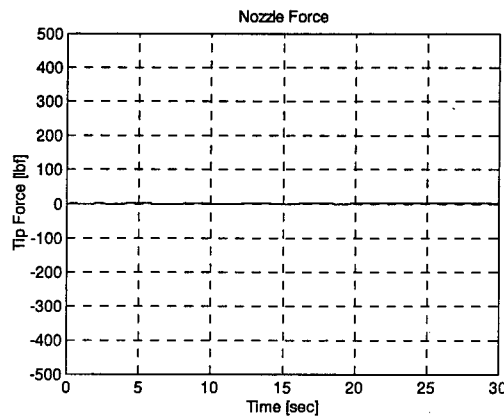


Figure 34: N.F., τ_{ff} and Rate Feedback $G = 1M$

The results of this run demonstrate the benefit of adding damping. The nozzle forces are negligible and the commanded torque hasn't changed in magnitude from the previous run with the gain set to 100,000. Of all the simulations, this combination of rate feedback and τ_{ff} promises the best performance for controlling the non-ideal rudder system. The following sections will discuss the performance of the controller when the rudder is non-ideal.

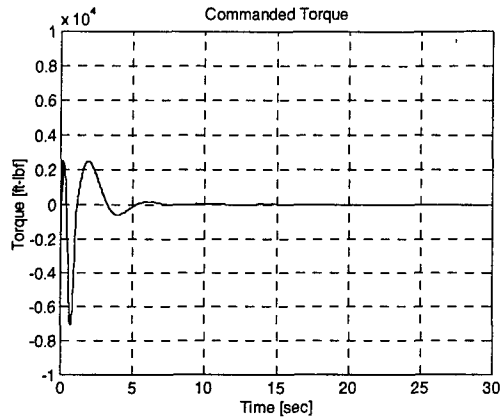


Figure 35 Torque Command for $G = 1M$

Closed Loop Controller With Non-Ideal Ruddevator Plant.

To simulate the real ruddevator, the direct feedback of the commanded torque, τ_{root} is disabled. In its place a model of the ruddevator plant which is commanded using a calculated ruddevator angle command, δ_r^c , derived from τ_{root} . δ_r^c is computed using the method outlined in chapter three using τ_{root} as the input command. The commanded ruddevator angle, δ_r^c is passed to the ruddevator plant which calculates the response to the command and outputs δ_r . Feed forward of the ruddevator characteristics provides the same benefits for the ruddevator as it did for the boom. It provides an additional signal which anticipates the magnitude of the error in the ruddevator angle which will occur. The signal, δ_r , is passed to the next module which calculates the actual aerodynamics. The equations used in this section are the same as those used to derive δ_r^c . This time however, the equations are solved in the forward direction to get $\tau_{root-actual}$. The plant is called a real plant because the inertia of the ruddevator, I_{rud} , $C_{m\dot{\alpha}}$, and hydraulic actuator lag are incorporated into the ruddevator plant. Additionally, the actual ruddevator angle, δ_r , is used as feedback to δ_r^c through a proportional, integral, derivative, (PID) controller. Regardless of the fidelity with which this PID controller is tuned, there will be error in the output

signal. This error will be propagated to the rudder aerodynamics module. To demonstrate the effect of this error, consider the following case. The boom is currently at rest. Its resting angle, q_2 is 0.981334 radians. Assume a δ_r^c of 0.5911 is commanded. Then using the relationship between AOA and rudder angle from chapter three, $\alpha = -(q_1+q_2) + \delta_r^c + \pi/2$, α will have a value of -0.0016 radians. Now, if an error in δ_r^c of just 0.0005 radians occurs as the PID works to match δ_r to δ_r^c , the result is an α of 0.0021 radians. This represents a change in α of 31.3 percent. So with a PID controller designed to work for one set of initial conditions there are going to be errors if the rudder system operates with a different set of initial conditions. This error in the PID controller is going to cause errors in the resulting AOA. Thus, this system represents a real, non-ideal rudder control system. Figure 36 is a sample taken from a plot where the feed forward and rate feedback to the boom plant are set to zero gain and the proportional controller on the feedback of δ_r is set to 10,000. Note the error between δ_r and δ_r^c . Though the external signals have been shut off, the rudder still has feed forward augmenting the commanded rudder angle. The hydraulic damping term is not included in any of the following plots except as noted below. Even with the gain tuned, there is error in the signal sent to the rudder. This is similar to the response in a real system. The signal produced by the controller is not perfect, some error is introduced into the output signal. The error in the signals appears as a phase shift where the output signal lags the input signal. Figure 37 shows the difference in the values of τ_{root} and $\tau_{root-actual}$. The error is more difficult to see because of the magnitudes of each signal.

To minimize this error, the gain on the proportional controller can be tuned to perform better. However, when the gain on the controller is tuned to accommodate one operating condition, its performance degrades quickly when the controller operates off this set point. To

demonstrate, the gain on the proportional controller was raised to 30,000. the result is shown in Figure 38 and Figure 39. The error in the signal is very small but still non-zero.

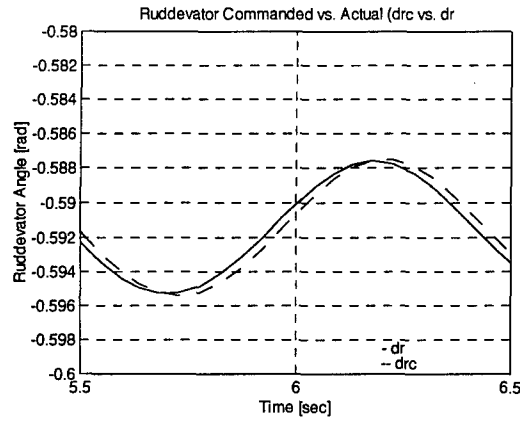


Figure 36: δ_r , δ_r^c Error, P controller gain = 10,000

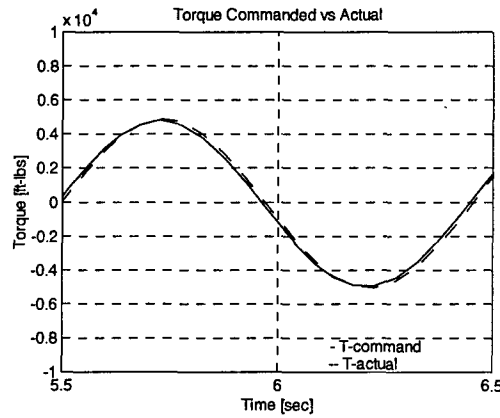


Figure 37: τ_{root} , $\tau_{root-actual}$ Error, P controller gain = 10,000

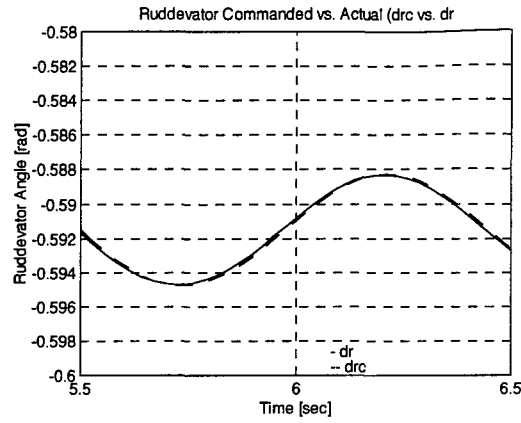


Figure 38: δ_r , δ_r^c Error, P controller gain = 30,000

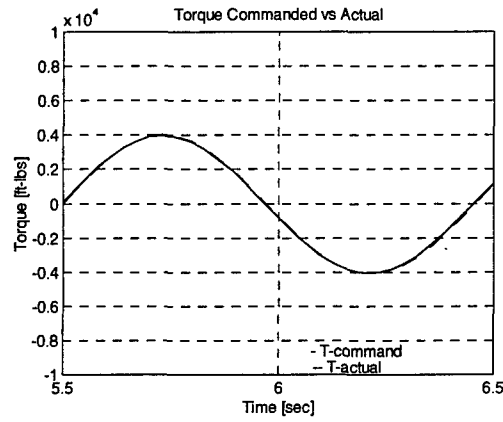


Figure 39: τ_{root} , $\tau_{root-actual}$ Error, P controller gain = 30,000

For this simulation run the elevator command used to excite the aircraft plant was only 3 degrees deflection. The error should increase if a different elevator command excites the aircraft plant.

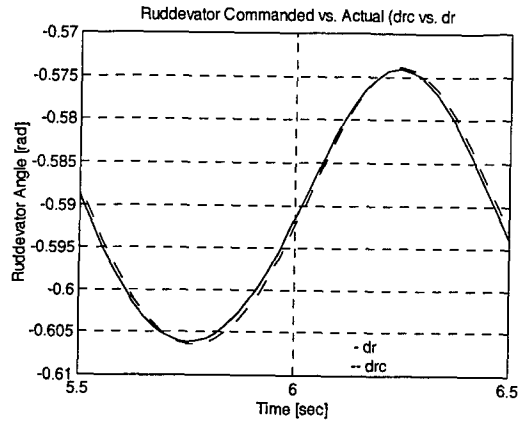


Figure 40: δ_r , δ_r^c Error, P gain = 30K, Elev. input = 15°

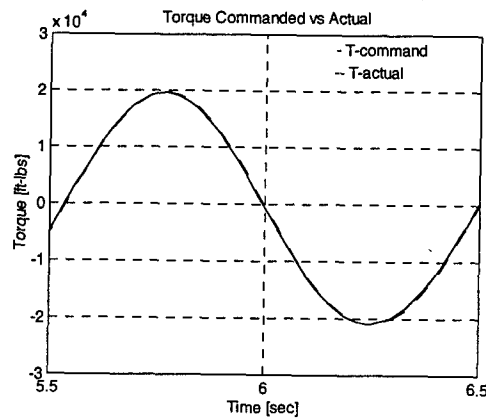


Figure 41: τ_{root} , $\tau_{root-actual}$ Error, P gain = 30,000, Elevator input = 15°

Figure 40 and Figure 41 verify this characteristic. The error in the phase of both δ_r and $\tau_{root-actual}$ is larger when excited by the larger 15 degree elevator input. This characteristic of controller design forces the designer to de-tune the gains in order to produce desirable performance over a large operating regime. The use of a non optimal gain for the operating conditions being simulated results in non-ideal performance of the ruddevator control system. All of the following simulations were run with the proportional controller gain on the ruddevator set equal to 10,000.

This section of chapter four will discuss the performance of each controller alternative, beginning with the least complex alternative. The first simulation is a verification run to ensure the model is stable with the non-ideal rudder plant. The following runs will examine feed forward, rate feedback, and the combination of both of these design options. There is one additional factor limiting the performance of the real rudder. In the case of the ideal plant it is assumed the rudder can supply any amount of force required. This is not true for the non-ideal plant. Here one must be aware that the rudder is only allowed a certain range of motion. This means that it cannot provide unlimited torque as was assumed in the ideal plant simulations. The rudder on the KC-135 currently has deflection limits in both the positive and negative directions of 0.2433 radians. As discussed earlier, if a specific commanded torque is not achievable by the rudders, the graph will show a τ_{root} signal where the peaks of the signal are chopped as a result of the rudder reaching the stop in either the positive or negative δ_r direction.

Closed Loop Performance With Non-Ideal Rudder Plant

It was expected that the non-ideal plant would tend to limit the responsiveness of the rudder and therefore cause the magnitude of the oscillation overshoots to increase. This would tend to drive the controller closer to instability. The nozzle force of Figure 42 is the same as that of the ideal rudder controller case, Figure 22. The maximum nozzle force is 125 lbs. The overshoot on Figure 43 is still approximately 5500 ft-lbs. The main difference between this run for the non-ideal case and the similar run for the ideal case, Figure 23, is that the signal doesn't decay as it did in the ideal case. Rather, the phase lag in the output signal results in a very small growth in the system oscillation. Increasing the gain in the PD controller may improve this response. The results of increased PD controller gains will be shown later. This unstable, oscillatory characteristic of the non-ideal rudder plant makes it a good candidate

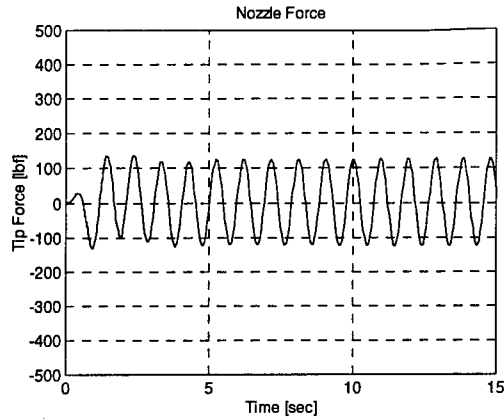


Figure 42: Nozzle Force of Non-Ideal Controller

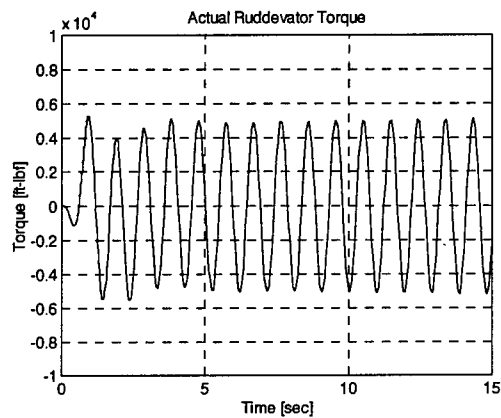


Figure 43: τ_{root} With Non-Ideal Ruddevator

for rate feedback. No other change has occurred in the response of the plain non-ideal boom controller compared with its ideal counterpart except for a lack of decay in the oscillation with time.

The ALAS boom controller architecture for the KC-10 is similar to the configuration used in this simulation run. This architecture uses the force at the boom tip as the signal to drive the ruddevators analogous to the ALAS using boom midspan bending stress to drive the ruddevators. In this simulation case, the goal is to zero out the error in the nozzle force. It will

be shown that one can improve on the performance of the KC-10's ALAS controller through the use of feed forward and rate feedback.

Non-Ideal Ruddevator Controller With Feed Forward

This simulation was performed with the feed forward gain set to unity. One expects the system response to decrease with the use of feed forward because of its ability to anticipate the required torque and augment the commanded torque accordingly. In a perfect system, the feed forward should be able to eliminate all error in the system response. The simulations using the ideal ruddevator plant didn't show a perfect response. The reason for this error was investigated after all feed forward simulations indicated the same type of error in feed forward occurred. A discussion of the likely reason for this error and a possible solution will be discussed at the end of this chapter. The non-ideal ruddevator system didn't show perfect performance with feed forward either. However, as shown in Figure 44, it did succeed in decreasing the magnitude of the boom bending because of its anticipatory nature. Where F_{tip} was 125 lbs in the basic controller design of Figure 42, the nozzle force was only 50 lbs for the feed forward

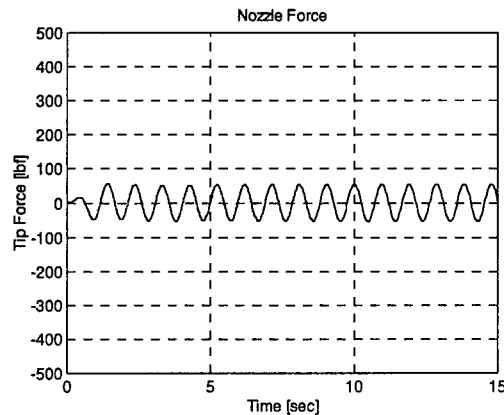


Figure 44: Nozzle Force With Feed Forward

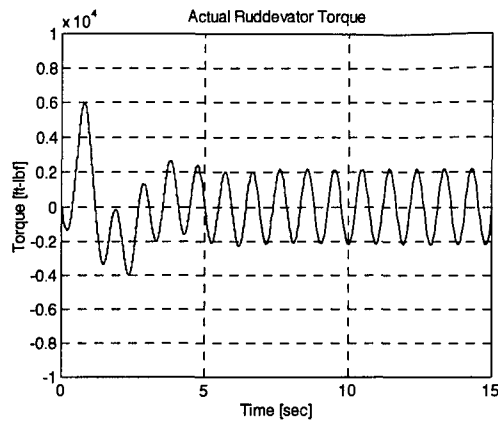


Figure 45: τ_{root} With Feed Forward

case. In the basic non-ideal controller, τ_{root} averages 5750 ft-lbs compared with an average torque of 2000 ft-lbs (Figure 45) when feed forward is added. The spike to 6000 ft-lbs seen in the first second of operation is the result of the feed forward signal augmenting the force which would normally be commanded in the basic controller. The basic controller had no similar initial burst of torquing. This indicates that the feed forward is helping the controller anticipate the required torques.

Non-Ideal Ruddevator Controller With Rate Feedback

As the gain on the rate feedback increased, the system response improved for the ideal ruddevator case. Additionally testing showed that if the gain were increased to one million the resulting nozzle force for the ideal controller was a flat line. Using a gain of one million caused the non-ideal plant to go unstable. Additional simulations showed that a gain of 400,000 was near the maximum magnitude gain which could be used and still maintain a stable system.

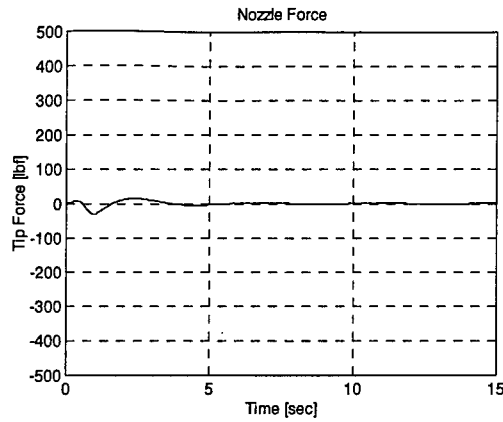


Figure 46: Nozzle Force With Rate Feedback, $G=400,000$

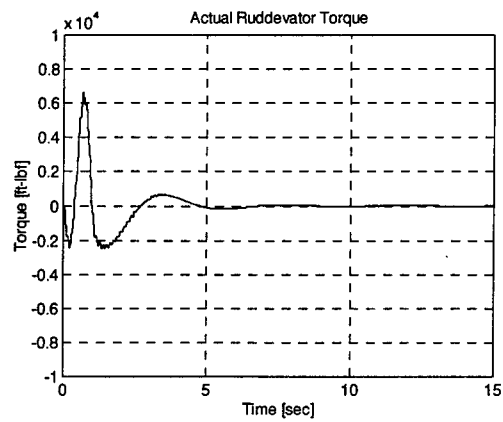


Figure 47: τ_{root} With Rate Feedback, $G=400,000$

The nozzle force in Figure 46 appears to be satisfactory but $\tau_{root-actual}$ of Figure 47 is larger than the response of the basic non-ideal controller. It has increased from approximately 5750 ft-lbs to nearly 7000 ft-lbs. While it is desirable to minimize the torques commanded of the rudder, the true purpose of this controller is to minimize the nozzle forces. Figure 46 is a definite improvement over the basic plant response of Figure 42. The nozzle force dropped from 125 lbs to only 25 lbs at the boom's maximum transient. This is a 125% improvement in system performance.

As shown the simulations for the feed forward and rate feedback are excellent tools for modifying the response of the non-ideal closed loop controller. Used in combination, the result is impressive.

Non-Ideal Controller With Rate Feedback and τ_{ff}

The expected result of combining feed forward and rate feedback is a system response with very small excursions during the time in which root motion occurs, with a flat line nozzle force response for the boom after the aircraft returns to a quiescent state. Figure 48 shows this is just what happened. There is a slight error in the nozzle force while the aircraft is moving about, but once the aircraft is quiescent the nozzle forces completely disappear. This is the controller

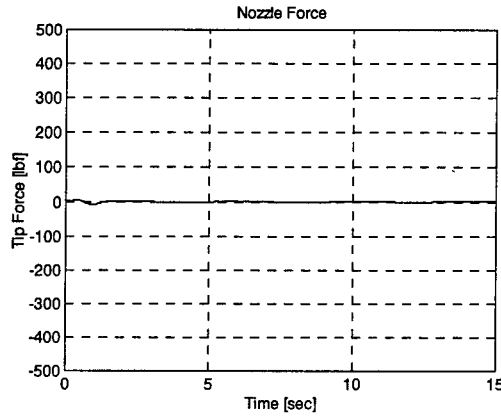


Figure 48: Nozzle Force with τ_{ff} and Rate Feedback, $G=400,000$

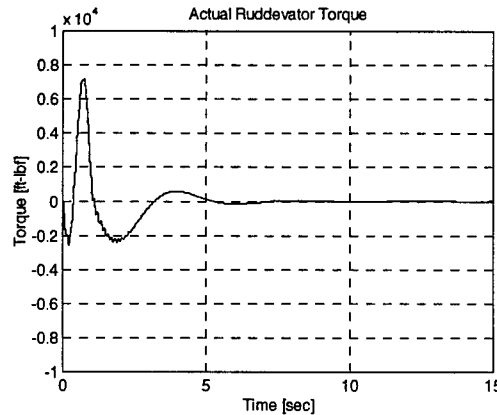


Figure 49: τ_{root} With τ_{ff} and Rate Feedback, $G=400,000$

which would best be incorporated onto the KC-135 for longitudinal automatic control. Note however, $\tau_{root-actual}$ increased even more than for the rate feedback only case. Figure 49 shows $\tau_{root-actual}$ increased from 5750 to about 6500 ft-lbs. The rate feedback is working extremely hard to damp the nozzle oscillations. While this occurs, the feed forward term is augmenting the signal to counter the lag in torque requirements occurring at the boom plant. Regardless, this required torque is still an order of magnitude less than the maximum available torque; roughly 50,000 ft-lbs. This controller, though more complex than the other alternatives, would effectively eliminate all nozzle forces when an input q_1 of the size of Figure 16 is used. It is arguable that the aircraft response this controller was tested against is entirely too benign to be a valid demonstration of nozzle force cancellation for the KC-135 refueling boom. In consideration of this viewpoint, the next section of this chapter introduces variations to the flight conditions of both the tanker and the refueled aircraft.

Operating Condition Variations

Once the controller's configuration was stable, the final step was to test the selected controller against other variations in the operating environment.

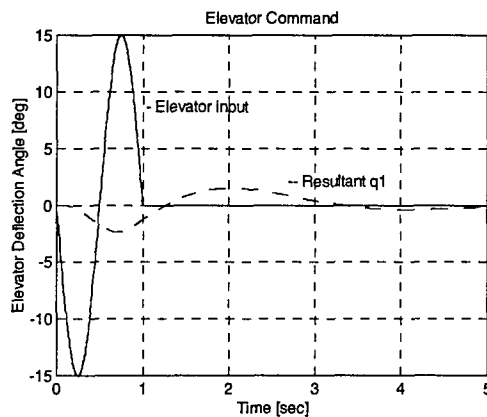


Figure 50: 15° Elevator Command and q_1 Result

Figure 50 is the commanded deflection of the elevator surface for the KC-135. The response is shown in the same plot. This is a very aggressive input for a tanker when it's refueling. The response of the boom controller is shown in Figure 51 and Figure 52. The Nozzle Force remained low, and the value of $\tau_{root-actual}$ is still within the capabilities of the rudder. At the beginning of this section the non-ideal plant was discussed. In that discussion the effect of inaccuracies in reproduction of the commanded signals was identified. This effect is further amplified when the model input is increased in magnitude. Additionally, if the feed forward

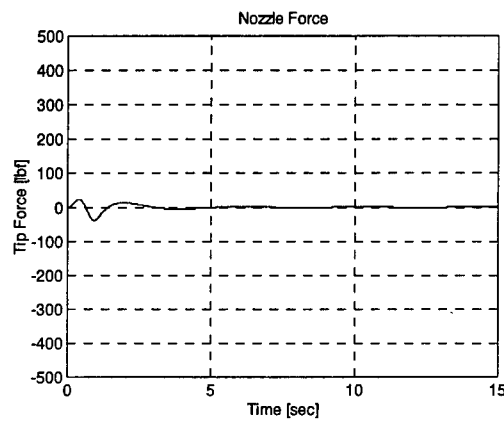


Figure 51: Nozzle Force Resulting From Large Magnitude Aircraft Motion

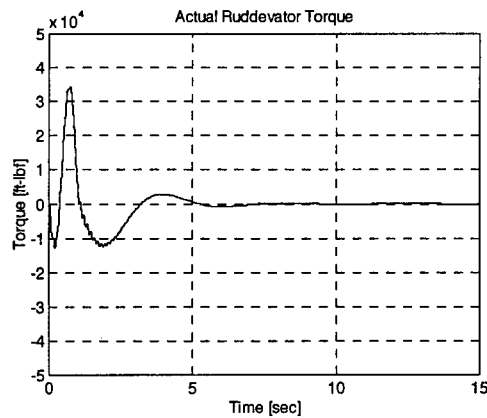


Figure 52: Torque Produced to Neutralize Aircraft Transient

term used to augment the rudder command does not exactly match the physical system it is modeling, the result is an increase in the error between the commanded response and the real result. In this next case, such a condition occurs. In the rudder plant a transfer function representing the hydraulic servo-actuators was inserted just after the PD controller of Figure 71 in appendix D. The effect was to increase the phase error in the output response. When compared with Figure 38, the error in the

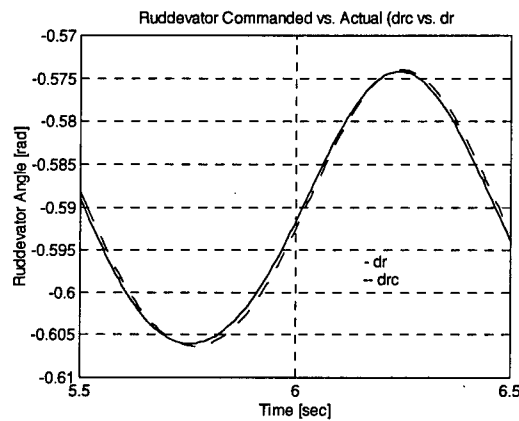


Figure 53: Rudder Error, P gain = 30K, Elev. comm = 15°, w/ hyd. T.F.

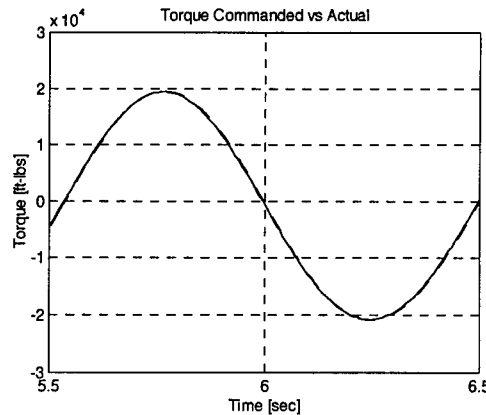


Figure 54: Torque Error, P gain = 30K, Elev comm = 15°, w/ Hyd. T.F.

rudder response, δ_r , has increased (Figure 53). Similarly, the error in the commanded torque has increased also (Figure 54). For the simulation run shown in Figure 53 and Figure 54, the

feed forward and the rate feedback were set to zero, and the rudder proportional controller gain was set to 30,000. With a hydraulic transfer function in the rudder plant of the form $500 / (s + 500)$, and the larger elevator input driving the model, the response was different but still controllable. The response of the controller with this additional lag and the larger elevator command is shown in Figure 55 and Figure 56. The nozzle force is greater than that seen in Figure 51 with no servo-actuator in the rudder plant, but the force is still well below the magnitudes seen in the basic non-ideal controller. These figures demonstrate the robustness of this controller. To make the controller remain stable in this condition, the gain on the rate feedback was decreased to 300,000 versus the original 400,000 of the case above.

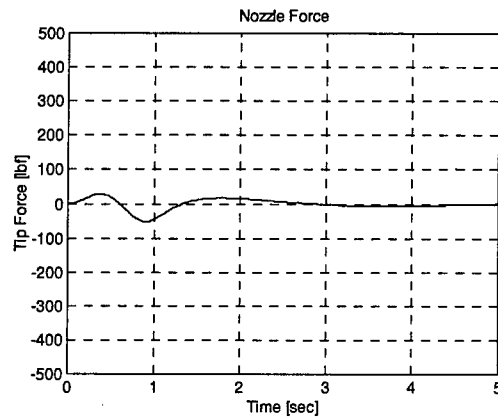


Figure 55: Nozzle Force With Large Elevator Input and Servo T.F

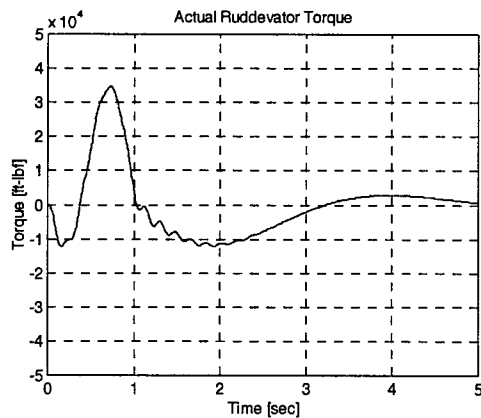


Figure 56: $\tau_{root-actual}$ to Minimize Nozzle Forces

Fine tuning this number would further flatten the nozzle force curve. The magnitude of $\tau_{root-actual}$ has increased dramatically for this case but is still within the limits of the rudder. Note the oscillatory nature of the torque $\tau_{root-actual}$. This high frequency torque output is the result of high rate motion of the rudder. A rate feedback gain should be chosen that minimizes this oscillation. To summarize the performance of the controller under conditions of large aircraft motion, the response is similar to that seen for the small amplitude aircraft motion, but, the magnitude of $\tau_{root-actual}$ grew an order of magnitude though still being within rudder performance limits. Additionally, the error between τ_{root} and the resultant $\tau_{root-actual}$ increased as a result of the de-tuning necessary to ensure the controller is stable for all of the cases tested.

The Coup de Grace

One more test demonstrates the utility of this controller. The most rigorous test of this controller is in a condition where both the tanker and the receiver aircraft are moving. The motion of the tanker has already been shown to be manageable. Performance of the controller can also be ascertained when the formation point is allowed to move relative to the tanker's CG. In this section two cases are shown. The first case demonstrates the controller's performance when the formation point is moving. A second case shown after this case shows the improvement in controller performance when the feed forward model for the boom has knowledge of the moving formation point. A sinusoidal motion of ± 1.4 feet was added to the initial position of the formation point to represent it moving vertically still within the bounds of the continuous refueling envelope. This represents an angular variation of 2 degrees above or below the ideal formation point. For this first simulation, the signal was only fed to the tip position calculation block. In the lower left corner of Figure 64 in Appendix D, the formation point is shown feeding into the mux prior to the kinematics and aerodynamic block and feeding

into the tip position calculation block. To simulate the motion of the formation point being a force the feed forward boom plant has no knowledge of, separate formation point drivers are used as input for the two locations currently fed by the one block. The block connected to the tip position error calculation had a sinusoidal signal added to the static formation point. This has the effect of moving the formation point while keeping the information on the motion of the formation point from the feed forward block. The controller's response to these conditions is shown below. The sinusoidal

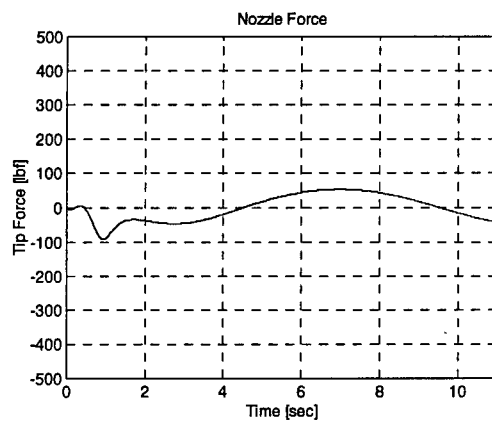


Figure 57: Nozzle Force, Controller w/ Moving F.P.

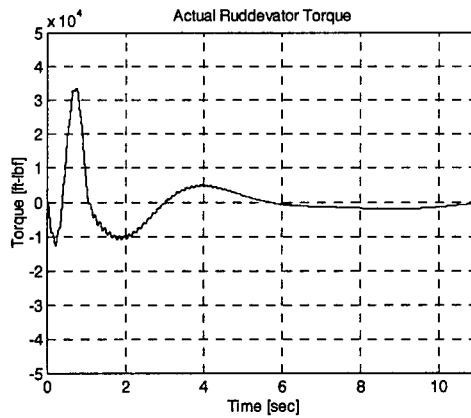


Figure 58: $\tau_{root-actual}$ Controller /w Moving F.P.

nature of the moving formation point is evident in Figure 60. After the aircraft's motion is damped out the controller has an oscillating error in the nozzle force. This is the result of the

feed forward term failing to accurately predict the boom error. The magnitude of the nozzle force shown in Figure 59 is still better than most of the controller options under ideal conditions. Finally, if the boom controller had knowledge about the position of the formation point as it moved relative to the CG of the tanker aircraft, this information could help drive the feed forward term. This is feasible if Trosen's formation hold autopilot were implemented. Then, the motion of the formation point would be a result of tracking error in the trailing aircraft's autopilot. This would give a more concrete indication of the boom controller's formation point tracking performance. To simulate the boom feed forward term having knowledge of the formation point's motion, the formation point block in Figure 64 of Appendix D is reconnected as shown in that figure and a sinusoidal signal is added. This would give an even flatter response than that seen in Figure 57 and Figure 58. This next set of plots demonstrates the benefit of accurate feed forward plant modeling.

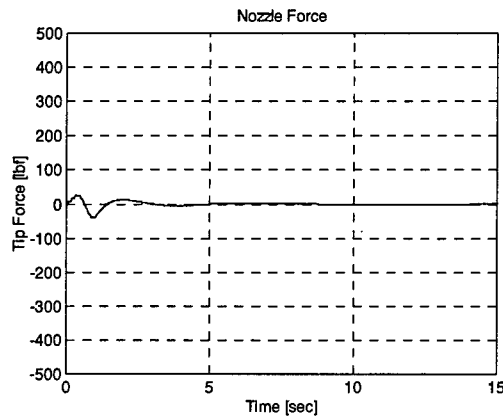


Figure 59: Nozzle Force, Controller w/ Feed Forward and Moving F.P.

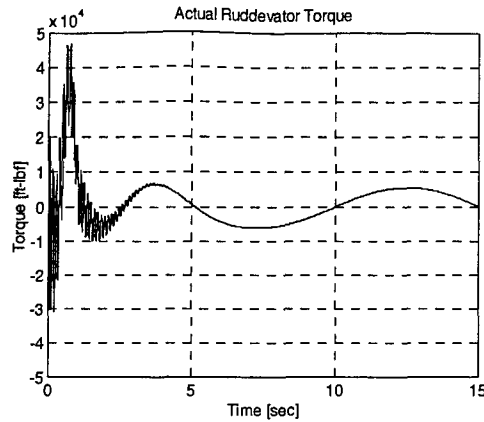


Figure 60: $\tau_{root-actual}$ Controller /w Feed Forward, Moving F.P.

The nozzle force dropped by half and the required torques are still achievable. Note however, oscillation is beginning in the rudder controller. This is a result of a gain on the rate feedback term being set too high. The importance of tuning the controller for the widest array of conditions becomes clear. One could attempt to use an ideally tuned controller for each condition occurring during the refueling operations. This could be accomplished by using a look up table for the gains to be used in the rudder proportional controller and the rate feedback based on the current angular rates of each joint. In this way the controller would gain robustness while maximizing the performance for a given set of conditions.

Feed Forward Imperfection

Throughout the analysis it was clear that the feed forward was not performing as an ideal feed forward even though the inverse boom plant used in the feed forward block is a duplicate of the boom plant with only minor changes made in order to output a torque instead of an angle for joint 2. After evaluating the two versions of the boom plant and comparing the signals from each of the subcomponents, it became clear that those terms in the boom plant which used any of the derivative signals derived in the block did not match the corresponding signals in the inverse boom plant block. This meant that either the integration algorithm used in the Simulink

integrator block was inaccurate or the time derivative block in Simulink was not performing well. To see if this was the cause of the problem, a demonstration was performed where a sinusoidal signal was passed through two derivative blocks and then passed through two integration blocks. Evaluation of the output of each block in the chain revealed that after passing through two derivative blocks the output signal was badly deformed. If a simple sinusoidal signal is differentiated twice, the expected result is a sinusoidal signal 180 degrees out of phase with the input signal. This was not the case. The output of the second derivative block was badly distorted. To verify that this was not a platform specific problem, the Matlab webpage was consulted. On the Matlab website there is a knowledge base article that stated that there is an inherent inaccuracy in the derivative block which MathWorks, the makers of Matlab, acknowledged. The error in the derivative block is noticeably exacerbated when the derivative block's output is fed into another derivative block.

To correct for this problem, there is another possible method which could be used to determine the derivative of a desired input. By using the Jacobian developed in the Robotica program, one could calculate a relation between the angular velocity of the controlled joint, q_2 with respect to the angular velocity of the prescribed motion joint, q_1 . This method is discussed in detail in Appendix D.

Impact of Controller Performance on UAV Refueling

The analysis shows that an order of magnitude reduction in the radial nozzle force occurred when the complexity of the controller was increased by adding rate feedback and feed forward. The research showed that when the boom controller is used in conjunction with a very rigid receiver where the formation point follows a trajectory driven by the receiver aircraft, the controller is very effective at minimizing nozzle forces due to boom bending. This analysis implicitly assumed then that the receiver was an infinitely stiff system which could not be moved

about by the boom. In reality, the compliance of a vehicle is not a zero compliance system. For example, a fighter sized aircraft gets moved around some if the boomer is not very agile on the boom control sticks. A fighter is more compliant than an aircraft the size of a transport. Therefore, the effect of large nozzle forces would be more detrimental on the fighter or a large UAV that is approximately the size of a small fighter. Consider then the effect of high nozzle forces on the lightweight or 6,000 lb class UAV. It inherently has less control authority than the larger vehicles because it requires less control authority to maneuver its smaller mass, and hence is more compliant than the larger UAVs. Therefore, unless the nozzle forces are decreased from those currently refueled aircraft experience, it is possible that the motion of the boom would override the small UAV's autopilot. With the order of magnitude reduction in the nozzle loading when the complex controller demonstrated in this study is used, the impact on the lightweight UAV is greatly reduced and rigid boom refueling may be feasible. The reduction in the nozzle force demonstrated with this study's controller is a good first indication that lightweight refueling is possible.

An analysis of the compliance of the different sizes of UAVs would allow the boom control designer to determine what level of nozzle force is acceptable when refueling a lightweight UAV. Unfortunately, the compliance of an aircraft is not easily determined. While we know from flying experience that the boom can move a fighter size aircraft around while it is connected, it is much more difficult to analyze the compliance represented by the motion of that aircraft as it is pushed about by a boom. The evaluator would have to know the characteristics of the force imparted to the coupled aircraft, and then be able to track the motion of the connected aircraft as it is pushed about. The analysis would require integration of the interaction between the boom controller and autopilot used to maintain flight formation of the tanker and receiver aircraft. To further determine the benefit of the decreased nozzle forces seen in this study's controller, the compliance of the vehicle to be refueled must be known.

Summary

Testing of the controller design was performed in three phases. The open loop plant was evaluated by exciting angle q_1 , with the result of an elevator pitch doublet command to the aircraft plant. The open loop controller proved stable but very oscillatory. Next, the controller was converted to a closed loop, ideal design by feeding back τ_b . This is analogous to feeding back the signal from an ideal rudder where $\tau_{root-actual}$ exactly matches τ_{root} . This proved to be stable but had an undesirable but expected increase in the controller's natural frequency. To damp out this oscillation, various modifying signals were applied to the input of the rudder plant. The best option appeared to be a combination of rate feedback and feed forward. With the gain on the rate feedback set to 1,000,000 and the feed forward working to correct the initial error, the nozzle force was nearly zero for the ideal rudder.

The data indicate that for the non-ideal boom controller the best alternative is to use feed forward in conjunction with τ_b to control the rudder. The anticipatory characteristic of the feed forward signal helps to minimize the error in the boom position during the period the aircraft is in motion. This results in a reduction of $\tau_{root-actual}$ because the controller is not required to correct for the large errors which occur when the plant operates with simple τ_b feedback. The rate feedback was decreased from 1,000,000 to 300,000, and the PD controller in the rudder plant was established at 10,000 to maintain stable controller operation under the largest range of refueling disturbances.

After performing the simulations and analyzing them, it was clear that the feed forward was not as effective as it should have been. Analysis showed the error in the feed forward signal resulted from use of the Simulink derivative block to calculate the first and second derivatives of q_{2d} which were needed to calculate the inertial and coriolis terms in the inverse boom plant.

Further analysis showed that another method could be used to determine the desired derivatives.

This method is outlined in Appendix E.

V. Conclusions and Recommendations

Conclusions

Through the use of a computer simulation model, the performance of an ideal KC-135 refueling boom controller was validated. As the complexity of the model increased, its ability to eliminate nozzle forces as the tanker moved from a steady state condition improved. Beginning with a basic open-loop controller, a pitch doublet was applied to joint one. The controller proved to be stable. Then the loop was closed on the controller with τ_b feedback as the input in order to represent a perfect rudder.

To this basic model, several different design alternatives were applied to determine their relative benefit or harmful effect. The use of a gain on the sensed nozzle force as a control concept proved to be detrimental to the system's performance. When the nozzle force was amplified, it had the effect of increasing the natural frequency of the refueling boom. The rudder was commanded to oscillate at a frequency which would likely prove catastrophic in a real rudder system. A gain of one order of magnitude on the bending torque resulted in an increase of the system's natural frequency from 0.9 Hz to 2.7 Hz.

Next a feed forward signal was added to the commanded rudder torque. This had the effect of decreasing the overshoot of the boom through the duration of the aircraft plant motion. This resulted in a reduction of the nozzle force from 125 lbs to 50 lbs. After feed forward was proven to be an effective method to anticipate the torque needed to keep the boom stationary, a rate feedback signal was tested to determine its ability to dampen the oscillations in the system response. Increasing the gain on this signal resulted in decreased settling time of the nozzle force and a decrease in its magnitude.

Finally, the ideal controller was tested with a combination of both rate feedback and feed forward. This combination proved to be most effective at reducing nozzle force. As the gain on

the rate feedback was increased, the nozzle force was damped out more effectively. The feed forward had the effect of minimizing the error in commanded torque during the pitch doublet. After the ideal rudder validated the performance of the control concepts, a non-ideal rudder plant was used to produce the commanded torques.

The non-ideal rudder plant didn't match the commanded torque because of the phase lag between the commanded rudder angle and the actual rudder angle. As the gain on the Proportional controller was tuned for a specific scenario the phase lag in the rudder angle decreased. Unfortunately, as the conditions changed in the subsequent simulations the gain had to be readjusted downward from 30,000 to 10,000 to ensure system stability. The controller was tested against the same combination of rate feedback and plant response feed forward as for the ideal design. The combination of rate feedback and feed forward resulted in the smallest forces being imparted to the nozzle. A rate feedback gain of 300,000 aided in damping out the nozzle force without contributing to the growth of the commanded torque. The only limitation to the use of rate feedback is that it has a tendency to increase the error in the system response during the period when the boom system is undergoing prescribed plant motion. High gains on the rate feedback result in large τ_{root} commands. This is a characteristic of the non-ideal rudder. The addition of an inertial term for the rudder resulted in a lag in the output signal. This lag acted to damp system overshoot independent of the rate feedback signal. Adding rate feedback at too high a gain resulted in a phase shift of $\tau_{root-actual}$. This shift had the effect of adding to the error instead of helping to eliminate the error. The best design alternative was found to be feed forward in conjunction with a rate feedback signal with a gain 300,000.

The nozzle forces produced using the most complex controller design are an order of magnitude less than those obtained using a simple force feedback design such as that of the KC-10's ALAS system. The nozzle forces determined for the basic controller are in the same range

as those seen in the KC-10 boom when the ALAS is operating. The KC-10 boom experiences bending loads of nearly 100 lbs [4] compared to 125 lbs seen in this study's basic controller. The reduction of nozzle force by an order of magnitude for the complex controller means that this controller is a better design to use when refueling light UAV's or other lightweight air vehicles.

Recommendations

The development of this design is the first step to creating a controller capable of operating the KC-135 refueling boom without a boom operator. The design gains must be adjusted once the controller is validated against the response characteristics of the actual boom. Some aerial testing of the boom response to a pitch doublet would help to verify the result of this study. Additionally, a lateral controller must be designed so all three axes of boom motion can be evaluated. Once a lateral model is designed, a comprehensive parametric study of the model should be performed. This study should evaluate the performance of the combined controller at different airspeeds and altitudes to verify its performance over the largest envelope of operating conditions.

It was noted that the boom's natural frequency with the closed loop controller was approximately 1.2 Hz when the closed loop controller was implemented. An evaluation of the effect of this rate of signal change to the rudder should be performed to ascertain whether operation at 1.2 Hz is within the capabilities of the real rudder.

The controller in this study was primarily designed to track a formation point which remains constant with respect to the tanker CG. If the controller were made to track moving formation point, the boom could be driven about its envelope by varying the formation point. A test was performed to demonstrate the boom's capability to minimize nozzle forces when the formation point moved. The results indicate that this method of controlling the boom merits

further development. Also, to demonstrate the effectiveness of the boom controller while tracking a moving formation point, Trosen's formation hold autopilot should be added to the simulation. Then the simulation could be tested to determine the boom performance in the presence of external disturbances such as wind gusts.

To ascertain the benefit of the nozzle force reduction, an analysis of the lightweight UAV's compliance should be conducted. This information would enable a comparison of the controller's performance with lightweight UAVs versus its performance with heavy transport aircraft. Another alternative would be to obtain a lightweight aircraft plant model and use it as the vehicle maintaining position at the formation point.

Past experience on boom controller design for the KC-10 proved that higher order modal analysis of the boom should be conducted.[4] This analysis could be used to modify the nozzle force equation in the boom controller in order to more accurately represent the real KC-135 boom.

Better data on the KC-135 boom's physical properties should be incorporated into the model to replace the estimates of rudder moment of inertia, boom stiffness and mass properties used in this study.

Finally, this controller architecture should be expanded to control both the lateral and longitudinal motions of the refueling boom.

Appendix A

Robotica Input and Results

This appendix outlines the method used to derive the boom transformation and dynamics matrices. The method is based on Spong[14]. The robotic development tool, Robotica is used to calculate all parameters.

Robotica Equations

The user must orient the coordinate frames according to the Denavit-Hartenberg (DH) method's criteria. Once the base coordinate frame, with origin O_0 , is drawn, the DH method guides the orientation of each joint with respect to the joint's origin frame. Specifically, if a joint is revolute, the Z-axis of the coordinate frame lies parallel with the joint's axis of rotation. If the joint is prismatic, the Z-axis lies in the direction of extension of the joint. The remainder of each coordinate frame is laid out following the right hand rule with some additional restrictions on the X-axis of each frame. After defining the coordinate frames, the DH method identifies the link parameters that must be documented. These parameters include each link's mass, moment of inertia, center of mass, and the direction gravity acts, represented as a vector in the system's base frame.

Because a robotic representation of the refueling system is used, some assumptions will make working with the DH method simpler. When a revolute joint is followed by a prismatic joint, as is the case at joint two and three, the DH method directs that both joints be co-located at the origin of the revolute joint. For this model, this means joint three, the telescoping joint of the boom is actually placed at the boom root, coincident with joint two. This has no effect on the mass distribution and the related center of mass calculations of the boom. The values for mass and center of mass of the boom are based on its actual configuration. Therefore d_3 is an input to the mass and center of mass function within Simulink, but the function uses it to determine the actual length of each segment of the boom. Because joints two and three are co-located, we can assume that link two has no mass or inertia. Instead, the mass of link two can be lumped in with the mass of link three. With these assumptions directing the robot representation, the data file is created and recorded in the Robotica program. The output of the program is a data file that includes the forward kinematic equations for both orientation and position, and the equations of

motion of the robot representation. While the basic system comprised of the aircraft, boom root, and telescoping joint can be modeled in the DH fashion, the transformations from the boom frame to the left and right ruddervators must still be calculated by hand. However, their mass and its effects on the boom arm are included in the boom dynamic equations.

This is the input data for the Robotica program. It includes all the orientation information and dynamics data for the robotic boom representation

A Robotica input data file for a six DOF simulation
of a KC-135 Refueling Boom

The base frame is an inertial reference frame that is "connected" to
the aircraft Center of Gravity by a spherical joint.

DOF = 3

The Denavit-Hartenberg Parameters:

joint1 = revolute

a1 = 49

alpha1 = 0

d1 = 0

theta1 = q1

joint2 = revolute

a2 = 0

alpha2 = 90

d2 = 0

theta2 = q2

joint3 = prismatic

a3 = 0

alpha3 = 0

d3 = d3

theta3 = 0

DYNAMICS

gravity vector = {0,-g,0}

mass1 = 0

center of mass = {0,0,0}

inertia matrix = {0,0,0,0,0,0}

mass2 = 0

center of mass = {0,0,0}

inertia matrix = {0,0,0,0,0,0}

mass3 = m3

center of mass = {0,0,-bx}

inertia matrix = {Ix3,0,0,Iy3,0,Iz3}

This file is the output of all data of the Robotica program. It includes all elements of the T (transformation), J (velocity jacobian), M (mass and inertia), C (coriolis), and G (gravity) matrices. They are listed by their cell position within the respective matrices. It is in original format to preserve organization.

```
T03[1,1] = Cos[q1 + q2]
T03[2,1] = Sin[q1 + q2]
T03[3,1] = 0
T03[4,1] = 0
T03[1,2] = 0
T03[2,2] = 0
T03[3,2] = 1
T03[4,2] = 0
T03[1,3] = Sin[q1 + q2]
T03[2,3] = -Cos[q1 + q2]
T03[3,3] = 0
T03[4,3] = 0
T03[1,4] = 49 Cos[q1] + d3 Sin[q1 + q2]
T03[2,4] = -(d3 Cos[q1 + q2]) + 49 Sin[q1]
T03[3,4] = 0
T03[4,4] = 1
J[1,1] = C1*C2*d3 - 49*S1 - d3*S1*S2
J[2,1] = 49*C1 + d3*Sin[12]
J[3,1] = 0
J[4,1] = 0
J[5,1] = 0
J[6,1] = 1
J[1,2] = C1*C2*d3 - d3*S1*S2
J[2,2] = d3*Sin[12]
J[3,2] = 0
J[4,2] = 0
J[5,2] = 0
J[6,2] = 1
J[1,3] = Sin[12]
J[2,3] = -(C1*C2) + S1*S2
```

$J[3,3] = 0$
 $J[4,3] = 0$
 $J[5,3] = 0$
 $J[6,3] = 0$
 $C[1,1] = m_3 (-bx d_3'[t]) + d_3 d_3'[t] + 49 \sin[q_2] d_3'[t] -$
 $> 49 bx \cos[q_2] q_2'[t] + 49 d_3 \cos[q_2] q_2'[t])$
 $C[2,1] = (-bx + d_3) m_3 (d_3'[t] - 49 \cos[q_2] q_1'[t])$
 $C[3,1] = m_3 (bx q_1'[t] - d_3 q_1'[t] - 49 \sin[q_2] q_1'[t] + bx q_2'[t] -$
 $> d_3 q_2'[t])$
 $C[1,2] = m_3 (-bx d_3'[t]) + d_3 d_3'[t] + 49 \sin[q_2] d_3'[t] -$
 $> 49 bx \cos[q_2] q_1'[t] + 49 d_3 \cos[q_2] q_1'[t] - 49 bx \cos[q_2] q_2'[t] +$
 $> 49 d_3 \cos[q_2] q_2'[t])$
 $C[2,2] = (-bx + d_3) m_3 d_3'[t]$
 $C[3,2] = (bx - d_3) m_3 (q_1'[t] + q_2'[t])$
 $C[1,3] = m_3 (-bx + d_3 + 49 \sin[q_2]) (q_1'[t] + q_2'[t])$
 $C[2,3] = (-bx + d_3) m_3 (q_1'[t] + q_2'[t])$
 $C[3,3] = 0$
 $M[1,1] = I_y^3 + 2401 m_3 + bx^2 m_3 - 2 bx d_3 m_3 + d_3^2 m_3 - 98 bx m_3 \sin[q_2] +$
 $> 98 d_3 m_3 \sin[q_2]$
 $M[2,1] = I_y^3 + bx^2 m_3 - 2 bx d_3 m_3 + d_3^2 m_3 - 49 bx m_3 \sin[q_2] +$
 $> 49 d_3 m_3 \sin[q_2]$
 $M[3,1] = -49 m_3 \cos[q_2]$
 $M[1,2] = I_y^3 + bx^2 m_3 - 2 bx d_3 m_3 + d_3^2 m_3 - 49 bx m_3 \sin[q_2] +$
 $> 49 d_3 m_3 \sin[q_2]$
 $M[2,2] = I_y^3 + bx^2 m_3 - 2 bx d_3 m_3 + d_3^2 m_3$
 $M[3,2] = 0$
 $M[1,3] = -49 m_3 \cos[q_2]$
 $M[2,3] = 0$
 $M[3,3] = m_3$
 $g[1] = -49 g m_3 \cos[q_1] + bx g m_3 \sin[q_1 + q_2] - d_3 g m_3 \sin[q_1 + q_2]$
 $g[2] = (bx - d_3) g m_3 \sin[q_1 + q_2]$
 $g[3] = g m_3 \cos[q_1 + q_2]$

Appendix B

Aircraft Plant Equations, Ruddevator Aerodynamics and Boom Mass Properties

Aircraft Plant State Space Equation and Coefficients

The state equation and coefficient development below is borrowed from William J. Locken's Thesis Work [8]

Assumptions:

Equations are assumed to have no coupling between motion in the lateral direction plane and the longitudinal plane.

The X, Y, and Z body axes lie in the plane of symmetry of the aircraft and the origin of the axis system is located at the aircraft center of gravity.

Aircraft mass is assumed to remain constant for a given flight condition.

The aircraft is a rigid body.

The earth is an inertial reference.

The equations are perturbation equations and represent the aircraft for small perturbations about the trimmed flight condition.

The freestream airflow is quasi-steady.

Thrust acts only in the X-axis direction.

Using these assumptions and following Locken's procedure (borrowed from Roskam [12]), the state space representation of the aircraft is:

$$\begin{aligned}\dot{x} &= Ax + Bu \\ y &= Cx\end{aligned}$$

where

$$\begin{aligned}\dot{x} &= [\dot{\phi} \dot{\beta} \dot{p} \dot{r} \dot{h} \dot{\theta} \dot{u} \dot{\alpha} \dot{q}]^T \\ x &= [\phi \beta p r h \theta u \alpha q]^T \\ u &= [\delta_r \delta_w \delta_e \delta_{sb} \delta_T]^T \\ y &= [h \theta u \alpha q]^T\end{aligned}$$

$$A = \begin{bmatrix} 0 & 0 & 1 & 0 & 0 & 0 & 0 & 0 & 0 \\ Y'_\phi & Y'_\beta & Y'_p & Y'_R & 0 & 0 & 0 & 0 & 0 \\ 0 & L'_\beta & L'_p & L'_R & 0 & 0 & 0 & 0 & 0 \\ 0 & N'_\beta & N'_p & N'_R & 0 & 0 & 0 & 0 & 0 \\ 0 & 0 & 0 & 0 & 0 & U'_0 & 0 & U'_0 & 0 \\ 0 & 0 & 0 & 0 & 0 & 0 & 0 & 0 & 1 \\ 0 & 0 & 0 & 0 & 0 & X'_\theta & X'_u & X'_\alpha & X'_q \\ 0 & 0 & 0 & 0 & 0 & Z'_\theta & Z'_u & Z'_\alpha & Z'_q \\ 0 & 0 & 0 & 0 & 0 & M'_\theta & M'_u & M'_\alpha & M'_q \end{bmatrix}$$

$$B = \begin{bmatrix} 0 & 0 & 0 & 0 & 0 \\ Y'_{\delta_r} & Y'_{\delta_w} & 0 & 0 & 0 \\ L'_{\delta_r} & L'_{\delta_w} & 0 & 0 & 0 \\ N'_{\delta_r} & N'_{\delta_w} & 0 & 0 & 0 \\ 0 & 0 & 0 & 0 & 0 \\ 0 & 0 & 0 & 0 & 0 \\ 0 & 0 & X'_{\delta_e} & X'_{\delta_{sb}} & X'_{\delta_T} \\ 0 & 0 & Z'_{\delta_e} & Z'_{\delta_{SB}} & 0 \\ 0 & 0 & M'_{\delta_e} & M'_{\delta_{SB}} & 0 \end{bmatrix}$$

The coefficients are calculated using the following two M-files in Matlab

```
%=====
% Adam Mortensen 19 Feb 97      Thesis aircraft model
%
% Non-Dimensional Derivatives for the KC-135.
%
% File Name derivatives.m
%
% Must be called before calculation of the commanded inputs can be calculated
% for the KC-135 aircraft model
%=====
```

```
H = 28500
mach = .77
W = 284000
CG = 24.2
Q = 279.6
S = 2433
SPAN = 130.83
C = 20.16
U = 760
G = 32.2
DTHETA = 2.4
DALPHA = 2.4
SIXX = 2930000
SIYY = 4660000
SIZZ = 7480000
SIXZ = 0
CMU = 0.0
CL = .426
CLU = 0
CLA = 4.727
CLQ = 4.825
CLDE = .1862
CLDSB = -.2751
CLB = -.198
CLP = -.345
CLR = .155
CLDR = .0315
CLDA = .0153
CM = 0
CMAD = -6.57
CMA = -.8595
CMQ = -14.65
CMDE = -.5988
CMDSB = .07639
CNB = .166
CNP = -.005
CNR = -.194
CNDR = -.113
CNDA = .00149
CD = .024
CDU = 0
CDA = .2143
CDDE = 0
CDDSB = .04779
CYB = -.762
CYP = -.211
CYR = .428
CYDR = .264
CYDA = -.0074
```

CXAD = 0.0
CZAD = 0.0

u0 = 13.2645

c = [0 0 0 0 1 0 0 0 0; 0 0 0 0 0 1 0 0 0; 0 0 0 0 0 0 1 0 0; 0 0 0 0 0 0 0 1 0; 0 0 0 0 0 0 0 0 1]

calcderv

```

%-----
% Adam Mortensen 19 Feb 97      Thesis aircraft model
%
% Calculation of the Dimensional Derivatives for an aircraft in the body
% axis system.
%
% File Name: calcdderiv.m
%
% Must must enter the nondimensional stability derivatives prior to running
% script
%-----

```

```

DPR = 360/(2.0*pi)

ALPHA=DALPHA/DPR
THETA=DTHETA/DPR

```

%LONGITUDINAL DERIVATIVE CALCULATIONS

```

SCZA = -CLA - CD
SCZQ = -CLQ
SCZU = -CLU - 2.0*CL
SCZDE = -CLDE
SCZDSB = -CLDSB
SCXA = -CDA + CL
SCXU = -CDU - 2.0*CD
SCXDE = -CDDE
SCXDSB = -CDDSB

```

```

CAL = cos(ALPHA)
SAL = sin(ALPHA)
COSSQ = CAL^2
SINSQ = SAL^2
COSSIN = CAL*SAL

```

```

%*****
%*Calc the body axis moments from the stab axis moments
%y=[SIXX
% SIZZ
% SIXZ]
%A = [COSSQ SINSQ -2.0*COSSIN
% SINSQ COSSQ 2.0*COSSIN
% COSSIN -COSSIN COSSQ-SINSQ]
%X = inv(A)*y
%*****

```

```

BIXX = SIXX
BIYY=SIYY
BIZZ=SIZZ
BIXZ=SIXZ

```

```

CZ = -CL*CAL - CD*SAL
CZA = SCZA*COSSQ + (SCZU+SCXA)*COSSIN + SCXU*SINSQ
CZQ = SCZQ*CAL
CZU = SCZU*COSSQ - (SCZA-SCXU)*COSSIN - SCXA*SINSQ
CZDE = SCZDE*CAL + SCXDE*SAL
CZDSB = SCZDSB*CAL + SCXDSB*SAL

```

$CX = -CD*CAL + CL*SAL$
 $CXA = SCXA*COSSQ + (SCXU-SCZA)*COSSIN - SCZU*SINSQ$
 $CXQ = CLQ*SAL$
 $CXU = SCXU*COSSQ - (SCXA+SCZU)*COSSIN + SCZA*SINSQ$
 $CXDE = SCXDE*CAL - SCZDE*SAL$
 $CXDSB = SCXDSB*CAL - SCZDSB*SAL$

$BCMA = CMA*CAL + (CMU + 2.0*CM)*SAL$
 $BCMAD = CMAD*CAL$
 $BCMU = (CMU + 2.0*CM)*CAL - CMA*SAL$

$Z1 = Q*S*G/W$
 $A = C/(2.0*U)$
 $PU = U/DPR$

%*****OUTPUT DATA*****

$Z = Q*S*CZ$
 $ZA = Z1*CZA$
 $ZAD = Z1*A*CZAD$
 $ZQ = Z1*A*CZQ$
 $ZU = (Z1/U)*CZU$
 $ZDE = Z1*CZDE$
 $ZDSB = Z1*CZDSB$

$X = Q*S*CX$
 $XA = Z1*CXA/DPR$
 $XAD = Z1*A*CXAD/DPR$
 $XQ = Z1*A*CXQ$
 $XU = (Z1/U)*CXU$
 $XDE = Z1*CXDE/DPR$
 $XDSB = Z1*CXDSB/DPR$

$M1 = Q*S*C/BIYY$

$M = Q*S*CM$
 $MA = M1*BCMA$
 $MAD = M1*A*BCMAD$
 $MQ = M1*A*CMQ$
 $MU = M1/U*BCMU$
 $MDE = M1*CMDE$
 $MDSB = M1*CMDSB$

$PZA = ZA/U$
 $PZQ = (ZQ/U) + 1.0$
 $PZU = ZU/U*DPR$
 $PZDE = ZDE/U$
 $PZDSB = ZDSB/U$
 $PZTHETA = -(G/U)*sin(THETA)$

$PMA = MA + MAD*PZA$
 $PMQ = MQ + MAD*PZQ$
 $PMU = MU + MAD*PZU$
 $PMDE = MDE + MAD*PZDE$
 $PMDSB = MDSB + MAD*PZDSB$
 $PMTHETA = MAD*PZTHETA$

$PXQ = XQ - U*ALPHA/DPR$
 $PXTHETA = -G*cos(THETA) / DPR$

%*****
%***END LONG OUTPUT DATA*****

BCLB = CLB*CAL - CNB*SAL
BCLP = CLP*COSSQ - (CLR+CNP)*COSSIN + CNR*SINSQ
BCLR = CLR*COSSQ - (CNR-CLP)*COSSIN - CNP*SINSQ
BCLDA = CLDA*CAL - CNDA*SAL
BCLDR = CLDR*CAL - CNDR*SAL
BCNB = CNB*CAL + CLB*SAL
BCNP = CNP*COSSQ - (CNR-CLP)*COSSIN - CLR*SINSQ
BCNR = CNR*COSSQ + (CLR+CNP)*COSSIN + CLP*SINSQ
BCNDA = CNDA*CAL + CLDA*SAL
BCNDR = CNDR*CAL + CLDR*SAL

BCYR = CYR*CAL + CYP*SAL
BCYP = CYP*CAL - CYR*SAL

N = (Q*S*SPAN)/BIZZ
L = (Q*S*SPAN)/BIXX
BN = SPAN/(2.0*U)
Y = (Q*S*G)/W
BNB = N*BCNB
BNP = N*BN*BCNP
BNR = N*BN*BCNR
BNDA = N*BCNDA
BNDR = N*BCNDR

BLB = L*BCLB
BLP = L*BN*BCLP
BLR = L*BN*BCLR
BLDR = L*BCLDR
BLDA = L*BCLDA

YB = Y*CYB
BYR = Y*BN*BCYR
BYP = Y*BN*BCYP
YDR = Y*CYDR
YDA = Y*CYDA

D = 1.0 - (BIXZ^2/(BIXX*BIZZ))
R1 = BIXZ/BIZZ
R2 = BIXZ/BIXX

PBNB = (BNB + R1*BLB)/D
PBNP = (BNP + R1*BLP)/D
PBNR = (BNR + R1*BLR)/D
PBNDR = (BNDR + R1*BLDR)/D
PBNDA = (BNDA + R1*BLDA)/D

PBLB = (BLB + R2*BNB)/D
PBLP = (BLP + R2*BNP)/D
PBLR = (BLR + R2*BNR)/D
PBLDR = (BLDR + R2*BNDR)/D
PBLDA = (BLDA + R2*BNDA)/D

PYB = YB/U
PBYP = BYP/U + ALPHA
PBYR = BYR/U - 1.0
PYDR = YDR/U

PYDA = YDA/U

A = [00100000;
G/U PYB PBYP BYR 00000;
0 PBLB PBLP PBLR 00000;
0 PENB PBNP PBNR 00000;
00000 PU 0 -PU 0;
000000001;
00000 PXTHEA XU XA PXQ;
00000 PZTHEA PZU PZA PZQ;
00000 PMTHEA PMU PMA PMQ]

B = [00000;
PYDR PYDA 000;
PBLDR PBLDA 000;
PBNDR PBNDA 000;
00000;00000;
00 XDE XDSB .034;
00 PZDE PZDSB 0;
00 PMDE PMDSB 0]

Structural/Mass Properties of KC-135 Boom

This structural data is borrowed from the 1989 GSE study [1]

Structure Derivation

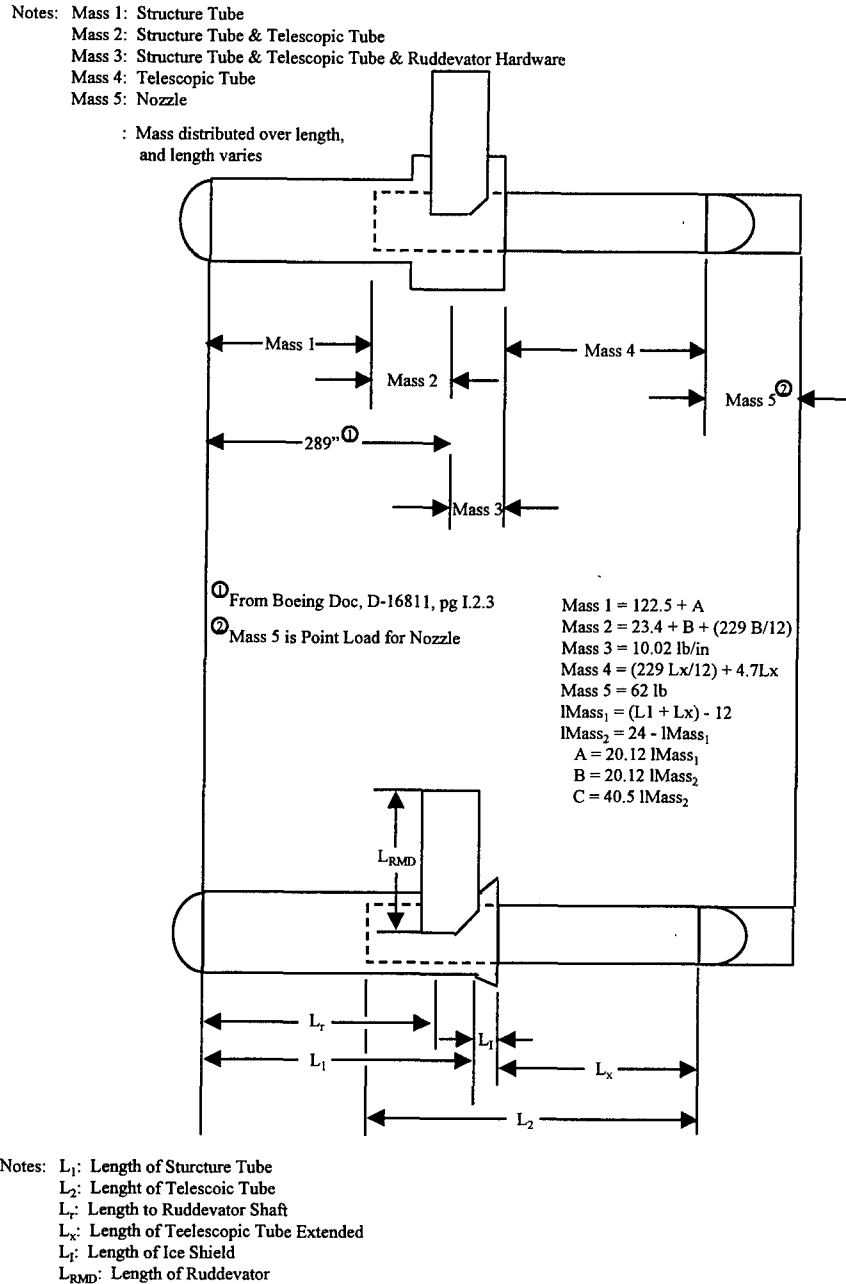
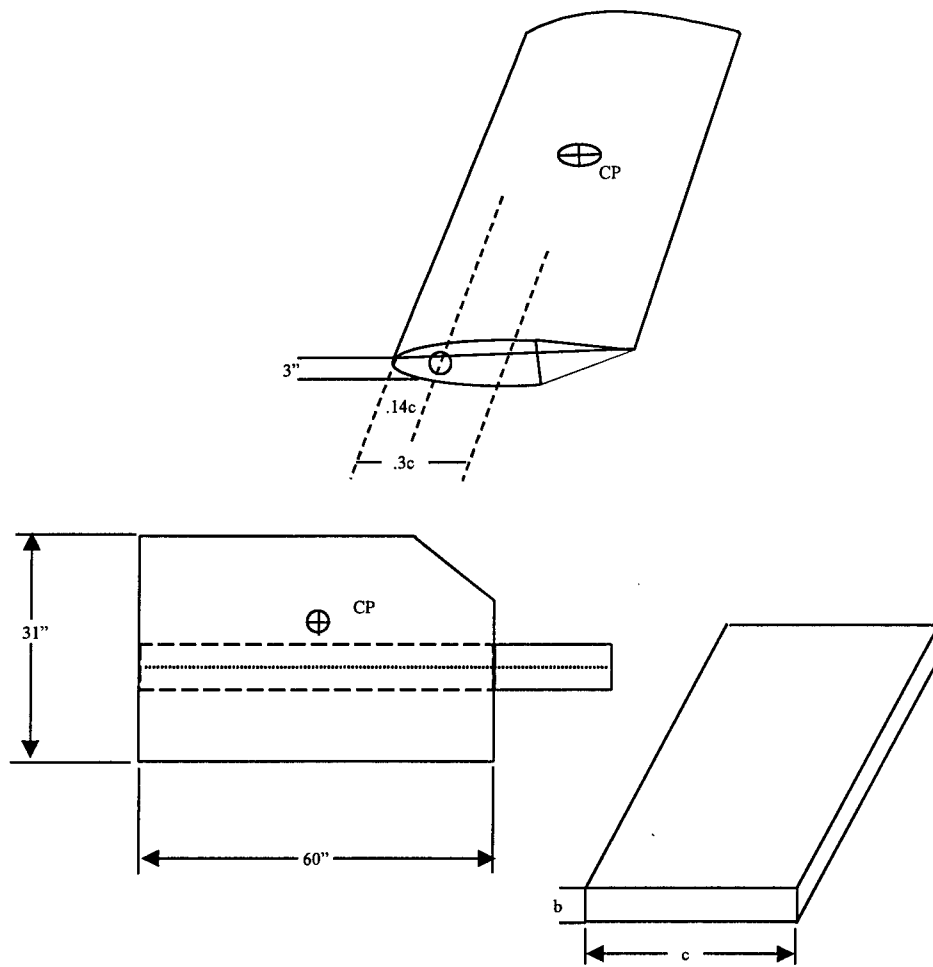


Figure 61: Structural and Mass Properties of Boom [1]



$$I_{rud} = 1/12 m(b^2 + c^2)$$

$$W_{rud} = 208 \text{ lbs}$$

$$M_{rud} = 208/32.2$$

Figure 62: Rudder Moment of Inertia Estimate[16]

Aerodynamic Coefficient Calculations

Derived using Etkin []

$$C_{l_\alpha} = 2\pi F(k) \Rightarrow F(k) = \frac{C_{l_\alpha}}{2\pi}$$

$$= \frac{5.959 / \text{rad}}{2\pi} = 0.9484 = F(k)$$

From $F(k)$ Pg.282 $k = 0.025$ and $G(k) = -0.11$

$$C_{e_\alpha} = \pi + 2\pi \frac{G(k)}{k} = \pi - 2\pi \frac{.11}{0.025} = -24.5044$$

$$Cm_\alpha = 2\pi F(k) \left(h - \frac{1}{4} \right)$$

$h = 0.3c$ for NACA65,-012

$$2\pi(0.9484)(0.3 - 0.25)$$

$$= 0.29795$$

$$Cm_{\dot{\alpha}} = \pi(h - 0.5) + 2\pi \frac{G(k)}{k} (h - 0.25)$$

$$= \pi(0.3 - 0.5) + 2\pi \frac{-0.11}{0.025} (0.3 - 0.25)$$

$$= -76.6549$$

$$\frac{Cm_{\dot{\alpha}}}{\ell_r} = \frac{-76.6549}{24.5} = -3.1288$$

Appendix C

Matlab Function M-Files

```

%-----
% Adam Mortensen 14/Jul/97 Thesis project
%
% kin_joints23
%
% input
%   -angle for joint one of the robot (remember the sign changes from the
%   aircraft model. Must be negative to agree with the robotic reference
%   frame notation)
%   -pipper point position (X,Y,Z)
%
% output
%   Joint angle for joint 2, jointsout(1), and length of joint three
%   d3, (jointsout(2)).
%
% Notes: This block calculates the value for q2 and d3 using geometry and
%   trig.
%   q1   pitch angle in degrees or the -tive of joint1's angle
%   q2   joint2 in degrees
%   d3   length of link 3 in feet
%-----

function[jointsout] = inv_kin_joints23(inputs)

% convert input joint one angle to be represented in robot base frame:
% Must be converted into radians for use with the cos, sin and tan.
joint1 = -inputs(1)*pi/180;

% baseline : "formation point" for the receiver aircraft
pos_j3 = [inputs(2) inputs(3) inputs(4)];

% Calculate the position of the second joint of the robot in base frame coords.
pos_j2 = [49*cos(joint1) 49*(sin(joint1)) 0];

% Determine joint 2 angle from relative positions of the pipper and xyz
% of joint2. Angle will always be positive

yval=pos_j3(2)-pos_j2(2);
xval=abs(pos_j3(1)-pos_j2(1));

jointsout(1) = joint1;
jointsout(2) = atan(yval/xval) +pi/2 - joint1;

% From the Pythagorean Theorem calculate d3:
jointsout(3)=sqrt((pos_j2(2)-pos_j3(2))^2 + (pos_j2(1)-pos_j3(1))^2);

```

```

%=====
% Adam Mortensen 15/Jul/97 Thesis project
%
% boomwgt.m (boom weight, centers of mass and centers of pressure
%
% input (1)
%   d3 telescoping boom segment length (ft).
%
% output (5)
%   centers of pressure of the 3 segments of boom (out(3-5))
%   Overall center of mass of boom (out(1))
%   Overall mass of boom (out(2))
%   Mass moment of inertia of boom about joint2 (out(6))
%   (not output currently --> moment due to gravity)
%
% Notes: Determines boom cp's for each segment, the boom mass and cm
%
%=====

function[out] = boomwgt(in)

boomlength = in;
l1 = 27.667;
lx = boomlength - l1;
l2 = 27.5;

dellength = l1 + lx;

lmass1 = dellength - l2;
lmass2 = 24.083 - lmass1;

mass1 = 122.5 + 20.12*lmass1;
mass2 = (23.4 + (20.12*lmass2))+229.7*lmass2/l2;
mass3 = 431.0;
mass4 = 229.7*(lx / l2) + 4.7 * lx;
mass5 = 62;
cm1 = lmass1/2;
cm2 = lmass1 + lmass2/2;
cm3 = 25.875;
cm4 = l1 + (lx / 2);
cm5 = dellength;

% Calculate total mass of boom (in lbm)
masst = mass1 + mass2 + mass3 + mass4 + mass5;

% Calculate the center of mass of the entire boom. Distance measured from nozzle
boomcmroot = (cm1*mass1 + cm2*mass2 + cm3*mass3 + cm4*mass4 + cm5*mass5)/masst;
cmnozzle = boomlength - boomcmroot;
out(4) = cmnozzle;

%output total mass of boom
out(5) = masst/32.174;

% Calculate the center of pressure of each segment of boom

%cp1 root segment
out(1) = 10.0;

%cp2 telescoping segment
out(2) = (lx / 2) + l1;

```

```

%cp3 ruddervator segment
out(3) = 23.8;

% compute the boom's moment of inertia about joint 2
inertia1 = (mass1*Imass1^2)/3 + (mass2*Imass2^2)/12 + (mass3*3.5833^2)/12 + (mass4*lx^2)/12 +
(mass2*(Imass1+.5*Imass2)^2) + (mass3*(Imass1+Imass2+1.791667)^2) + (mass4*(Imass1+Imass2+3.5833 +
.5*lx)^2) + (mass5*(Imass1+Imass2+3.5833+lx)^2);

% compute the boom's moment of inertia about the boom center of mass
moicm = inertia1 - mass*boomcmroot^2;

% units of inertia are (lbf-ft-sec^2)
inertia = moicm/32.174;

% units of gravity moment are (lbf-ft)
gmt = mass1*cm1 + mass2*cm2 + mass3*cm3 + mass4*cm4 + mass5*cm5;

out(6) = inertia;

%out(7) = gmt;

```

```
% Adam Mortensen 14/Jul/97 Thesis project
%
% Convaxes.m
%
% input
%   - joint angles with respect to the robot base frame
%   - vector to be converted to the boom frame
%
% output
%   vector converted to the boom frame
%
% Notes: This block converts things like freestream velocity to the AC boom
%        fram to aid in calculation of the boom loads
```

```
function[out] = convaxes(input)
```

```
q1 =input(1);
q2 =input(2);
```

```
c12 = cos(q1+q2);
s12 = sin(q1+q2);
```

```
c1 = cos(q1);
c2 = cos(q2);
s1 = sin(q1);
s2 = sin(q2);
```

```
tst = [input(3) input(4) input(5)];
```

```
t02 = [c12 0 s12;s12 0 -(c12);0 1 0];
```

```
out = inv(t02)*tst;
```



```

%=====
% Adam Mortensen 14/Jul/97 Thesis project
%
% pos_kinematics
% input
%     Joint angles q1, q2, and d3
%
% output
%     Position of the tip of the boom (3x1)
%
% Notes: This block calculates the position of the end of the boom
%         using the d03 portion of the t03 Denavit Hartenberg robot
%         transformation matrix equations for the Xboom and Yboom directions.
%
%     q1     pitch angle in radians or the -tive of joint1's angle
%     q2     joint2 in radians
%     d3     length of link 3 in feet
%=====

function[positionsout] = pos_kinematics(joint)

% use joints to calculate the positions
%q1 = joint(1)
%q2 = joint(2)
%dd3 = joint(3)

% Calculate the x position
positionsout(1) = 49*cos(joint(1)) + joint(3)*sin(joint(1)+joint(2));

% Calculate the y position
positionsout(2) = -(joint(3)*cos(joint(1) + (joint(2)))) + 49*sin(joint(1));

% The Z direction for this problem is zero
positionsout(3) = 0;

```

```

%=====
% Adam Mortensen 14/Jul/97 Thesis project
%
% tip_pos
%
% input
%     position vector of the piper point in robot base frame
%     position vector of the boom end point due to boom dynamics
%
% output
%     direction vector from piper to endpoint position in base frame coord
%     system
%
% Notes:
%=====

function[posvect] =tip_pos(input)

% baseline "piper point" for the receiver aircraft (X,Y,Z)_base
pippos= [input(4) input(5) input(6)];

% Calculate the position of the second joint of the robot in base frame coords.
endpos = [input(1) input(2) input(3)];

% Determine vector from difference between piper and boom end

yval=endpos(2)-pippos(2);
xval=endpos(1)-pippos(1);

posvect(1) = xval;
posvect(2) = yval;
posvect(3) = 0;

```

```

%-----
% Adam Mortensen 14/Jul/97 Thesis project
%
% boomtorudframe
%
% input
%   angle of the dihedral and the current estimate for the angle
%   of the right and left ruddervators
%   the vector to be transformed to the ruddervator frame
%
%
% output
%   velocity vector converted to the rud frame
%
% Notes: This block converts velocity from the boom frame to the
%        left and right ruddervator frames
%        qd      dihedral angle
%        qr      right ruddervator angle estimate
%        ql      left ruddervator angle estimate
%
%-----

```

```

function[out] = boomtorudframe(input)

qd =input(1);
qr =input(2);
%ql =input(2);

cg = cos(qd);
cr = cos(qr);
%c3 = cos(ql);
sg = sin(qd);
sr = sin(qr);
%s3 = sin(ql);

tst = [input(3) input(4) input(5)];

tbr = [cg*cr -(cg*sr) sg; cr*sg -(sg*sr) -cg; sr cr 0];
tbrl = [cg*cr -(cg*sr) -sg; -(cr*sg) sg*sr -cg; sr cr 0];

out(1:3,1) = inv(tbr)*tst;
out(4:6,1) = inv(tbrl)*tst;

```

```

% Adam Mortensen 15/Jul/97 Thesis project
%
% rud_aero_force (Aero rudder forces)
%
% input (7)
%   -Magnitude of velocity in the Ruddervator frame
%   -Angle of attack
%   -Ruddervator angle
%   -Rate of change of angle of attack
%
% output (1)
%   forces in the ruddervator frame due to lift and drag
%
% Notes:
%   I included the Cld (lift coefficient due to aoa rate of change) to give a
%   more realistic response for the ruddervators.

```

```
function[out] = rud_aero_force(in)
```

```

wind = in(1);
aoa = in(2);
rudangle = in(3);
aoadot = in(4);
sarea = 6.01;
cl = 5.959;
cld = 0 ;
cd0 = 0.006;
rho = .00093;

```

```

saoa = sin(aoa);
caoa = cos(aoa);

```

```

% Calculate the lift and drag forces in the rudder frame
lift = (cl * aoa + cld * aoadot) * (sarea * rho * wind^2);
drag = sarea * rho * wind^2 * (cd0 + 7.878 * aoa^2);

```

```

% Divide the lift and drag into the rudder axis coordinate system
xrforce = lift * caoa + drag * saoa;
yrforce = -lift * saoa + drag * caoa;
zrforce = 0;

```

```

out(1) = xrforce;
out(2) = yrforce;
out(3) = zrforce;

```

```
% Adam Mortensen 14/Jul/97 Thesis project
%
% rdtoboomframe1.m
%
% input
%   angle of the dihedral and the current estimate for the angle
%   of the right and left ruddervators
%   the vector to be transformed from rudder to the boom frame
%
% output
%   left ruddervator velocity vector converted to the boom frame
%
% Notes: This block converts velocity from the boom frame to the
%        left ruddervator frame
%        qd      dihedral angle
%        qr      right ruddervator angle estimate
%        ql      left ruddervator angle estimate
%
```

%=====

```
function[outl] = rudtoboomframe1(input)
```

```
qd =input(1);  
qr =input(2);  
%ql =input(2);
```

```
cg = cos(qd);  
cr = cos(qr);  
%c3 = cos(ql);  
sg = sin(qd);  
sr = sin(qr);  
%s3 = sin(ql);
```

```
tst = [input(3) input(4) input(5)]';
```

```
tbrl = [cg*cr -(cg*sr) -sg; -(cr*sg) sg*sr -cg; sr cr 0];
```

```
outl(1:3,1) = (tbrl)*tst;
```

```

%=====
% Adam Mortensen 14/Jul/97 Thesis project
%
% rdtboomframer.m
%
% input
%   angle of the dihedral and the current estimate for the angle
%   of the right and left ruddervators
%   the vector to be transformed from rudder to the boom frame
%
%
% output
%   velocity vector converted to the boom frame
%
% Notes: This block converts velocity from the boom frame to the
%        right ruddervator frame
%        qd      dihedral angle
%        qr      right ruddervator angle estimate
%        ql      left ruddervator angle estimate
%
%=====

```

```

function[outr] = rdtboomframer(input)

qd =input(1);
qr =input(2);
%ql =input(2);

cg = cos(qd);
cr = cos(qr);
%c3 = cos(ql);
sg = sin(qd);
sr = sin(qr);
%s3 = sin(ql);

tst = [input(3) input(4) input(5)]';

tbrr = [cg*cr -(cg*sr) sg; cr*sg -(sg*sr) -cg; sr cr 0];

outr(1:3,1) = (tbrr)*tst;

```

Appendix D

Simulink Model Diagrams

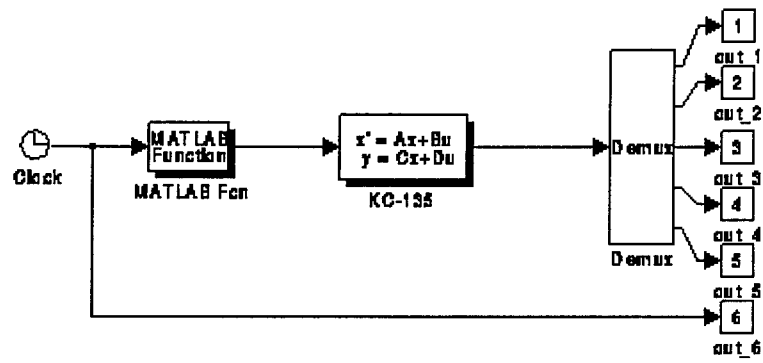


Figure 63: Aircraft Plant Block

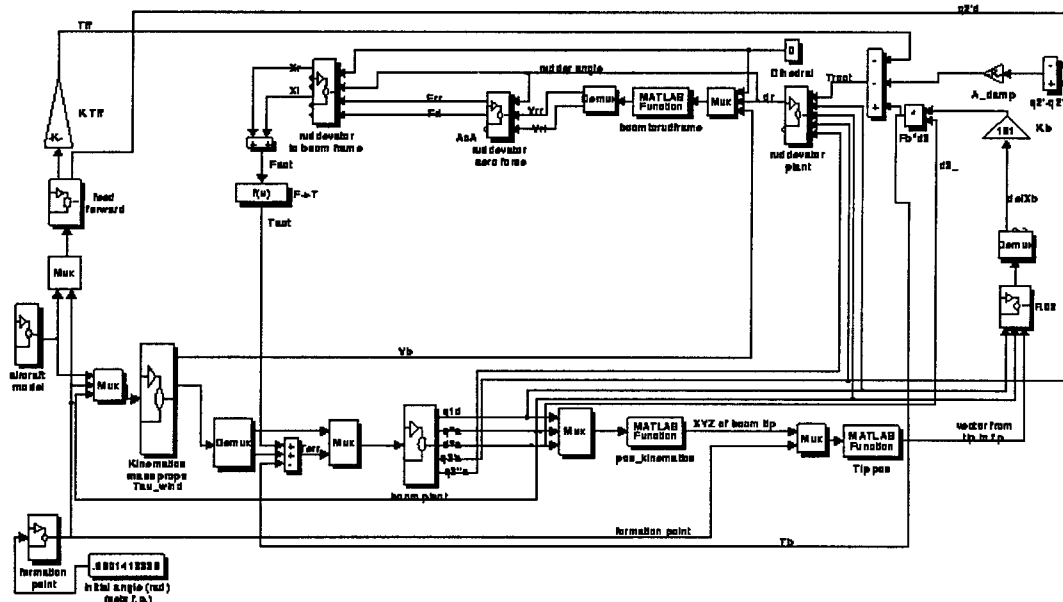


Figure 64: Controller Model

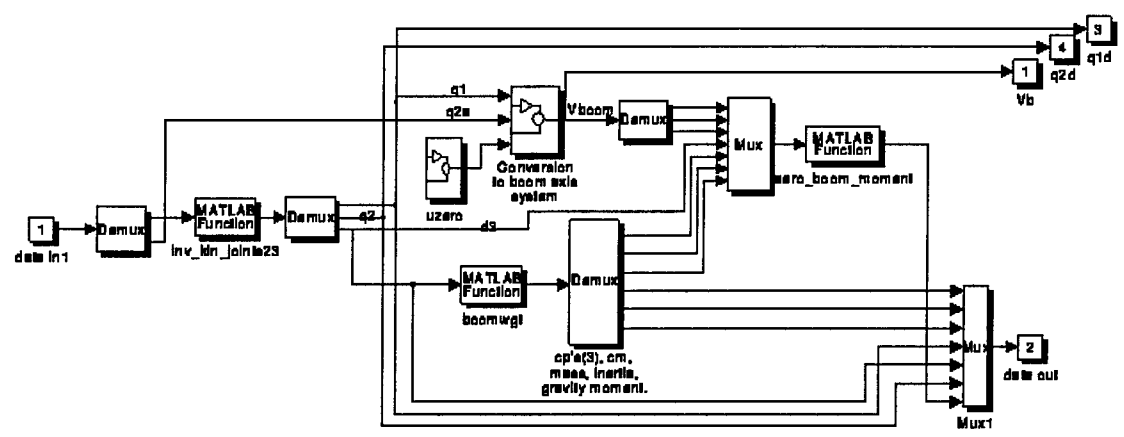


Figure 65: Kinematic, Boom Mass and Aerodynamics Calculation Block

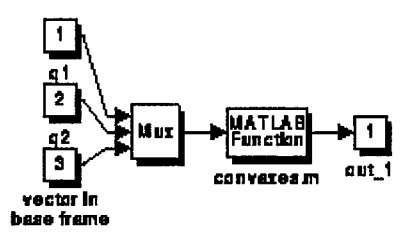


Figure 66: Freestream Wind Conversion to Boom Axes Block

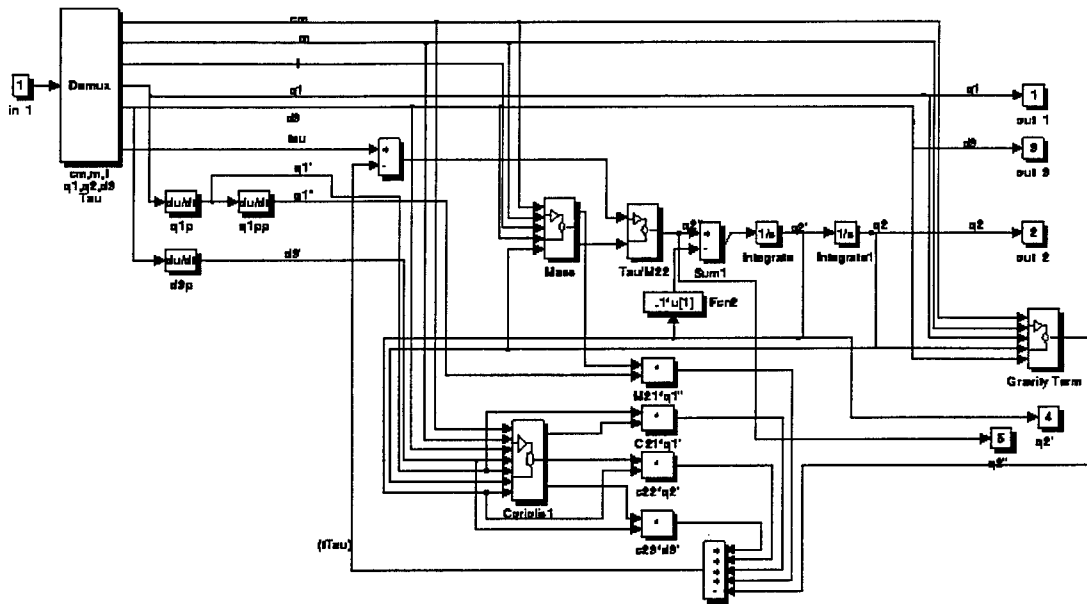


Figure 67: Boom Dynamic Plant Block



Figure 68: Inertia Block and Division Block

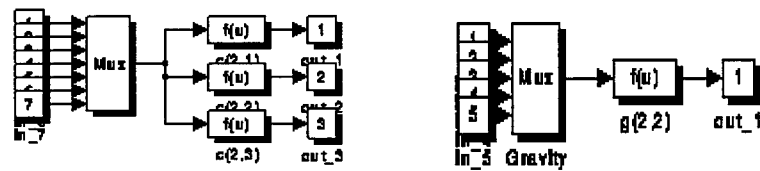


Figure 69: Boom Dynamics Coriolis and Gravity Calculation Blocks

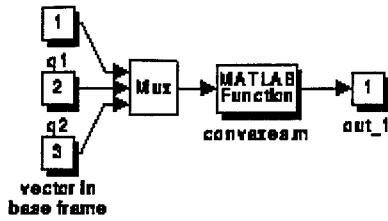


Figure 70: Conversion of Position Error, ΔX , ΔY , ΔZ Vector from Inertial Frame, "R03"

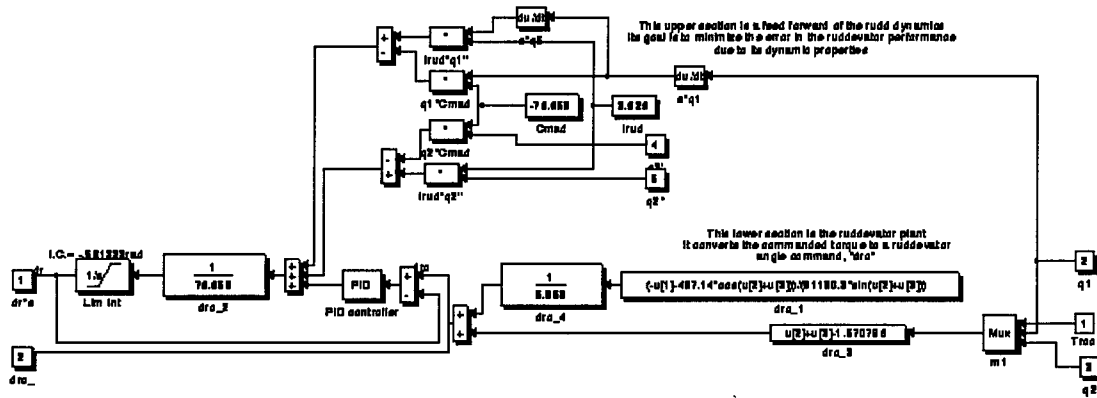


Figure 71: Ruddevator Plant and Feed Forward Inputs

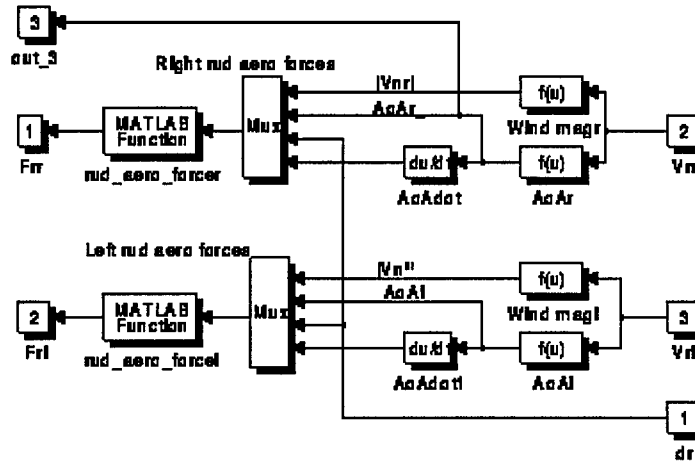


Figure 72: Ruddevator Aerodynamics Calculation Block

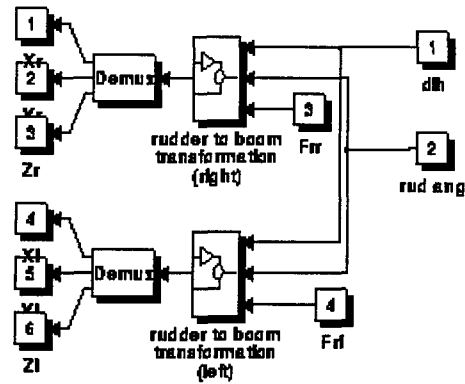
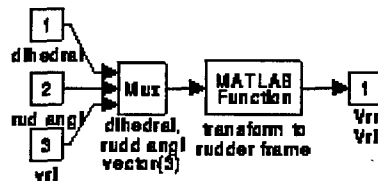


Figure 73: Transformation of Rudder Deviator Forces to Boom Frame



Right and Left Transformations
Are Identical

Figure 74: Subblock of Figure 73, Actual Transformation Block

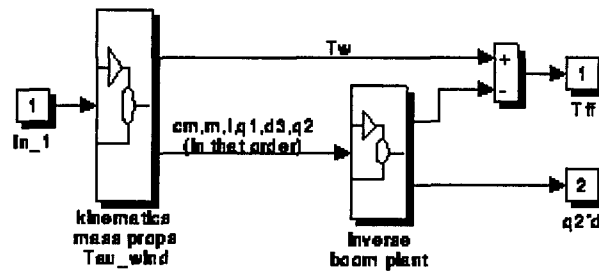


Figure 75: Feed Forward Signal Calculation Block

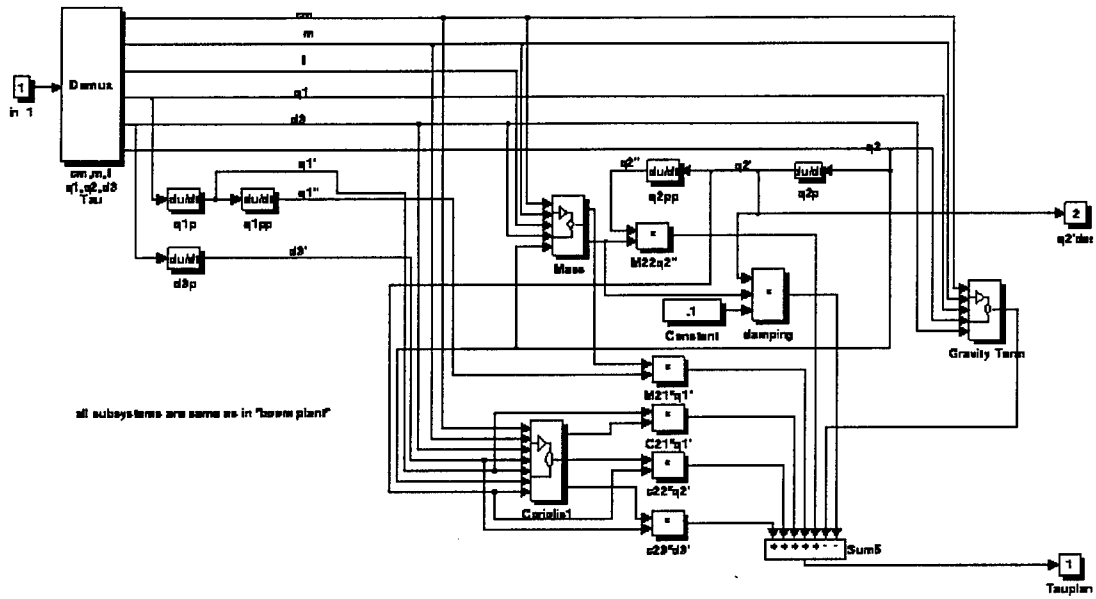


Figure 76: Inverse Boom Plant Subsystem from Figure 75

Appendix E

Feed Forward Plant Error Analysis

As indicated in chapter four, the cause of the error in the feed forward signal was due to the lack of precision of the Simulink program's derivative block. The MathWorks website verified this imperfection in the derivative block. While it is true that one can achieve a reasonable good estimation of the derivative using numeric methods, the estimated value obtained is still just that, an estimation. To determine the solution to this problem it was necessary to consider the main difference between the boom plant shown in Figure 67 of Appendix D and the inverse boom plant used in the feed forward block, Figure 76 of Appendix D. The primary difference between the two plants is caused because the boom plant is solved for the actual angle q_2 where the inverse boom plant is solved for the torque due to dynamic forces. In the boom plant the angular acceleration of q_2 is integrated twice to arrive at a value for q_2 . Conversely, in the inverse boom plant the angular velocity and acceleration of q_2 are derived by taking the numerical derivative twice of the angle q_2 . Other than these two differences, the two plant systems are identical. Error being a result of the integrator blocks was ruled out through simple tests where the sin was integrated to verify the proper result was obtained. When the derivative block was tested using a sinusoid input, the result of two derivatives being taken was not what one would expect. The signal did not look like a sinusoidal signal with a 180 degree phase lag. Instead the signal was pinched at the peaks with a lot of noise occurring at the peaks.

While both plant systems use the same derivative block network to calculate the angular velocity and acceleration of q_1 and the velocity of d_3 , the fact that both plants use the same network means that there should be no net error in the signal produced as a result of these derivatives. The problem remains then, to identify an alternative method for calculating the first and second derivatives of the angle q_2 . If one could relate the rate of change of the angle q_2 to the known angle q_1 , without using the derivatives of q_2 in the process, the problem of the inaccurate angular velocity and acceleration of angle q_2 could be eliminated. This relationship

can be found by using the velocity jacobian calculated as part of the forward kinematics in the Robotica program. This Jacobian is included in Appendix A.

The standard form of the velocity jacobian is

$$\dot{\vec{x}} = J\dot{\theta} \quad (E.1)$$

where

$$\dot{\vec{x}} = \begin{Bmatrix} \dot{x} \\ \dot{y} \\ \dot{z} \end{Bmatrix}$$

$$\dot{\theta} = \begin{Bmatrix} \dot{q}_1 \\ \dot{q}_2 \\ \dot{d}_3 \end{Bmatrix}$$

for the upper three rows of this problem's jacobian, which gives the linear velocity of the boom frame with respect to the base frame. (The last three rows of the velocity jacobian represent the angular velocity of the last frame.) By setting the r.h.s. of equation (E.1) to zero, which means we are representing the initial condition where there is no motion in the nozzle, we get two equations with three unknowns. As shown below, it is then possible to represent the angular velocity of q_2 in terms of the angular velocity of q_1 times a coefficient. From rows one and two of the velocity jacobian, equation (E.1),

$$0 = \dot{x} = (d_3(c_1c_2 - s_1s_2) - 49s_1)\dot{q}_1 + d_3(3(c_1c_2 - s_1s_2)\dot{q}_2 + s_12\dot{d}_3) \quad (E.2)$$

$$0 = \dot{y} = (d_3s_12 + 49c_1)\dot{q}_1 + d_3s_12\dot{q}_2 + (-c_1c_2 + s_1s_2)\dot{d}_3 \quad (E.3)$$

then, solving equation (E.3) for \dot{d}_3

$$\dot{d}_3 = \frac{1}{-c_1c_2 + s_1s_2} [-(d_3s_12 + 49c_1)\dot{q}_1 - d_3s_12\dot{q}_2] \quad (E.4)$$

equation (E.4) can be substituted for \dot{d}_3 in equation (E.2) to get a relationship between the angular velocities of q_1 and q_2 with undifferentiated values.

$$0 = \left[d_3(c_1c_2 - s_1s_2) - 49s_1 + \frac{s_1^2}{c_1c_2 - s_1s_2} (d_3 3s_1^2 + 49c_1) \right] \dot{q}_1 + \left[d_3(c_1c_2 - s_1s_2) + \frac{s_1^2}{c_1c_2 - s_1s_2} (d_3 s_1^2) \right] \dot{q}_2 \quad (E.5)$$

Finally, solving equation (E.5) for \dot{q}_2 , a relationship is found which does not require the differentiation of q_2 .

$$a = \frac{d_3[(c_1c_2 - s_1s_2)^2 + s_1^2] - 49[s_1(c_1c_2 - s_1s_2) - s_1^2c_1] / c_1c_2 - s_1s_2}{d_3[(c_1c_2 - s_1s_2)^2 + s_1^2] / c_1c_2 - s_1s_2} \quad (E.6)$$

Which reduces to

$$a = \frac{d_3 - 49(s_1c_1c_2 - s_1^2c_1)}{d_3(c_1^2 + s_1^2)} \quad (E.7)$$

and finally becomes

$$a = 1 + \frac{49}{d} (s_1^2d_1 - s_1c_1c_2) \quad (E.8)$$

then,

$$\dot{q}_2 = -a\dot{q}_1 \quad (E.9)$$

Equation (E.9) could be inserted in place of the first derivative block in Figure 76, Appendix D.

This same method can be used to calculate the relationship between the angular acceleration of q_1 and q_2 . By first differentiating the velocity jacobian, equation (E.1) with respect to time, then making the substitution for \ddot{d}_3 as was done above.

The effect on the system of implementing this option was beneficial. Just replacing the first of the two derivative blocks on the q_{2d} signal resulted in a small decrease in the resulting error. The impact to the feed forward block's performance did not clearly indicate the derivative was the only problem. Because of this, additional simulations were performed in an attempt to clarify the problem. After analyzing the model it became clear that there was no gain on the primary source of feedback for the controller, the bending torque, τ_b . This implied that the basic closed loop controller had no gains on its feedback. For the basic closed loop controller, the author didn't properly select the gain for the bending torque input to the t_{root} signal. The result was that the controller didn't zero out the error in the input signal very effectively. Recall, one example tested for the ideal controller was the use of a gain on the spring constant. That simulation resulted in excessive oscillation with little improvement in the required torque. The error in the simulation occurred as a result of the location chosen to insert the feedback gain on the τ_b signal. This gain was mistakenly placed on the F_{tip} signal instead of being placed only on the τ_b signal path that feeds into the t_{root} command. The result was an unforeseen feedback gain on the boom tip reaction force as well as on the intended line which becomes part of t_{root} . If the gain had only been added to the τ_b signal feeding the t_{root} command, shown in the bottom right corner of Figure 4, selection of the gain would have been successful and resulted in a better system response than that shown in chapter four. After determining this to be the source of the error, additional testing was done first to select a reasonable gain and then to verify that the results for simulation runs similar to those covered in the body were an improvement on what was shown. With the proper gain inserted in τ_b , the feed forward and rate feedback signals were disabled and the basic closed loop ideal controller was run with various gains. For the ideal case, the result was a flat line F_{tip} response that only got flatter as the gain value increase. The gain selected for the ideal rudder was 15. At this magnitude the ideal plant response for the feed

forward only case was an F_{tip} value of nearly zero while the value of t_{root} changed very little. After the gain on τ_b was selected several simulations were run to determine the effect of this gain when rate feedback and feed forward were added. In each case improvement was seen. In the feed forward only case, the resulting signal was a virtual flat line F_{tip} response. When rate feedback was added to the feed forward, the result was a flatline F_{tip} response during the period of prescribed aircraft plant motion with no oscillation after the prescribed motion ended.

After verifying the ideal case, numerous simulations were run with different combinations of gains and elevator deflection commands. The results of these runs are summarized in Table 7. This table is not a complete list of all simulations run but it is a sample of the simulations that show the trend in the controller's performance. The best results were

Table 7: Summary of Additional Simulation Runs

Case	Elevator Command (deg)	Gains				Results		Notes
		Tau_b	Rate Feedback	Feed Forward	Ruddevator P/	Ftip (lbs)	Tau_root (ft-lbs)	
1	3	10	0	0	10,000 / 0	23	9300	Signal growth ~ 5-10% in 15 sec.
2	3	10	400,000	0	10,000 / 0	14	7800	Choppy rudd tracking, no oscillation
3	3	10	0	1	10,000 / 0	8	8000	Oscillatory, 3% growth in 15 sec
4	3	15	0	0	70,000 / 500	11	6500	Simple controller with better PD
5	3	15	0	1	70,000 / 500	0.4	7500	Good response small oscillation
6	3	15	400,000	1	70,000 / 500	0.25	7250	Getting better, no oscillation
7	15	15	0	0	70,000 / 500	55	31,000	relatively large tip force
8	15	15	400,000	0	70,000 / 500	55	35,000	Strange behaviour in Ftip
9	15	15	0	1	70,000 / 500	2.5	35,000	some oscillation but very slow growth
10	15	15	400,000	1	70,000 / 500	1.5	35,000	Good response
11	15	50	0	0	70,000 / 500	21	40,000	Seem to have found a sweet spot
12	15	50	400,000	0	70,000 / 500	17	38,000	Better response than w/ lower T_b
10	15	50	0	1	70,000 / 500	1.7	36,000	good performance trend
11	15	50	400,000	1	70,000 / 500	0.5	35,000	excellent performance
12	15	50	400,000	1	70,000 / 500	3.75	37,000	moving F.P, no F.F knowledge

obtained when the PD controller gains were tuned to 70,000 for proportional feedback and 500 for the Derivative feedback. Just the inclusion of the derivative feedback made a noticeable difference in the controller's performance with feed forward. These gain settings were arrived at after many simulation iterations. The values used represent a "sweet spot" for this controller. Shifting either of these values by a little as 10% resulted in degraded system performance.

Without the addition of the τ_b feedback gain, it wasn't possible to use gains on the proportional path of the PD controller in the rudder plant above approximately 40,000. The additional testing made it clear that the performance of the feed forward signal is very dependent upon the fidelity with which the rudder plant PD controller is tuned. If the commanded root torque is not produced accurately by the rudder plant the feed forward term's performance degrades.

Summary

The failure of the feed forward term to perfectly augment the non-ideal simulation cases is a result of two main problems. The use of the Simulink derivative block produces error that would normally not be present in a real system. The second reason for the feed forward plant's limited performance was found to be related to the gain on τ_b and how well the rudder PD controller plant is tuned to a specific simulation scenario. The performance of the feed forward degrades when the controller is operated away from the conditions for which it was tuned. Because of this, there will always be some error present in this controller as it is run through a large range of conditions.

VITA

Captain Adam L. Mortensen [REDACTED]

[REDACTED] graduated from Clovis High School in California in June of 1982. He was accepted to the U.S. Air Force Academy, USAFA, in the Spring of 1986. At USAFA he studied Aeronautical Engineering and taught as a soaring instructor for two years. He received his Bachelor of Science degree in Aeronautical Engineering on 30 May 1990 from USAFA. He received his commission in the United States Air Force that same day.

His first permanent assignment was to Los Angeles Air Force Base, CA, as a member of the Defense Meteorological Satellite Program, DMSP, System Program Office. His primary duty while there was as Launch Operations Manager coordinating all program office preparations for launch at the launch base. In April of 1995 he was married to Ms. Sabrina L. Stegman while in Los Angeles. Then, after three successful launches with DMSP, he entered the School of Engineering at the Air Force Institute of Technology in June 1995. His first child, Aydan Lukas Mortensen, was born during his time at AFIT.

His follow on assignment is with the Electronic Countermeasures office, Wright Patterson AFB, OH.

[REDACTED]

Bibliography

1. Campbell, Terry G. et.al. System Study of the KC-135 Aerial Refueling System. MS thesis, Air Force Institute of Technology, Wright-Patterson AFB, OH, December 1989.
2. Carmichael, Bruce W. and others. "Strikestar 2025," Air Force 2025. Maxwell AFB, AL: Air University, August 1996.
3. Dargan, John L. Proportional Plus Integral Control of Aircraft for Automated Maneuvering Formation Flight. MS thesis, Air Force Institute of Technology, Wright-Patterson AFB, OH, December 1991.
4. Dodge, Don. Manager Automated Flight Systems, Avionics Dept, Douglas Products Division, Boeing Aircraft Company, Long Beach, Ca. Telephone Interview, 4 Sept 1997.
5. Etkin, Bernard. Dynamics of Atmospheric Flight. John Wiley & Sons, Inc., 1972.
6. Lahey, Mike, Chief UAV Applications Branch, ASC/RAV, Wright Patterson AFB. OH, Personal interview, 2 Sep 1997.
7. Lester, Rick W. and others. "Counterair: The Cutting Edge," Air Force 2025. Maxwell AFB, AL: Air University, August 1996.
8. Locken, William J. Digital Multivariable Tracker Control Laws for the KC-135A. MS thesis, Air Force Institute of Technology, Wright-Patterson AFB, OH, December 1993.
9. McFadden, Russell. Aeronautical Engineer, Boeing Company, Wichita, KS. Telephone interview. 13 August 1997.
10. Nawrocki, Debra A. Investigation of Aerodynamic Alterations for Improving the KC-135 Boom Performance During Aerial Refueling. MS thesis, Air Force Institute of Technology, Wright-Patterson AFB, OH, December 1995.
11. Phillips, Janel. Weights and Structure Engineer, Boeing Aircraft Company, Wichita, KS. Telephone interview. 17 July 1997.
12. Roskam, Jan. Airplane Flight Dynamics and Automatic Flight Controls. Roskam Aviation and Engineering Corporation, 1982.
13. Russell, Harvey H. Design of Robust Controllers for a Multiple Input-Multiple Output Control System with Uncertain Parameters Application to the Lateral and Longitudinal modes of the KC-135 Transport Aircraft. MS thesis, Air Force Institute of Technology, Wright-Patterson AFB, OH, December 1984.
14. Spong, Mark W., M. Vidyasagar Robot Dynamics and Control. John Wiley and Sons, Inc. 1989
15. Spong, Mark W. Robotica for Engineers. A Robotics Frontend for Mathematica. WWWeb, <http://decision.csl.uiuc.edu/pub/spong/robotica/rob2.m>. Computer software. University of Illinois at Urbana-Champaign, 1991.
16. Timoshenko, S. and Young, D.H. Elements of Strength of Materials. D. Van Nostrand Company, Inc., January 1962.
17. Trosen, Dennis W. Development of an Air-To-Air Refueling Automatic Flight Control System Using Quantitative Feedback Theory. MS thesis, Air Force Institute of Technology, Wright-Patterson AFB, OH, June 1993.
18. Unterreiner, Ronald J. and others. "Close Air Support (CAS) in 2025 'Computer, Lead's in Hot'," Air Force 2025. Maxwell AFB, AL: Air University, August 1996.

REPORT DOCUMENTATION PAGE			Form Approved OMB No. 0704-0188	
Public reporting burden for this collection of information is estimated to average 1 hour per response, including the time for reviewing instructions, searching existing data sources, gathering and maintaining the data needed, and completing and reviewing the collection of information. Send comments regarding this burden estimate or any other aspect of this collection of information, including suggestions for reducing this burden, to Washington Headquarters Services, Directorate for Information Operations and Reports, 1215 Jefferson Davis Highway, Suite 1204, Arlington, VA 22202-4302, and to the Office of Management and Budget, Paperwork Reduction Project (0704-0188), Washington, DC 20503.				
1. AGENCY USE ONLY (Leave blank)	2. REPORT DATE September 1997	3. REPORT TYPE AND DATES COVERED Master's Thesis		
4. TITLE AND SUBTITLE Improved Load Alleviation Capability for a KC-135			5. FUNDING NUMBERS	
6. AUTHOR(S) Adam L. Mortensen, Capt., USAF				
7. PERFORMING ORGANIZATION NAME(S) AND ADDRESS(ES) Air Force Institute of Technology AFIT/ENY 2950 P Street WPAFB OH, 45433-6583			8. PERFORMING ORGANIZATION REPORT NUMBER AFIT/GE/ENY/97S-1	
9. SPONSORING/MONITORING AGENCY NAME(S) AND ADDRESS(ES) ASC/GRR 2590 Loop Road WPAFB OH, 54533-7142			10. SPONSORING/MONITORING AGENCY REPORT NUMBER	
11. SUPPLEMENTARY NOTES				
12a. DISTRIBUTION AVAILABILITY STATEMENT Approved for Public Release; Distribution Unlimited			12b. DISTRIBUTION CODE A	
13. ABSTRACT (Maximum 200 words) The Air Force will greatly increase its use of Unmanned Aerial Vehicles (UAVs) in the next century and the latter part of this decade. These UAVs will require refueling like their manned counterparts. The KC-135 and the KC-10 are candidates to provide this refueling task. The KC-10 is equipped with an automatic load alleviation system on its refueling boom which minimizes radial loads at the receiver of the aircraft being refueled. The KC-135 does not have such a system on its boom. Because the boom operator relies on visual cues to tell him when the boom is bending to adjust the boom's ruddvators, large loads may be imparted to receiver aircraft at the fuel receiver port. While load alleviation is required for all aircraft in order to ensure that binding of the nozzle does not prevent disconnect, load alleviation may also be important for the lightweight UAV in order to prevent unwanted disturbance to its flight control system. A Controller was designed to control the longitudinal motion of the boom. This controller can control the angle of the boom so no forces are imparted to the nozzle as the tanker moves from its nominal orientation. The optimal controller design uses both feed forward and rate feedback to modulate the commanded torque signal sent to the ruddvators. The results show that using an automatic controller promises to provide accurate control of the KC-135 refueling boom during refueling operations with minimal forces being imparted to the receiver aircraft.				
14. SUBJECT TERMS KC-135, Refueling, Boom Controller, Automatic Control, Tanker Aircraft, Robotics, Automation, Simulation			15. NUMBER OF PAGES 145	
			16. PRICE CODE	
17. SECURITY CLASSIFICATION OF REPORT UNCLASSIFIED	18. SECURITY CLASSIFICATION OF THIS PAGE UNCLASSIFIED	19. SECURITY CLASSIFICATION OF ABSTRACT UNCLASSIFIED	20. LIMITATION OF ABSTRACT UL	